NATURAL RESOURCES

GEOLOGIC MAP OF THE CENTRALIA 7.5-MINUTE QUADRANGLE, LEWIS COUNTY, WASHINGTON

by Andrew J. Sadowski, William E. Keller, Michael Polenz, Todd R. Lau, Recep Cakir, Elizabeth Nesbitt, Jeffrey H. Tepper, S. Andrew DuFrane, and Gabriel Legoretta Paulín

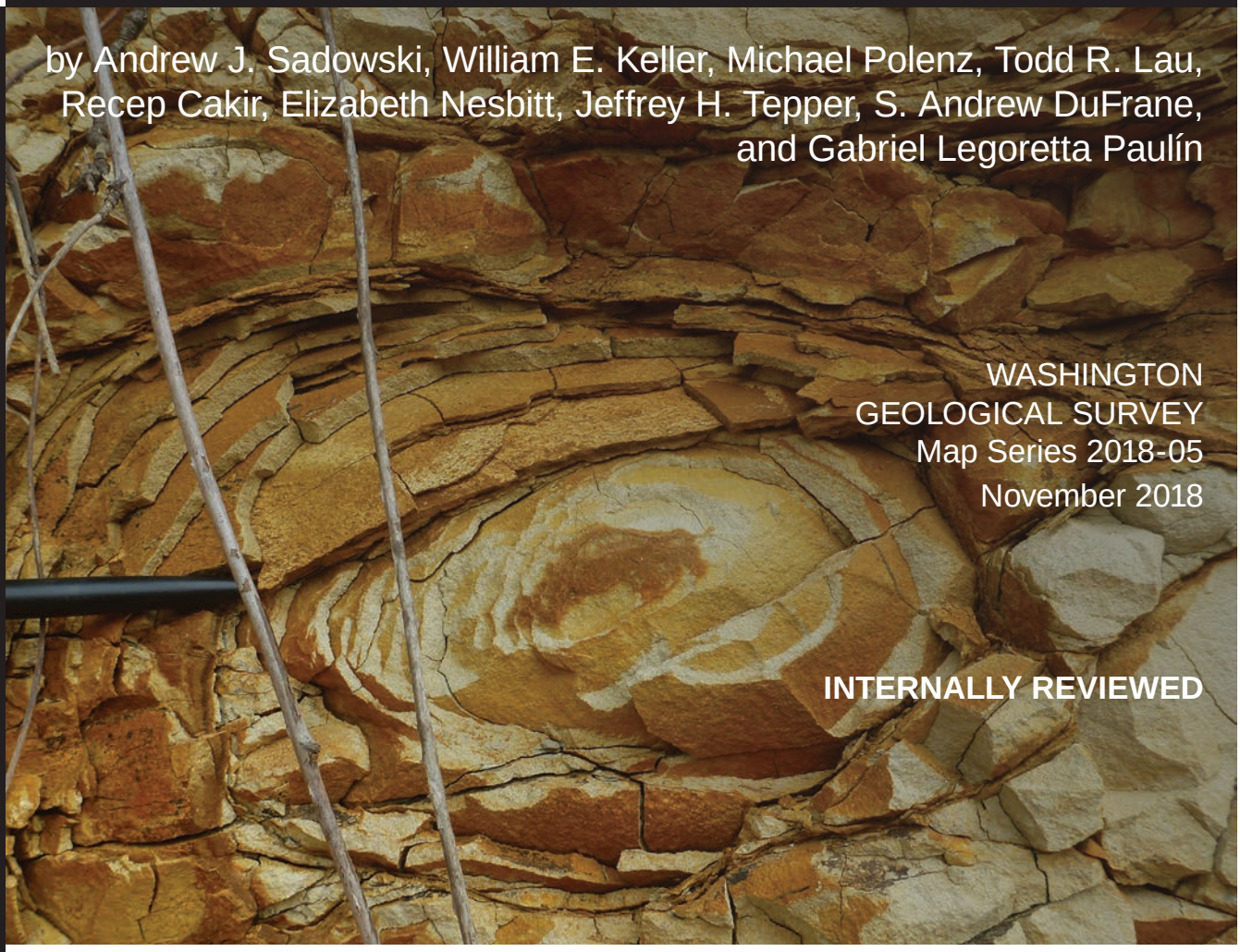

WASHINGTON
GEOLOGICAL SURVEY
Map Series 2018-05
November 2018

INTERNALLY REVIEWED

WASHINGTON STATE DEPARTMENT OF
NATURAL RESOURCES
WASHINGTON GEOLOGICAL SURVEY

GEOLOGIC MAP OF THE CENTRALIA 7.5-MINUTE QUADRANGLE, LEWIS COUNTY, WASHINGTON

by Andrew J. Sadowski, William E. Keller, Michael Polenz, Todd R. Lau, Recep Cakir, Elizabeth Nesbitt, Jeffrey H. Tepper, S. Andrew DuFrane, and Gabriel Legoretta Paulín

WASHINGTON
GEOLOGICAL SURVEY
Map Series 2018-05
November 2018

This geologic map was funded in part by the USGS National Cooperative Geologic Mapping Program, award no. G17AC00262

This publication has been subject to an iterative technical review process by at least one Survey geologist who is not an author. This publication has also been subject to an iterative review process with Survey editors and cartographers.

WASHINGTON STATE DEPARTMENT OF
NATURAL RESOURCES
WASHINGTON GEOLOGICAL SURVEY

DISCLAIMER

Neither the State of Washington, nor any agency thereof, nor any of their employees, makes any warranty, express or implied, or assumes any legal liability or responsibility for the accuracy, completeness, or usefulness of any information, apparatus, product, or process disclosed, or represents that its use would not infringe privately owned rights. Reference herein to any specific commercial product, process, or service by trade name, trademark, manufacturer, or otherwise, does not necessarily constitute or imply its endorsement, recommendation, or favoring by the State of Washington or any agency thereof. The views and opinions of authors expressed herein do not necessarily state or reflect those of the State of Washington or any agency thereof.

INDEMNIFICATION

Research supported by the U.S. Geological Survey, National Cooperative Geologic Mapping Program, under USGS award number G17AC00262. The views and conclusions contained in this document are those of the authors and should not be interpreted as necessarily representing the official policies, either expressed or implied, of the U.S. Government.

WASHINGTON STATE DEPARTMENT OF NATURAL RESOURCES

Hilary S. Franz—*Commissioner of Public Lands*

WASHINGTON GEOLOGICAL SURVEY

David K. Norman—*State Geologist*
John P. Bromley—*Assistant State Geologist*

Washington State Department of Natural Resources
Washington Geological Survey

Mailing Address:
MS 47007
Olympia, WA 98504-7007

Street Address:
Natural Resources Bldg, Rm 148
1111 Washington St SE
Olympia, WA 98501

Phone: 360-902-1450
Fax: 360-902-1785
Email: geology@dnr.wa.gov
Website: http://www.dnr.wa.gov/geology

Publications and Maps:
www.dnr.wa.gov/programs-and-services/geology/publications-and-data/publications-and-maps

Washington Geology Library Searchable Catalog:
www.dnr.wa.gov/programs-and-services/geology/washington-geology-library

Suggested Citation: Sadowski, A. J.; Keller, W. E.; Polenz, Michael; Lau, T. R.; Cakir, Recep; Nesbitt, Elizabeth; Tepper, J. H.; DuFrane, S. A.; Legoretta Paulín, Gabriel, 2018, Geologic map of the Centralia 7.5-minute quadrangle, Lewis County, Washington: Washington Geological Survey Map Series 2018-05, 1 sheet, scale 1:24,000, 43 p. text. [http://www.dnr.wa.gov/publications/ger_ms2018-05_geol_map_centralia_24k.zip]

© 2018 Washington Geological Survey
Published in the United States of America

Contents

Introduction 1
Geologic Overview 2
    Bedrock 2
    Surficial Deposits 2
    Tectonic Framework 2
Methods 3
    Geologic Mapping 3
    Data Collection and Analysis 3
    Geochronology 3
    Geochemistry and X-ray Diffraction 3
    Sedimentary Provenance of Quaternary Units 4
    Quaternary Geochronology 4
Description of Map Units 4
    Quaternary Unconsolidated Deposits 4
    Tertiary Volcanic and Sedimentary Bedrock 5
Geochemistry Results 13
    Volcanic Geochemistry 13
    Sedimentary Geochemistry 13
    X-Ray Diffraction 15
Ages of Deposits and Paleoenvironmental Interpretations 15
    Bedrock Units 15
    Quaternary Surficial Units 18
Structures in the Map Area 19
    Faults 21
    Folds 23
    Lincoln Creek Uplift 24
Geophysical Data and Interpretation 25
    Gravity and Magnetic Geophysical Data 25
    Active and Passive Seismic Interpretation 25
Structural Synthesis 26
Conclusions 27
    Recommendations for Future Work 28
Acknowledgments 30
References 30
Appendix A. Geophysical Methods: Data Collection and Analysis 34
Appendix B. New U-Pb Age Estimates 37
Appendix C. New Radiocarbon Age Estimate 42

FIGURES

Figure 1. Clast compositional charts 6
Figure 2. Weathering of clasts 7
Figure 3. Photograph of U-Pb age site GD06 7
Figure 4. Photograph of U-Pb age site GD08 8
Figure 5. Photographs of significant site S05 9
Figure 6. Photograph of significant site S06 11
Figure 7. Photograph of paleomagnetic site M02 12
Figure 8. Photograph of fossil site GD33 13
Figure 9. Geochemistry data 14
Figure 10. Compilation probability distribution plot of U-Pb analyses of zircon grains 16
Figure 11. *Thalassinoides (Glossifungites* ichnofacies) trace fossils 17
Figure 12. Schematic map showing inferred paleogeography of the Centralia area 18
Figure 13. Photo of sand dike at GD07 19
Figure 14. Structural map of the Centralia quadrangle and adjacent areas 20
Figure 15. Lidar images showing the Salzer Creek fault 22
Figure 16. South Scheuber Road geophysical survey results 26
Figure 17. All dispersion curves from ambient noise data processing 27
Figure 18. Two-dimensional shear-wave velocity image 28
Figure 19. Hypothetical stress regime in the greater Centralia quadrangle area 29
Figure A1. Geometry of the long-range passive seismic array 35
Figure A2. Long-range passive array measurement locations 36
Figure A3. Comparison of simplified dispersion curves 36
Figure B1. Younger zircon age peaks for sample from site GD10 39
Figure B2. Younger zircon age peaks for sample from site GD09 39
Figure B3A. Younger zircon age peaks for sample from site GD08. 40
Figure B3B. Older zircon age peaks for sample from site GD08. 40
Figure B3C. Concordia diagram for sample from site GD08. 40
Figure B4A. Younger zircon age peaks for sample from site GD07. 40
Figure B4B. Older zircon age peaks for sample from site GD07. 40
Figure B4C. Concordia diagram for sample from site GD07. 40
Figure B5A. Younger zircon age peaks for sample from site GD06. 41
Figure B5B. Older zircon age peaks for sample from site GD06. 41
Figure B5C. Concordia diagram for sample from site GD06. 41
Figure C1. Radiocarbon age diagram for sample from site GD01. 42

TABLES

Table B1. U-Pb data 38
Table C1. Radiocarbon data 42

MAP SHEET

Geologic Map of the Centralia 7.5-minute Quadrangle, Lewis County, Washington

Figure M1. Regional geologic map of the Centralia quadrangle and surrounding areas
Figure M2. Aeromagnetic map of the Centralia quadrangle and vicinity
Figure M3. Complete Bouguer gravity anomaly map of the Centralia quadrangle and vicinity

Geologic Map of the Centralia 7.5-minute Quadrangle, Lewis County, Washington

by Andrew J. Sadowski[1], William E. Keller[1], Michael Polenz[1], Todd R. Lau[1], Recep Cakir[1], Elizabeth Nesbitt[2], Jeffrey H. Tepper[3], S. Andrew DuFrane[4], and Gabriel Legoretta Paulín[5]

[1] Washington Geological Survey
MS 47007
Olympia, WA
98504-7007

[2] The Burke Museum of Natural History and Culture
University of Washington
Box 353010
Seattle, WA 98195

[3] Geology Department
University of Puget Sound
1500 N Warner
Tacoma, WA 98416

[4] University of Alberta
Department of Earth and Atmospheric Sciences
1-26 Earth Sciences Building
Edmonton, Alberta, Canada T6G 2E3

[5] Instituto de Geografía
Universidad Nacional Autónoma de México
Ciudad Universitaria, Del Coyoacán
cp 04510, México, D.F.

ABSTRACT

New 1:24,000-scale geologic mapping of the Centralia quadrangle focuses on improving geologic understanding of a populated area affected by natural hazards. Critical among these are potential seismic hazards related to the Doty–Salzer Creek fault system, which may pose a hazard to a proposed flood retention dam near Pe Ell, WA.

New mapping and geophysical data build on previous work by characterizing geologic structures in greater detail, refining fault locations, and updating structural interpretations. Northwest- and west-striking oblique faults in the quadrangle may be capable of producing damaging earthquakes and may be responding to a local transpressive stress regime. Newly acquired gravity, ground magnetic, and passive seismic geophysical data constrain the locations of several concealed fault strands, and strongly suggest a structural high—the Lincoln Creek uplift—underlies the Chehalis River valley from Chehalis to Fords Prairie, WA.

Radiometric dating (U-Pb) of detrital zircons also refines the stratigraphic framework for southwest Washington. Analyses reveal new maximum depositional ages for the base and middle of the Lincoln Creek Formation (36.70 ±0.32 Ma and 30.58 ±0.35 Ma, respectively), the previously unrecognized Wilkes Formation (8.57 ±0.92 Ma and 7.54 ±1.04 Ma), and the Logan Hill Formation (1.68 ±0.97 Ma youngest age).

Numerous previously unrecognized landslides are identified from lidar and field mapping. The lower contact of the early Pleistocene Logan Hill Formation is commonly concealed by landslides, which suggests that the base of this formation may form a slide plane for landslides and may warrant future geotechnical work.

INTRODUCTION

The Centralia 7.5-minute quadrangle (hereinafter also referred to as "the map area") is located in northwestern Lewis County, Washington, about 30 mi south of Olympia, WA, and encompasses the towns of Centralia and Chehalis, WA. The Chehalis River flows north through the map area, merging with the Newaukum and Skookumchuck rivers. Much of the lowland near Centralia and Chehalis has been developed as residential or commercial property, while areas away from the population centers have remained agricultural land. Most of the higher elevation areas are forested and managed for timber resources. Coal production played an important economic role in the area until the early to mid-20th century, and mining continued at the Centralia coal mine northeast of the map area until the early 2000s.

The map area contains the economically vital I-5 corridor, which runs subparallel to the north-flowing stretch of the Chehalis River. Flooding in 1989, 1996, 2007, and 2009 closed the interstate and resulted in widespread damages, economic losses, and harm to the citizens of Washington, especially those in Lewis County. These disasters prompted the development of hazard mitigation plans for the region, one of which proposed a flood retention dam on the upper Chehalis River, south of Pe Ell, WA. However, understanding of geologic hazards that may affect construction and stability of this dam is currently limited. The new 1:24,000-scale geologic mapping presented here will help identify natural hazards, inform resource management, and guide urban planning within the Centralia quadrangle and beyond. Critical among these concerns are landslide hazards and seismic hazards related to potentially active faults that can be traced westward toward the proposed dam site south of Pe Ell. The new geologic mapping is part of a larger multi-year effort to map bedrock, surficial, and structural geology across the southern Puget Lowland and westward through the Willapa Hills. The new work aims to better characterize crustal faults and deformation in the Doty–Willapa Hills area. Geologic hazards in this area

include earthquakes (both regional subduction-zone events and relatively local crustal-scale events), shallow and deep-seated landslides, and floods. The mapping will assist in geologic hazard assessment, geotechnical engineering, groundwater hydrology, earth resource management, academic research, and investigations for urban development planning.

GEOLOGIC OVERVIEW

Bedrock

Paleogene and Neogene bedrock exposures are limited in the map area due to widespread vegetation, severe weathering, and modification by human activity. Paleogene sedimentary units are derived from distal eroded material from central and eastern Washington as well as local interfingering volcanic suites, such as the Northcraft Formation. The Neogene sedimentary units are derived from these underlying Paleogene units and volcanic rocks of the Cascade arc. This entire stratigraphic section overlies Eocene-age Crescent Formation, which is not exposed in the Centralia quadrangle (Snavely and others, 1951, 1958; Dragovich and others, 2002; Walsh and Logan, 2005; Logan and others, 2009; Wells and others, 2014; Kant and others, 2015).

The two principal Paleogene units exposed in the map area are the middle to late Eocene Skookumchuck Formation and the latest Eocene to Oligocene Lincoln Creek Formation (Snavely and others, 1951; 1958). The Skookumchuck Formation is part of the upper Puget Group and represents the near-shore to deltaic depositional facies equivalent to a portion of the Eocene Cowlitz Formation of southwestern Washington and northwestern Oregon (Weaver 1937; Armentrout and others, 1983; Wells and others, 2014). The Skookumchuck Formation was mined extensively as a coal resource throughout the 20th century at 20 small coal mines in the map area. The formation is the only bedrock unit in the area that contains coal beds.

Weaver (1912, 1937) used the name Lincoln Formation to describe marine siltstone and sandstone at the mouth of Lincoln Creek, near Galvin, WA. Weaver (1944) later expanded the type section to include outcrops along the Chehalis River from Centralia to Porter, WA. The name Lincoln Formation (of Weaver) was later changed to Lincoln Creek Formation (Beikman and others, 1967), to avoid confusion with other North American geologic units.

Neogene bedrock units in the Centralia quadrangle include the Miocene Grande Ronde Basalt of the Columbia River Basalt Group and the Miocene Wilkes Formation. The Wilkes Formation was formerly recognized as an unnamed Tertiary nonmarine unit composed of semi-consolidated sedimentary rock types from fluvial, lacustrine, and brackish-water depositional environments (Roberts, 1958; Snavely and others, 1958).

Surficial Deposits

Glacial and nonglacial surficial deposits are present in the Centralia quadrangle. Glacial units include outwash from Vashon continental glaciations and outwash from pre-Vashon alpine glaciations. The map area lies south of the maximum extent of the Puget Lobe ice sheet (Bretz, 1913; Lea, 1984). Vashon-aged outwash from this Cordilleran ice sheet drained to the south and west through the Skookumchuck River valley (Bretz, 1913; Lea, 1984). This drainage pattern resulted in glacial units with a distinct northern provenance in the northern half of the quadrangle compared to the alluvium of the Chehalis River to the south.

Pre-Vashon outwash from alpine glaciation(s) includes the Pleistocene Logan Hill Formation. This formation was first described by Bretz (1913) as the "pre-Vashon red gravels of the Chehalis Valley" and formally named by Snavely and others (1951). It mantles topography and forms broad, flat landforms composed of severely weathered, alpine glacial outwash of Cascades-sourced material. The new geologic mapping shows that the Logan Hill Formation is less extensive than previously mapped throughout the map area and is more common to the south and east of the quadrangle, especially in the Logan Hill 7.5-minute quadrangle to the east.

Nonglacial units include alluvium and landslides. The Chehalis River valley occupies a large portion of the map area, and consists of a broad floodplain with elevated fluvial terraces composed of variably-sorted clastic material. Above the Chehalis River valley, the map area hosts numerous large landslides, landslide complexes, and other mass-wasting deposits. These areas of concern should be evaluated on an individual basis as potential geologic hazards.

Tectonic Framework

The Centralia quadrangle lies within the forearc of the Cascadia subduction zone, where oblique subduction of the Juan de Fuca plate beneath the North American plate has resulted in structural complexity (Wells and others, 1998; Lewis and others, 2003; Johnson and others, 2004; McCaffrey and others, 2007, 2013). Clockwise rotation of the Washington forearc accompanies about 4.4 to 4.6 mm/year of ongoing, north-south shortening against the relatively stable Coast Mountains of British Columbia (Johnson and others, 2004; McCaffrey and others, 2013; Wells and McCaffrey, 2013). This shortening combined with oblique subduction, transpression, and rotation resulted in a series of basins and uplifts bounded by mostly west-striking faults and folds in the Puget Lowland (Clowes and others, 1987; Johnson and others, 1996; Wang, 1996; Pratt and others 1997; Wells and others, 2017; Bowman and Czajkowski, 2016).

Faults in the Centralia quadrangle broadly fit into two regional-scale patterns related to the segmented, upper crustal structure associated with the Cascadia subduction zone (Wells and others, 2017). These fault patterns are defined as the west-striking faults, exemplified by the Doty–Salzer Creek fault system, and the northwest-striking faults, exemplified by the main strand of the Kopiah fault. These fault patterns intersect in the Logan Hill quadrangle, and form the center of a broad zone of interaction between regional fault systems that also encompasses the Centralia quadrangle (Fig. M1). Similar to the segmented faults related to the Cascadia megathrust, the tremor density within the map area is "segmented" or sparse as well (Well and others, 2017). Numerous active structures have been recognized farther north in the Puget Lowland (Johnson and others, 2004; McCaffrey and others, 2013; Wells and McCaffrey, 2013), and these fault systems are likely reacting to the modern compressional stress regime. This regional stress regime has been steady since Miocene time (Wells and McCaffrey, 2013) and it has exhibited clockwise-rotational

behavior since Eocene time (Wells and Coe, 1985). Therefore, these active northern faults exhibit similar geometries to faults in the map area. Also north of the map area, fault activity has been linked to the modern transpressional stress regime, which has been largely similar in orientation since the late Miocene. Although clear evidence for fault activity on structures in the map area is arguable, their similarity in orientation to active structures farther north raises the possibility that they may be active as well.

METHODS

Geologic Mapping

Lithologic units were identified from field observations between July 13 and November 9, 2017. Field data was collected using traditional geologic field methods and digitally recorded in the field with Esri ArcCollector. The geologic map was refined using prior 1:48,000 geologic mapping (Snavely and others, 1958), 21 historic coal mine records (Snavely and others, 1958), six historic coal mine maps, and recent aerial orthophotos. Bedding attitudes, sedimentary structure, foliation, joints, and shears in bedrock were collected where the feature did not appear to be a randomly oriented crack, brecciation of unknown origin, or columnar jointing in basalt. Due to poor exposure, most outcrops are small, and no measured features could be traced beyond individual exposures. Orientations were evaluated using Stereonet 10.1.0 software (Allmendinger and others, 2018; Cardozo and Allmendinger, 2013). Elevation data from the SWWA Foothills 2017 lidar project (USGS, 2016) with a 3-ft grid resolution were used to derive hillshade images, contours, and other terrain products that served as base maps for directing field investigations.

Data Collection and Analysis

Multiple datasets were reviewed, including well logs, boring records, geotechnical reports, geophysical data (aeromagnetics and ground magnetics, gravity, seismic reflection, passive seismic, seismic tomography), petrographic analysis of thin sections, geochemical analyses (major element, trace element, and x-ray diffraction), and identification of geomorphic features using lidar. More than 2,400 water wells and geotechnical borings within ~1 mi of the Centralia quadrangle were reviewed. Of these, fewer than 715 were precisely located and used to inform our mapping. Eleven wells were used to construct the cross section. Five of the 41 field borings that were drilled during the fieldwork of Snavely and others (1958) aided understanding of subsurface relationships and identification of concealed minor faults in the Centralia quadrangle. Numerous test holes drilled prior to the investigation of Snavely and others (1958) in the Centralia–Chehalis coal district further supported field observations and guided interpretations.

GEOPHYSICAL DATA COLLECTION AND ANALYSIS

Ground magnetics, gravity, and passive and active seismic surveys were performed along with paleomagnetic sampling. Data acquisition procedures and analytical methods are described in detail in Appendix A.

Geochronology

PALEONTOLOGY AND BIOSTRATIGRAPHY

Ellington and Associates, Inc. (Houston, TX, division of ALS) prepared biostratigraphy samples for microfossil analysis. Fossil content was analyzed by Elizabeth Nesbitt and Ruth Martin of the Burke Museum (Univ. of Wash.) to provide biostratigraphic age controls and constraints on paleoenvironment (Table DS1).

U-PB ANALYSIS OF DETRITAL ZIRCON GRAINS

U-Pb analysis of zircon grains extracted from five samples in the Centralia quadrangle provides new information about sediment provenance and depositional age for the Lincoln Creek, Wilkes, and Logan Hill Formations. Two zircon age analyses targeted tuffs within the lower and middle stratigraphic positions of the Lincoln Creek Formation (age sites GD10, GD09, respectively). Three other detrital zircon samples were collected from sedimentary units, including two samples from the Wilkes Formation (age sites GD07, GD08) and one from the overlying Logan Hill formation (age site GD06)(Appendix B, Tables DS2–DS6).

A maximum depositional age represents the oldest possible age of the deposit (although it could have been deposited more recently), and can be determined from either a single-event age or detrital samples. Depending on the geologic context of the sample and the source area, the maximum depositional age is either the average of the youngest population of zircons or the age of the youngest single zircon. Where the zircon ages of a sample are thought to represent a single geologic event, such as an airfall tuff, an average age of the youngest population is preferred (Dickinson and Gehrels, 2009). Where deposition is more continuous than a single event, such as fluvial deposition of detrital zircons, the youngest single grain is preferred in our study.

Geochemistry and X-ray Diffraction

A total of 46 samples of volcanic and sedimentary bedrock, drift, and weathering products of those rock types were analyzed for major and trace element composition (Tables DS7 and DS8). ALS, a geochemistry laboratory in North Vancouver, BC, Canada, analyzed 44 samples using ICP-AES (major elements), ICP-MS (trace elements), and a combustion oven (loss on ignition [LOI]). Three samples of Columbia River Basalt were analyzed using x-ray fluorescence (XRF) and ICP-MS under the direction of John Wolff at the Peter Hooper GeoAnalytical Lab at Washington State University (WSU), Pullman, WA. As a quality assurance check, a single basalt sample (geochemistry site G02) was analyzed at both labs and returned similar results.

Clay mineral analysis by x-ray diffraction (XRD) was performed by Washington Geological Survey (WGS) staff on 31 samples in the Centralia quadrangle (27 bedrock and 4 surficial materials) and 16 samples from the Violet Prairie quadrangle (15 sedimentary rocks and 1 northern-sourced pre-Vashon till)(Table DS9). Samples were prepared using standard procedures outlined in Starkey and others (1984) and analyzed using a Rigaku MiniFlex 600 with copper radiation at 40kV and 15 mA. Qualitative phase analysis of orientated clay samples was performed following Starkey and others (1984).

Sedimentary Provenance of Quaternary Units

Pebble and cobble clast rock types and weathering were recorded to determine provenance and help assess relative deposit ages, respectively. Observations from clast counts (Table DS10), petrographic review of matrix content, sedimentary attributes (such as bedding style, grain size, and textural changes), and field relations among unlithified deposits are used to infer provenance of sedimentary units and help determine their depositional setting (glacial, nonglacial, or undivided).

Quaternary Geochronology

WEATHERING

The relative ages of Quaternary units were assessed using clast weathering and thin-section petrographic assessment of matrix weathering. The results are summarized below. The degree of weathering is used as a proxy for age, where thinner weathering rinds represent younger units and severely weathered and rotten clasts are oldest.

RADIOCARBON ANALYSIS

Conventional radiocarbon analysis was performed on a large stick lodged into a steep bank of the Chehalis River in the southern portion of the map area (age site GD01) between the Doty and Salzer Creek faults. Conventional "radiocarbon plus" analysis was performed by Beta Analytic (Miami, FL)(Appendix C).

Description of Map Units

Quaternary Unconsolidated Deposits

POSTGLACIAL DEPOSITS

Postglacial deposits in glaciated parts of the map area are in most cases readily identified by their lack of compaction. However, in unglaciated parts of the map area glacial/postglacial distinctions are difficult and variations are discussed in more detail below (see *Nonglacial Deposits*).

Holocene Nonglacial Deposits

af **Artificial fill**—Rubble of mostly northern-sourced cobbles, pebbles, sand and boulders in varied amounts and rock types; poorly sorted and unconsolidated; used to raise roadbeds and other infrastructure throughout the map area; most of these represent built environments (for example, Chehalis–Centralia municipal airport, Interstate 5).

ml **Modified land**—Rubble of northern-sourced cobbles, pebbles, sand and boulders in varied amounts and rock types; locally sourced but redistributed to modify topography; includes most industrial zones (for example, warehouse districts, railyards, timber storage) and downtown commercial corridors, hospitals, sports field complexes, some rock quarries, and some large housing developments; excludes local roads, individual homes, golf courses, farms and harvested timber lands. Also excludes some pits where underlying units can be readily identified, fill areas appear minor, excavation exposes the same unit as the surrounding surface, or exposure of underlying units was deemed likely to be permanent. The mapping of alluvial and glacial Quaternary units takes priority over delineating modified land, therefore, contact relationships between Quaternary units are shown preferentially.

Qp **Peat**—Organic and organic-rich sediment; includes peat, gyttja, muck, silt, and clay; typically in closed depressions; mapped in wetland areas and distinctly flat-bottomed depressions; also mapped on the basis of spectral analysis of Landsat data and (or) evaluation of infrared and color aerial photos. The thickness of most peat deposits is largely unassessed and unknown. Small peat deposits are scattered throughout the map area, typically within alluvium and related to ponding of stagnant water.

Qls **Landslide deposits**—Sand, silt, clay, cobbles, pebbles, boulders and diamicton of sandstone and siltstone of varied amounts; degree of weathering varies; clasts angular to rounded; unsorted; generally loose, jumbled and unstratified, but locally retaining primary bedding and compaction; rock types varied but sandstone and siltstone dominate; derived from units upslope (or underfoot in some landslide toes). Unit thickness varies throughout the map area and is mostly unassessed. Landslides are common, vary in overall extent, and are more densely concentrated in the Centralia quadrangle than in other areas that were previously mapped by the WGS landslide hazards group. Very large landslide complexes are common along hillslopes and are mapped mostly from lidar, typically based on the interpretations of the WGS landslide hazards group. A "mass wasting" overlay is also used to delineate more ambiguous deposits with landslide-like characteristics. Absence of mapped landslides or mass-wasting features does not imply stability or the absence of hazard. The ages, timing, and recurrence of both deposit types are uncertain.

Pleistocene to Holocene Nonglacial Deposits

Qa, Qoa **Alluvium**—Stream channel deposits, flood plains, and older terrace deposits; pebbles, cobbles, sand, silt, clay, peat, and boulders in varying amounts along stream channels and on flood plains; color ranges from light tanish gray to dark brown, depending on the amount and source of fines; fresh to lightly weathered except where streams have incorporated older deposits, resulting in a bimodal weathering distribution; not compacted and not cemented; typically well rounded and moderately to well sorted; lithology of the clasts varies based on what deposits the stream flows through; clasts are dominantly extrusive volcanic rocks with lesser gabbro, metamorphic rocks, chert, and granite; active alluvium is 70 to 100 ft thick based on well logs and an interpreted seismic reflection profile to the west of

Chehalis–Centralia airport along NW Airport Road (W. Stephenson, written commun., 2018). Mapped as unit Qa where youngest, lowest lying, and alluvium is active. Mapped as unit Qoa where low-lying older alluvial terraces (5–20 ft thick) reside more than 5 ft above the active alluvial surface. Older alluvium also includes alluvium (<20 ft thick?) incised into the uppermost portions of the Logan Hill Formation. Age of unit Qa is 1,650 ±30 years before present (radiocarbon age site GD01, Appendix C), and other ages are not constrained.

Qaf **Alluvial fines, silt**—Fine alluvial overbank material near the main alluvial deposits that lacks meandering channel morphologic texture; tanish gray to light brown color; fresh to lightly weathered; not compacted and not cemented; silt to very fine sand; rounding unclear; well sorted(?); unit thickness is inferred to be less than 5 ft; restricted to the southern half of the map area, in the Chehalis River floodplain, where it drapes over poorly sorted floodplain alluvium (unit Qa) of the Chehalis River and below higher elevation deposits (unit Qoa or bedrock). Distinction from other alluvial units is primarily textural, based on lidar analysis.

PLEISTOCENE GLACIAL DEPOSITS

Vashon Drift of the Fraser Glaciation

Qgog **Vashon recessional outwash, gravel**—Northern-sourced pebble to cobble gravel with a coarse sandy matrix; clast rock types are northern sourced; tan, red-orange where iron stained; lightly weathered, with most weathering rinds less than 2 mm thick; loose; may be lightly cemented; cobble- to pebble-size clasts with sandy matrix; well-rounded to subrounded; moderately sorted; massive to bedded with localized interbeds or lenses of sand with little to no silt or clay; lithic clasts are appreciably northern-sourced and include about 57% extrusive volcanic rocks, 17% granitic rock types, 15% metamorphic rocks, 4% of both gabbro and chert, and 3% sedimentary rocks from three clast counts (Fig. 1, and Table DS10); the unit makes up most of the Waunch Prairie along the Skookumchuck River and Fords Prairie to the north of the Chehalis River, both in the northern half of the map area, and found locally along the eastern margin of the Chehalis River valley. Discrete coloring of the DEM (1 foot-interval color ramp) shows conspicuous fan-like depositional pattern used to delineate the outwash deposit. This pattern of outwash gravels suggests glaciofluvial processes from meltwater flowing south and west from ice north of the Centralia quadrangle. The southern maximum ice extent of the Puget Lobe is mapped in the adjacent Violet Prairie quadrangle to the north (Polenz and others, 2018). The unit is well exposed at clast count site C03.

Pre-Vashon Glacial Deposits

Qapolh **Logan Hill Formation (Pleistocene)**—Cascade-sourced, pebbles and cobbles in a matrix of sand, silt, and clay; multicolored, yellowish light gray, grayish brown, dark brown, rusty orange, and reddish brown, previously described as "ferretto" colored by Bretz (1913); strongly to severely weathered to the point of being able to cut clasts with a knife or break them open by hand; weathering rind thicknesses are far greater than 2 mm with many exposures entirely weathered to clay; slightly to very compact; weakly cemented; grain size varies widely from cobbles (<20 cm) to silt; on average cobble- and pebble-sized clasts in a medium-grained sand matrix; rounded to subangular, with clasts commonly bullet-shaped or oblate and less commonly equant and disc-shaped; moderately to poorly sorted; massive; lithic clasts are dominantly Cascade-sourced and include about 68% extrusive volcanic rocks, 13% quartz and chert, 8%, gabbro rock types, 7% sedimentary rocks, and 4% metamorphic rocks from 16 clast counts (Figs. 1 and 2; Table DS10); includes sand-sized grains composed of monocrystalline and polycrystalline quartz, with rare mica; <250 ft thick. Deposit is widespread and most extensive in the southern half of the map area, and patchy to uncertain in the northern half. The unit mantles topography and unconformably overlies bedrock. The rocks are interpreted to be part of a poorly understood, Pleistocene (or younger) glaciofluvial environment. Based on weathering, the unit is older than the Double Bluff Formation (Dethier and Bethel, 1981), and therefore, pre-Vashon. U-Pb analysis of detrital zircons yields a maximum depositional age interpreted at ≤1.86 ±0.19 Ma (GD06, youngest single grain, Fig. B5, Table DS6). Unit is well exposed at age site GD06 (Fig. 3).

Tertiary Volcanic and Sedimentary Bedrock

Mcw **Wilkes Formation (Miocene)**—Pebbly sandstone to sandy conglomerate; light grey to medium brown with occasional olive tint; sands are weakly to moderately cemented; very coarse- to fine-grained sand matrix with pebbles and cobbles; subangular to subrounded; moderately to well sorted; where observed, pebbly conglomerate is subangular to rounded, moderately to strongly weathered, similar to the Logan Hill Formation, but less severely weathered; bedding is massive to cross laminated to undulatory, encompassing lenses of coarser material; heterolithic clasts include basalt to andesite (10–80%, 0.2–10 mm), quartzite (10–17%, as low as 3%, 0.2–0.5 mm), with trace sandstone, siltstone, and chert; minerals include quartz (5–20%, <0.2 mm), potassium feldspar (sanidine?)(2–8%, 0.25–0.5 mm), plagioclase (<1–3%, <0.2 mm), mica (muscovite and biotite)(<1–2%, 0.2–0.5 mm), and trace chalcedony and pyroxene. Overall, a QFL ternary shows 20–50% quartz, 5–35% feldspar, and 30–70% lithics; in general L > Q >> F. Unit thickness is poorly constrained to greater than 200 ft; sparsely and irregularly distributed, and best exposed in the northern half of the quadrangle. Deposits are terrestrial to nearshore (nonmarine), formerly named the Tertiary nonmarine unit by Snavely and others (1958).

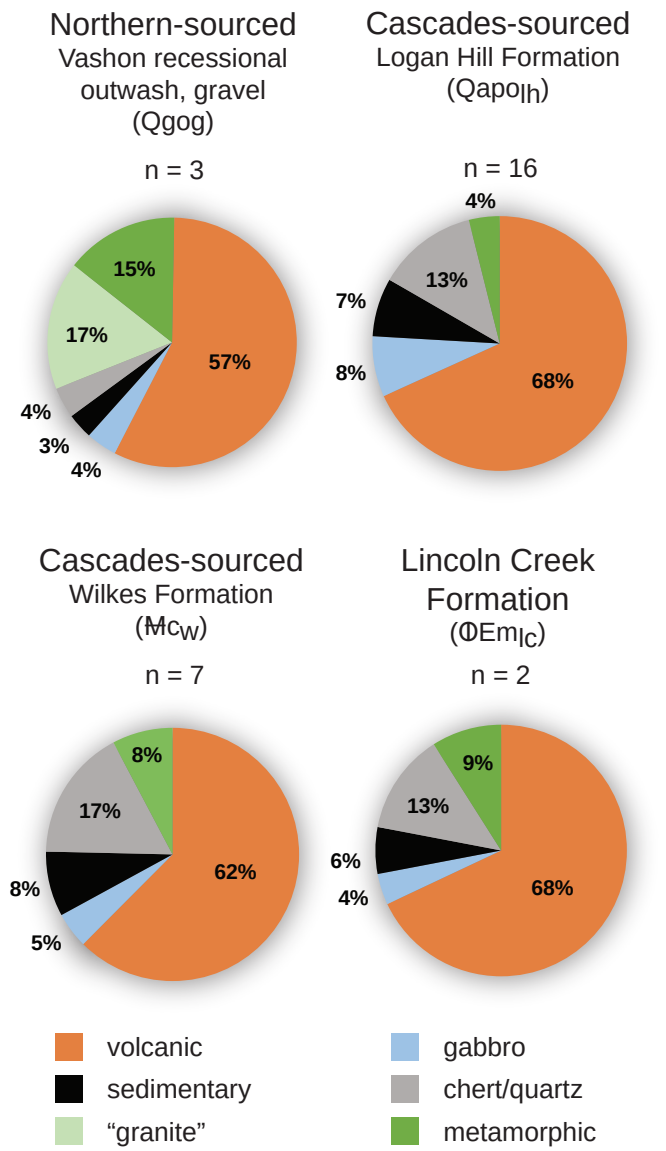

Figure 1. Clast compositional charts . Pie charts showing lithological composition of clasts from unlithified units (Qgog and Qapo$_{lh}$) and bedrock units (ꝶc$_{w}$ and ΦEm$_{lc}$). Charts are constructed from averages of (n) clast counts in each sample group (see Table DS2 for details). A clear compositional distinction is seen between the Cascades-sourced pre-Vashon Logan Hill Formation and northern-sourced Vashon outwash unit Qgog. The latter contains an appreciable proportion of granitic and metamorphic rock clasts.

Contact relationships show relict, northwest-southeast oriented, channel(?) geometries flanked by exposures of Lincoln Creek Formation. At age site GD08, a paleo-erosional surface shows Wilkes Formation rocks lying unconformably above the less heterolithic Lincoln Creek Formation. Dip directions are typically different by as much as 90° from underlying attitudes in the Lincoln Creek Formation, further suggesting a possible angular unconformity. The Logan Hill Formation unconformably overlies this unit at age site GD07 with a distinct contact. Two U-Pb analyses on youngest single detrital zircon grains yield a maximum depositional age interpreted at ≤8.57 ±0.92 Ma (GD08, Fig. B3) and ≤7.54 ±1.04 Ma (GD07, Fig. B4), and constrain the age of the unit to Late(?) Miocene, which correlates with the age range of the Wilkes Formation (Roberts, 1958)(see Tables DS4 and DS5). The unit is well exposed at age sites GD07, GD08, and clast count site C08 (Fig. 4).

ꝶvb$_{gr}$ **Grande Ronde Basalt of Columbia River Basalt Group (Miocene)**—Aphanitic basalt to basaltic andesite; bluish medium gray to dark gray when fresh, weathered to orangeish brown and dark yellowish brown; well indurated where fresh, moderately indurated where weathered; aphanitic; euhedral to subhedral; well sorted; no pillows observed, flow-top autobreccia common; microphenocrysts include plagioclase (40–>70%, <0.3–0.6 mm, euhedral laths, pilotaxitic/felty), olivine (1–10%, <0.4–0.6 mm, equant subhedral, moderately altered with >40% altered to iddingsite), and rare clinopyroxene (augite?)(1%, <0.2 mm). Geochemical analyses (50.9–55.5 wt. % SiO_2, 3.0–3.9 wt. % MgO) (Tables DS7 and DS8); the unit is less than ~100 ft thick; sparsely distributed but best exposed on the west flank of Newaukum Hill in the southwestern corner of the map area; subaerial to submarine(?) eruptive environment; contact relationships are poor, and the unit is unconformably overlain by the Logan Hill Formation. The basal contact of the Grande Ronde Basalt is not exposed in the map area, but the basalt interfingers with the Miocene Astoria Formation in areas mapped to the west (Snavely and others, 1958; Pease and Hoover, 1957). Major and trace element geochemistry show basalt to basaltic andesite compositions that overlap and correlate with geochemical analyses of the Grande Ronde Basalt. Geochemistry shows that MgO is too low for the Sentinel Bluffs Member and therefore suggests that this unit lies stratigraphically below that member (J. Wolff, Washington State Univ., written commun., 2018). Paleomagnetic analyses of this unit exhibit consistent reverse magnetization based on 12 hand specimens measured using a portable fluxgate magnetometer. These readings may correspond with one of the reversely magnetized polarity intervals of the Grande Ronde Basalt (Riedel and Tolan, 2013). The age of the unit is poorly constrained to middle to late Miocene (Armentrout and others, 1983; Reidel and Tolan, 2013; Reidel and others, 2013) by major and trace element compositions characteristic of the Grande Ronde Basalt of the Columbia River Basalt Group (geochemistry sites G02, G44, and G47)(Figs. 9A–D) (GeoRoc database at http://georoc.mpch-mainz.gwdg.de/georoc/). The unit is well exposed at geochemistry site G43.

ꝶma? **Astoria(?) Formation (Miocene)(cross section only)**—marine to continental sedimentary rocks that interfinger with Grande Ronde Basalt (Pease and Hoover, 1957; Snavely and others, 1958). This unit is exposed west of the map area (Pease and Hoover, 1957; Snavely and others, 1958). The unit unconformably overlies the Lincoln Creek Formation and is inferred to be less than ~1,000 ft thick in the Centralia–Chehalis area.

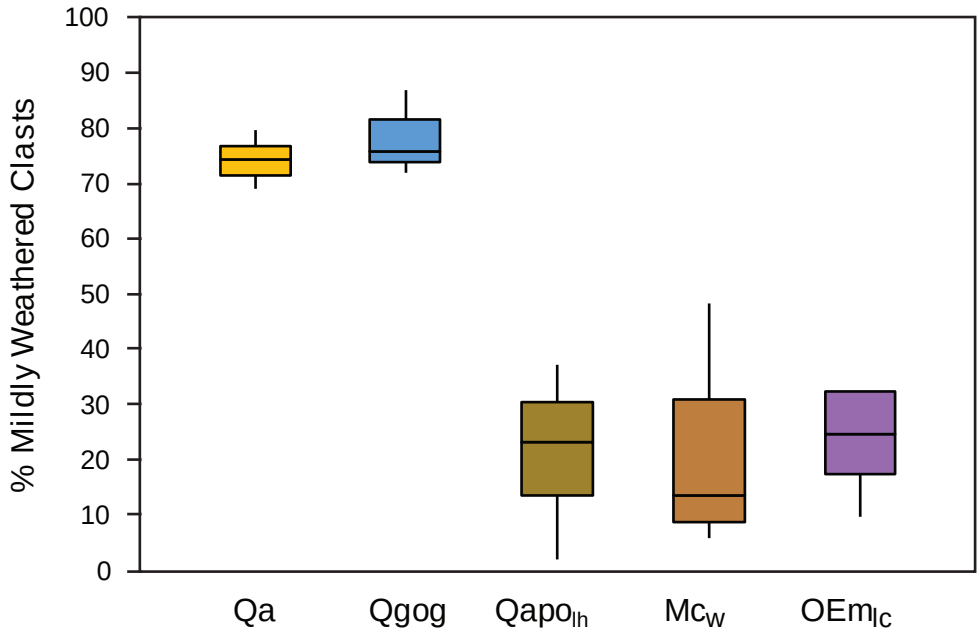

Figure 2. Weathering of clasts . Box-and-whisker plots show ranges of clast weathering for Quaternary and Tertiary bedrock units. Older units lack significant amounts of mildly weathered clasts (not controlled for clast type). However, clasts from these older units are generally more weathered than those from alluvial and Vashon units (see Table DS2 for details).

ΦEm$_{lc}$ **Lincoln Creek Formation, undivided (latest Eocene to Oligocene)**—Very fine sand to siltstone with rare medium sandstone; dull ivory to pale gray when fresh, weathers buff tan to orangeish brown; weakly to moderately indurated; very fine-grained sand, silt, and rare medium-grained sand; subangular to subrounded; moderately to well sorted; massive with rare planar bedding. Sedimentary structures are difficult to discern due to pervasive hackly and spheroidal weathering, which is somewhat diagnostic of the unit and can be easily confused with bedding at localities with limited exposure. Liesegang banding (iron-oxidation) is not uncommon and fracture surfaces often weather to a dark brownish red. Mineral percentages are a combination of the percentages from the tuffaceous and volcaniclastic members (see following unit descriptions), but generally tuffaceous(?), poor in mica (<2%), and containing volcaniclastic fragments including appreciable glass shards with lesser basalt and ash. Also contains trace glauconitic pellets (coprolites), and very rare carbonaceous material with associated pyrite. Unit thickness is greater than 2,000 ft. The undivided unit is mapped sparsely in the map area, where the distinction between the sub-units is unclear or where a poorly understood area likely contains a variant of the Lincoln Creek Formation. Variants of the Lincoln Creek Formation include the following members: tuffaceous, volcaniclastic, and basaltic sedimentary members as well as lithic tuff and lapilli tuff pyroclastic members. Deposits are marine to nearshore and conformably(?) overlie the late Eocene Skookumchuck Formation in the map area (Armentrout and others, 1983; Armentrout, 1987; Wells and others, 2014). Essentially, this undivided unit groups the tuffaceous siltstone, volcaniclastic siltstone, and basaltic sandstone sub-units of the Lincoln Creek Formation. Age ranges from latest Eocene to Oligocene (Snavely and others, 1958; Armentrout and others, 1983; Prothero and Armentrout, 1985; Wells and others, 2014). The unit is well exposed at significant site S05 (Fig. 5). Divided into:

Figure 3. Photograph of U-Pb age site GD06 showing multi-colored and severely weathered Logan Hill Formation along Centralia Alpha Rd east of Centralia, WA on Logan Hill (shovel for scale).

ΦEm$_{lct}$ **Tuffaceous siltstone**—Tuffaceous siltstone; ivory to pale gray when fresh, weathers tan; weakly to moderately indurated; subrounded to subangular; silt to very fine-grained sand;

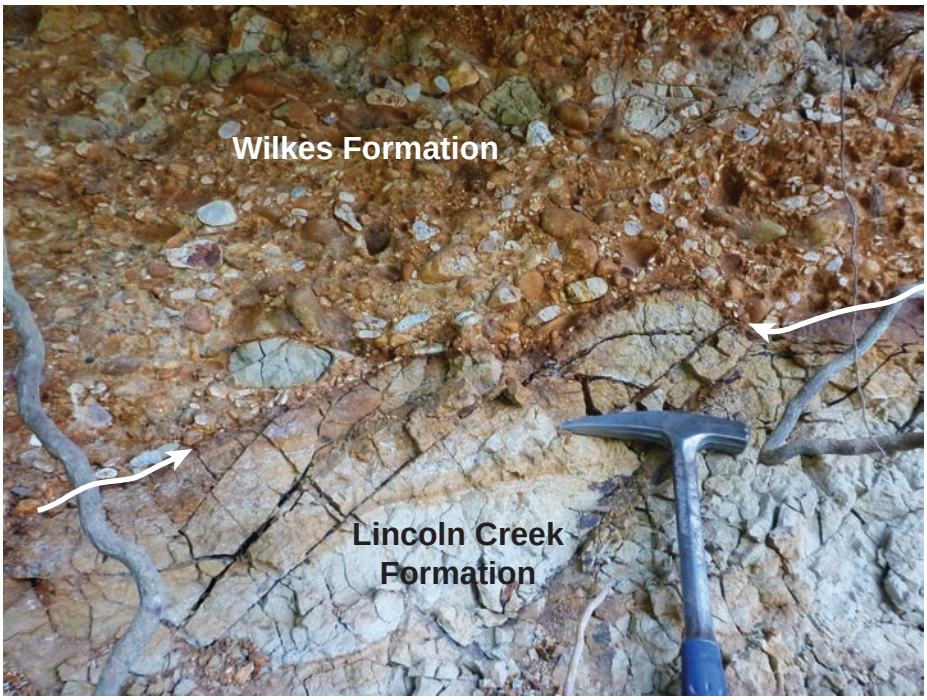

Figure 4. Photograph of U-Pb age site GD08 showing irregular, paleoerosional surface (unconformity indicated with white arrows) of volcaniclastic siltstone of the Lincoln Creek Formation, which is unconformably overlain by sandy conglomerate of the Wilkes Formation (hammer for scale).

well sorted; massive with lesser hackly and spheroidal weathering; variably composed of volcanic ash (as high as 95% with <2% total microphenocrysts entirely of plagioclase <0.1 mm), plagioclase (10–40%, 0.07–0.4 mm), quartz (10–40%, <0.07 mm), mica (biotite and muscovite)(<2%, <0.2 mm), glauconitic pellets (coprolites)(~1%, 0.1–0.2 mm), trace potassium feldspar (<<1%, <0.2 mm), and rare lithic fragments (volcanic rocks)(0–5%, 1.0–2.0 mm); the unit thickness is greater than 400 ft; mapped in upsection areas in south-central and northern portions of the map area; deposits are marine (to nearshore); deposits grade and interfinger with the volcaniclastic member of the Lincoln Creek Formation. The unit also irregularly interfingers with a glauconite-rich, fine sandstone in the map area. The mineral content of the glauconitic sandstone includes plagioclase (10–40%, 0.1–0.4 mm), potassium feldspar (5–10%, <0.05 mm), glauconitic pellets (coprolites)(10–20%, 0.4–0.6 mm), quartz (>5%, 0.2 mm), mica (biotite and muscovite) (1–3%, 0.5 mm), lithic fragments (quartzite) (1–3%, 0.2 mm). Glauconitic sandstone may exist at multiple stratigraphic intervals within the Lincoln Creek Formation including the basal and upper sections. The unit contains sparse marine macro and microfossils. The unit is well exposed at sites G22, X09, and X10.

ⓅEvtlcc **Lithic tuff**—poorly welded, lithic dacite tuff; light bluish gray to pinkish gray; moderately to well indurated; medium- to fine-grained particles; subangular (subhedral); poorly sorted (lithic fragments from 0.5–5.0 mm); massive, and exhibits partially developed microscopic fiammé, suggesting poor welding; composition includes lithic fragments (volcanic rocks)(<4%, <1.0 mm), pumice (<3%, as high as 10%, <0.8 mm). Total phenocrysts (<6%): clear white plagioclase (<3%, as high as 10–20%, 0.3–1.4 mm), potassium feldspar(?) (1%, amorphous sodium cobaltinitrite staining), and black biotite(?) (2%, 1.0–2.0 mm). Geochemistry classifies this unit as calc-alkaline dacite and is more silica-rich than Ohanapecosh Formation type localities farther east (Polivka, 1984; Shultz, 1988; Phillips and others 1989). Thickness is less than 200 ft. The unit is only exposed at one locality in the map area (age site GD09) and is inferred to pinch out to the northwest and southeast. Likely subaqueous deposition(?) in a shallow marine environment(?). Poorly exposed contact relationships weakly suggest that this unit serves as a stratigraphic marker between the volcaniclastic members below and tuffaceous members above. Outcrop description is similar to the Wildcat Creek facies of the Ohanapecosh Formation (Shultz, 1988). U-Pb analysis of zircon crystals yields a maximum depositional age peak interpreted at ≤30.58 ±0.35 Ma (GD09, “single-event” average age of youngest population, Fig. B2, Table DS3). The unit is well exposed at age site GD09.

ⓅEmlcv **Volcaniclastic siltstone**—Volcaniclastic, very fine sandstone to siltstone; commonly tan to buff, but bluish medium gray when fresh, weathers tan to orangeish brown; weakly to

moderately indurated; very fine-grained sand to silt, rarely fine sand; subangular; moderately to well sorted; massive with rare planar bedding. Sedimentary structures are difficult to discern due to pervasive hackly and spheroidal weathering, which is somewhat diagnostic of the unit and can be easily and erroneously confused with bedding at various scales (Fig. 5). Fracture surfaces often weather to a dark brownish red. Mineral content includes plagioclase (>5–13%, as high as 30%, 0.05–0.15 mm, as large as 0.35 mm), quartz (3–10%, as high as 15%, 0.08–0.2 mm), black glass shards (3–10%, <0.1 mm, angular to subangular), mica (muscovite ≥ biotite)(<1–2%, 0.1–0.2 mm), potassium feldspar (0–7% typically <1–2%, 0.18–0.25 mm), trace glauconitic pellets (coprolite)(0–5%, <0.15 mm), minor pyroxene (2–3%, 0.05–0.07 mm), rare hornblende, and rare lithic fragments (quartzite >> basalt + andesite ≥ pumice). Overall, a QFL ternary shows 5–45% quartz, 40–80% feldspar, and 1–15% lithics; in general F ≥ Q >> L, with very rare basaltic lithic fragments. Unit thickness is greater than 1,800 ft. The unit is mapped extensively, especially in the central map area; deposits are marine (lower shoreface to offshore) and conformably(?) overlie the late Eocene Skookumchuck Formation (Armentrout and others, 1983; Armentrout, 1987). Contact relationships show that the unit serves as an erosional surface upon which the Miocene Wilkes Formation was deposited. Upsection to the west and southwest, the unit grades and is synchronous with and interfingers with the tuffaceous siltstone member of the Lincoln Creek Formation. The volcaniclastic siltstone described here serves as an intermediate lithology between the western tuffaceous siltstone and the eastern basaltic sandstone (Snavely and others, 1958). This gradation reflects both westward-deepening depositional environments and overall basin subsidence and consequent marine transgression (Armentrout, 1987). The volcaniclastic member effectively splits the previously described basaltic sandstone of Snavely and others (1958) into a basalt-poor siltstone (common in the map area) and a basalt-rich sandstone (uncommon and poorly exposed in the map area, likely more common farther to the east). The unit is broadly folded into wide, gentle synclines. It is commonly fossiliferous and contains marine macrofauna fossils and microfossils throughout, which generally indicates a shallow water paleoenvironment. Diagnostically, this unit has appreciable black glass shards, slightly less mica, generally a finer grain size, slightly more induration, and is more commonly spheroidally-weathered compared to the similar-looking Skookumchuck Formation. The unit is well exposed at age and geochemistry sites GD14, GD17, GD18, G34, G35, G40, and at the cliff underlying age site GD08.

ΦEm$_{lcb}$ **Basaltic sandstone**—Basaltic lithic fragment-rich, coarse sandstone; medium brown overall with multi-colored lithic fragments of light brown, light orange, light red, maroon, red, pinkish brown, and light to dark gray,

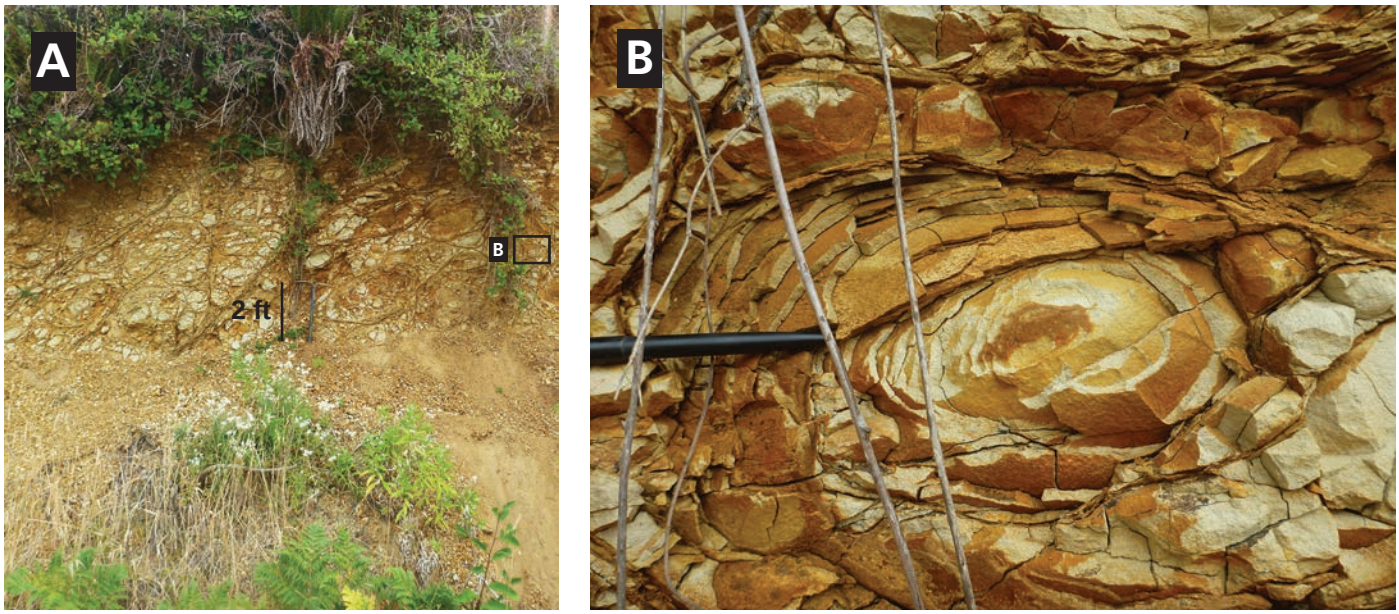

Figure 5. Photographs of significant site S05 showing common hackly and spheroidally weathered Lincoln Creek Formation. Formation is generally massive where fresh. Scale indicated by ~2 foot geopick and pen. Locality is slightly outside of the map area, ~1,100 ft to the east of the eastern map boundary, and ~3,110 ft to the northeast of significant site S02.

weathers to orangeish light brown; mildly indurated; moderately cemented; medium- to very coarse-grained sand to granules; subangular; poorly to moderately sorted; massive and varies from matrix- to clast-supported, though matrix-support is more common; dominantly composed of lithic fragments including, in order of decreasing abundance: scoria, aphanitic basalt with <0.3 mm vesicles or empty phenocryst sites, pumice, tuff(?), and siltstone; unit thickness is greater than 100 ft; unit is irregularly distributed in small areas in the western and northwestern portions of the map area within the Lincoln Creek Formation; depositional environment is inferred to be marine to near-shore equivalent of the farther offshore and possibly synchronous tuffaceous siltstone sub-unit of the Lincoln Creek Formation; the unit conformably(?) overlies unit ΦEvc?, which contains porphyritic basaltic andesite (geochemistry site G52), and also underlies and likely interfingers with other sub-units of the Lincoln Creek Formation, particularly the tuffaceous siltstone sub-unit in the western map area; the unit is possibly better exposed and more common to the east of the Centralia quadrangle where paleogeography is inferred to be a shallower marine depositional environment (Snavely and others, 1958); age is inferred to be latest Eocene or earliest Oligocene.

ΦEvt$_{lcp}$ **Lapilli tuff**—Unwelded, lapilli dacite ash flow tuff; light bluish gray, weathers to dark gray or medium brown, heavily saprolitized in some areas; moderately indurated; ash matrix is smaller than silt size, and lapilli pumice are up to 5.0 mm in diameter; angular to subangular; poorly sorted; massive with possible pyroclastic foliation (subtle layering); dominantly ash with total microphenocrysts (<2%): plagioclase (~1–2%, 0.10–0.35 mm). Also contains lapilli pumice (~10%, 0.5–5.0 mm) and trace volcanic lithic fragments (palagonitized and clayified basalt-andesite)(0.3–1.0mm). Geochemistry classifies this unit as calc-alkaline dacite and is more silica-rich than Ohanapecosh Formation type localities farther east (Polivka, 1984; Shultz, 1988; Phillips and others 1989). Unit thickness is less than 500 ft and likely thinner due to interfingering with the volcaniclastic siltstone member. The unit is sparsely distributed across the map area. The pyroclastic texture is consistent with a water-lain deposition or subaqueous eruptive paleoenvironment (shallow marine). Contact relationships place the unit consistently near the bottom of the Lincoln Creek Formation in the map area, interfingering with the volcaniclastic siltstone member, and directly overlying the Skookumchuck Formation, where it serves as a useful marker horizon. The unit is not necessarily located at the bottom of the Lincoln Creek Formation outside of the map area. The outcrop description is similar to the Wildcat Creek facies of the Ohanapecosh Formation (Shultz, 1988), but with smaller lapilli clasts. U-Pb analysis of zircon crystals yields a maximum depositional age peak interpreted at ≤36.70 ±0.32 Ma (age site GD10, "single-event" average age of youngest population, Fig. B1, Table DS6). Unit is well exposed at significant site S06 and age site GD10 (Fig. 6).

ΦEvc? **Volcaniclastic breccia(?)**—Dacitic volcaniclastic breccia(?); dark gray to dark brown, weathering reddish brown; very well indurated; medium-grained; subangular/subhedral; mineral content includes plagioclase (>8%, <4.0 mm) and trace potassium feldspar. Depositional environment is possibly a distal volcanic facies. Geochemistry classifies this unit as calc-alkaline dacite and the rocks are more silica-rich than Ohanapecosh Formation type localities farther east (Polivka, 1984; Shultz, 1988; Phillips and others 1989). The outcrop description is similar to the Timberwolf Mountain facies of the Ohanapecosh Formation (Shultz, 1988). Unit thickness is unknown (>20 ft?). The unit is exposed in the map area in a large, poorly exposed block within a landslide (unit Qls)(geochemistry site G55) and possibly exposed near the base of the tuffaceous siltstone of the Lincoln Creek Formation (unit ΦEm$_{lct}$) in the western portion of the map area (geochemistry site G52). Within the large landslide block, the unit directly underlies the volcaniclastic siltstone member of the Lincoln Creek Formation. The age is poorly constrained to late Eocene to Oligocene from its stratigraphic relationship with the Lincoln Creek Formation. The unit is well exposed at geochemistry sites G52 and G55.

En$_{sk}$ **Skookumchuck Formation, undivided (middle to late Eocene)**—Micaceous and tuffaceous(?) sandstone; feldspathic sandstone with abundant mica; light gray to medium brown, weathers white, tan, medium brown, and yellowish brown with very common orangeish brown liesegang banding. Where fresh and carbonaceous, color is rich bluish medium gray with dark gray to black coal beds with a sulfurous smell; generally highly friable, weakly indurated and mildly compacted; mildly to moderately indurated where fresh; medium- to fine-grained sand, rarely coarse-grained; subrounded to subangular; moderately to well-sorted; medium bedded to thinly laminated (parallel) with common mica-rich lamina (compare Fossen and others, 2007), or massive, common trough crossbedding. Iron staining common along bedding planes, joints, and millimeter-scale deformation bands(?) (Fig. 7); mineral content includes potassium feldspar (sanidine >> microcline) (7–12%, as high as 20%, 0.25–0.5 mm), plagioclase (3–15%, typically <8%, as high as 40%, 0.06–0.5 mm,

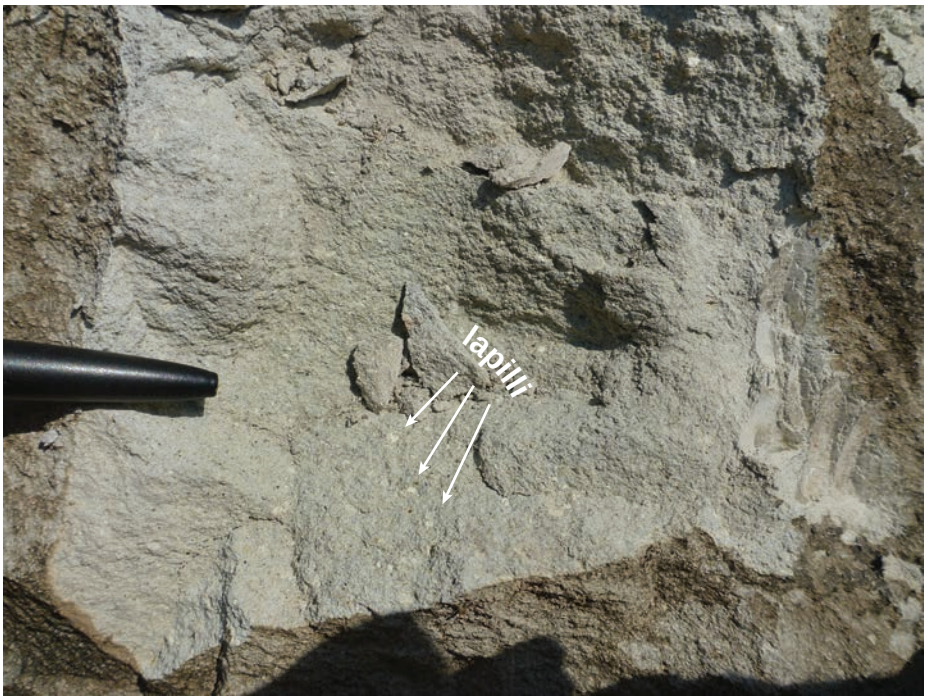

Figure 6. Photograph of significant site S06 (pen for scale) showing lapilli ash flow tuff (unit ΦEvt_{lcp}), which is interpreted to have been deposited in a subaqueous setting near the base of the Lincoln Creek Formation in the Centralia quadrangle. This lithology conformably overlies the Skookumchuck Formation in the map area but may not necessarily be at the bottom of the Lincoln Creek Formation outside of the map area (see Prothero and Armentrout, 1985). The unit is likely correlative with the Wildcat Creek facies of the Ohanapecosh Formation described by Shultz (1988). There are more lapilli in the photograph than indicated. Maximum depositional age from U-Pb analysis of detrital zircons shows a single event age of ≤36.70 ±0.32 Ma (site GD10) from this unit along the railroad section in the northern portion of the quadrangle.

commonly 0.2 mm), quartz (typically 5–10%, ranging from 3–35%, 0.4–0.6 mm), mica (muscovite > biotite) (1–6%, 0.05–0.4 mm, biotite > muscovite where mica percentage is greater), lithic fragments (quartzite, chert) (4–7%, as high as 20%, 0.3–0.5 mm), trace pyroxene (augite?)(<1%, <0.15 mm), and rare hornblende. Overall, a QFL ternary shows 5–45% quartz, 30–70% feldspar, and 1–25% lithics; in general F > Q >> L. Unit thickness is at least 2,000 ft, but is approximately 3,500 ft in most locations. The unit is found extensively throughout the map area, especially in the central and northern portions, and constitutes about half of the bedrock outcrops in the entire quadrangle. The unit contains several coal beds, and has been studied and mined as a coal resource for more than 100 years (Snavely and others, 1958; Flores and Johnson, 1995). Its depositional environment was likely nearshore marine (foreshore to upper shoreface) within a broader deltaic setting of distributary channels and interdistributary interfluves (Buckovic, 1979; Flores and Johnson, 1995). The basal contact is not exposed in the map area, and the upper contact may be locally conformable with the Lincoln Creek Formation. The unit is folded, faulted, and locally fossiliferous. *Turritella uvasana washingtoniana* (Weaver and Palmer, 1922) were identified at biostratigraphic age site GD38, and had previously been recorded only from the Cowlitz Formation. Compared to the similar-looking Lincoln Creek Formation, the unit diagnostically has coal beds, lacks fine black glass shards, has slightly more mica, has a larger grain size, is poorly indurated, and is less commonly spheroidally-weathered. Age is constrained to the late Eocene (Snavely and others, 1958; Armentrout and others, 1983). Subdivided into:

En_{skc} **Carbonaceous sandstone**—Micaceous and carbonaceous sandstone. Essentially texturally and compositionally equivalent to the undivided Skookumchuck Formation and contains coal beds as mapped by Snavely and others (1958). Coal rank is lignite to sub-bituminous B, and most of it is subbituminous C (Snavely and others, 1958). Unit is well exposed at geochemistry and age sites G15–16, GD22, GD33, and GD36–38 (Fig. 8).

Within the carbonaceous sandstone, some coal beds contain ash partings (tonsteins) that are late Eocene (40–41.5 Ma, K-Ar, unpublished locations, D. M. Triplehorn, Univ. of Alaska, written commun., 1991, as cited in Flores and Johnson, 1995). The tonstein observed in the map area is pale brown to pale gray with a brownish orange coating of iron oxidation, but only mild to moderate weathering. It is putrid to sour smelling. The tonstein is well compacted and moderately indurated. It is very fine-grained with angular-euhedral clasts. It is well sorted and thinly bedded with parallel layers that form excellent surfaces to take bedding attitudes. The tonstein is composed of 90% ash with feldspar (plagioclase >> alkali feldspar) (<7%, <0.12 mm), pyroxene (1%, <0.09 mm), and trace carbonaceous material; tonstein thickness is ~5 cm (~2 in.). The sole exposure in the map area is too small to map and restricted to a coal bed (Upper Thompson or Big Dirty coal bed?) in the northern portion of the map area along the railroad tracks. The tonstein was deposited on terrestrial coal surfaces. The outcrop had <1 gallon per minute of steady groundwater seepage. The age is

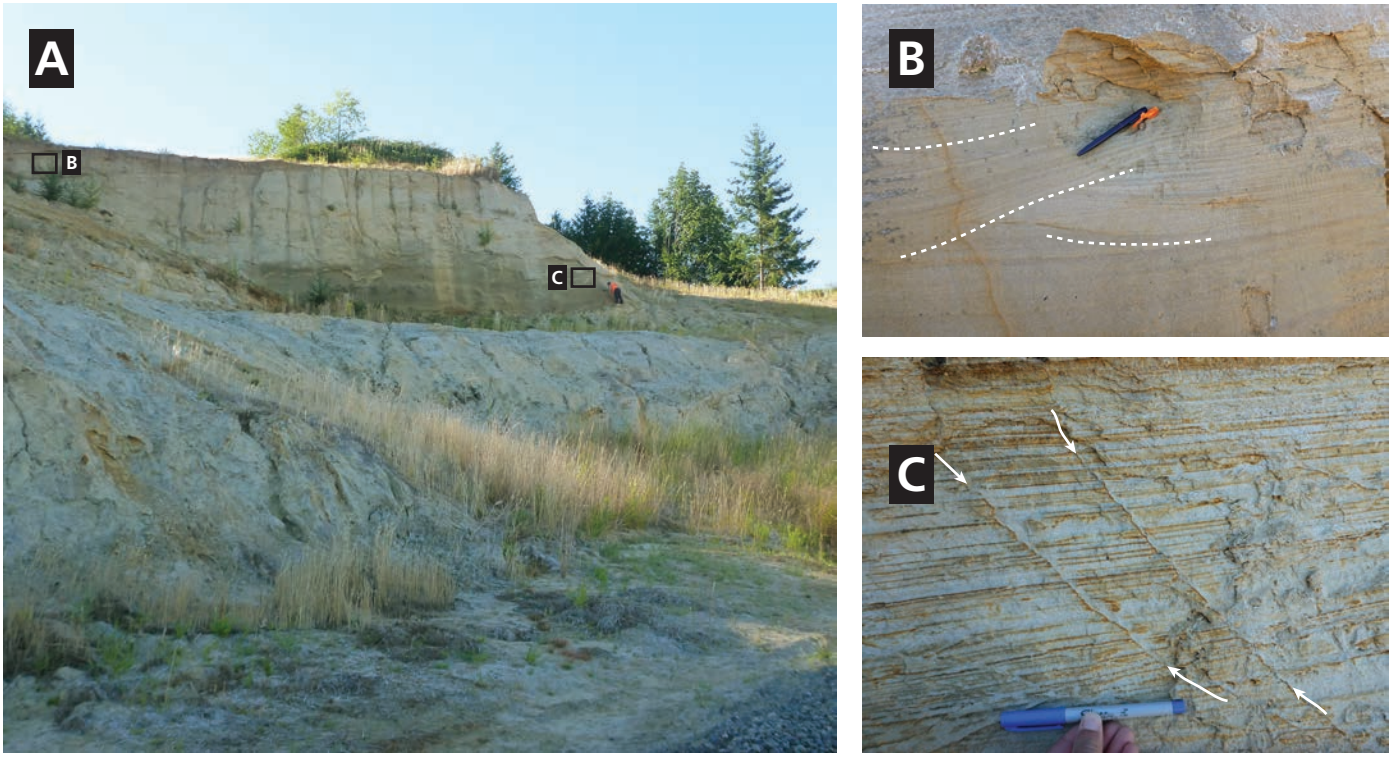

Figure 7. Photograph of paleomagnetic site M02 showing cliff exposure of Skookumchuck Formation (A) along the axis of the Chehalis anticline. Trough crossbedding (B) and deformation bands (C) are common. Brown liesegang banding follows laminations of the micaceous sandstone.

poorly constrained to late Eocene and is the same location as fossil site GD32.

En_{skg} **Glauconitic sandstone**—Glauconitic, micaceous sandstone; tan to yellowish brown, moderately weathered; friable and poorly indurated; medium-grained sand; subangular to subrounded; well sorted; mineral content includes quartz (3–10%,<0.2 mm), plagioclase (3–10%, <0.2 mm), mica (muscovite > biotite) (~5%, 0.2–0.3 mm), potassium feldspar (<4%, <0.1 mm), glauconitic pellets (coprolites) (<3%, <0.3 mm), lithic fragments (chert > quartzite)(<2%, <0.25 mm). Overall, a QFL ternary shows 35% quartz, 55% feldspar, and 1–10% lithics; in general F > Q >> L; unit is approximately 100–350 ft thick; irregularly distributed, located in the core of the Chehalis anticline at lower stratigraphic levels of the Skookumchuck Formation; glauconitic pellets look very similar to basaltic lithic fragments. Pellets are highly fragile, with a "breadcrust" texture, and segmented like a colon. Pea green to translucent brown in thin section. Unit is well exposed at age site GD21.

ΦEvc_n **Northcraft Formation (Oligocene–Eocene)(cross section only)**—Basalt to andesite, volcaniclastic debris flows, and volcanic breccias of the Northcraft Formation. The unit crops out in the northern portion of the Violet Prairie quadrangle, the adjacent quadrangle to the north (Polenz and others, 2018). Given the distance from the inferred Northcraft eruptive center near Morton, WA (Buckovic, 1979), lateral continuity is inferred to be variable and thickness is inferred to be minimal (<250 ft) in the map area. The Northcraft Formation conformably overlies and interfingers with the McIntosh Formation and locally unconformably overlies the Skookumchuck Formation (Snavely and others, 1958).

Em_m **McIntosh Formation (Eocene)(cross section only)**—Marine sandstone with volcanic and pyroclastic interlayers. The unit crops out in quadrangles to the north (Violet Prairie and Littlerock; Polenz and others, 2017, 2018). The McIntosh Formation in Cross Section A–A′ is undivided, whereas other quadrangles (for example, Violet Prairie and Littlerock) specify an upper member, unit Em_m, and Pease and Hoover (1957) recognize a lower member, unit Tml. Thickness is poorly constrained in the quadrangle and inferred to be ~3,000 ft (Cross Section A–A′). Other studies report varying thicknesses for the McIntosh Formation including >2,500 ft in the Violet Prairie quadrangle (Polenz and others, 2018) and ~4,000 ft (Snavely and others, 1951). The McIntosh Formation interfingers with the Northcraft Formation and has gradational and interfingering(?) contacts with the Skookumchuck Formation farther west of the map area (Pease and Hoover, 1957; Snavely and others, 1958).

Evc **Crescent Formation (Eocene)(cross section only)**—Submarine basalt and volcanic rocks associated with the Siletzia terrane underlie the Chehalis–Centralia area (Finn, 1990; Trehu and others, 1994). Unit includes thin sedimentary interbeds. The unit crops

out in the Black Hills of the Littlerock quadrangle (Polenz and others, 2018) and the Doty Hills (Pease and Hoover, 1957). The unit is several miles thick, and its base is not exposed.

GEOCHEMISTRY RESULTS

Volcanic Geochemistry

Nine igneous hand samples from the Centralia quadrangle were selected for whole-rock chemical analysis (Tables DS7 and DS8): three Columbia River Basalt samples, three tuffs from the Lincoln Creek Formation, and three volcaniclastic rocks that could not be confidently assigned to a formation in the field.

Compositions of the Columbia River Basalt samples (50.9–55.5 wt. % SiO_2, 3.0–3.9 wt.% MgO) are consistent with the composition of the Grande Ronde member (avg. = 54.3 wt. % SiO_2, 4.8 wt. % MgO)(Figs. 9A, B, and C). The geochemical data are insufficient to characterize the exact flow found in the map area, but the unit is likely older than the Sentinel Bluffs Member (J. Wolff, written commun., 2018). Geochemistry site G52 (56.4 wt. % SiO_2, 3.8 wt. % MgO) is similar in both major and trace element composition to the Ohanapecosh Formation data (Figs. 9A–D) and is likely that lithology, heavily derived from those lavas, or correlative with volcanism of that age.

The three Lincoln Creek Formation tuffs (sites G21, G26, and G01), volcanic breccia (site G55), and a sample from site G52 classify as calc-alkaline volcanic rocks (Figures 9A and B), where most are dacites and the sample from site G52 is basaltic andesite. These five samples have very similar patterns on rare earth element plots (Fig. 9C) and MORB-normalized spider diagrams (Fig. 9D), suggesting they share a common origin. Their enrichments in large ion lithophile elements (K, Rb, Ba) and depletions in high field strength elements (Ta, Nb) on the spider diagram (Fig. 9D) and their calc-alkaline affinities are diagnostic of a subduction zone setting. Taken together, these chemical traits and the U-Pb age of ~36 Ma on a sample from site G26 indicate these dacites are products of early Cascade arc volcanism and may be correlative with the Ohanapecosh Formation. The dacites in the map area are higher in silica than any published Ohanapecosh Formation analyses (Fig. 9E), but the available Ohanapecosh Formation dataset is limited to 18 major element analyses and probably does not reflect the full range of compositions present within that formation (Polivka, 1984; Shultz, 1988; Phillips and others, 1989). The Centralia quadrangle dacite samples are more silica-rich than the Goble and Northcraft volcanic rocks, and, with that higher silicic composition, they plot as a likely extension of the Ohanapecosh Formation data array, consistent with the suggestion that they represent some variation of that formation (Fig. 9E). Distal silica-rich ashy samples are under-represented in the existing analyses, which focus on thicker, near-source localities. These Centralia dacite samples could be extensions of the Goble and Northcraft volcanic suites instead of the Ohanapecosh Formation given the overlapping, subparallel trends shown on Figure 9E. However, with most Goble and Northcraft samples exhibiting <58 wt. % SiO_2 and <60 wt. % SiO_2, respectively, the high silica content suggests these samples are related to the Ohanapecosh Formation with >60 wt. % SiO_2. Additional geochemical samples are needed for comparison with other volcanic units, including the Goble Volcanic suite, Northcraft Formation, Hatchet Mountain Formation, and Ohanapecosh Formation.

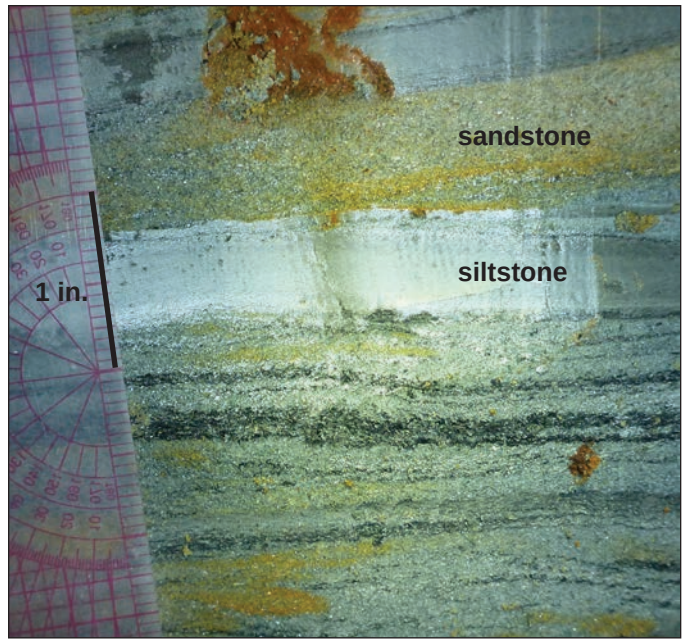

Figure 8. Photograph of fossil site GD33 showing close-up of carbonaceous material (black) interlayered in bluish gray micaceous sandstone and siltstone laminations. This photograph shows a characteristic exposure of the carbonaceous sandstone unit of the Skookumchuck Formation. The outcrop surface has been scraped clean to improve exposure of the sedimentary texture.

Other early Cascade arc formations in the Centralia area include the Goble Volcanics and the Northcraft Formation, but both of these are dominantly basaltic to andesitic in composition (Fig. 9E) and thus less likely to be correlative with the dacitic rocks of the Centralia quadrangle. The composition of a sample from site G53, a tuffaceous siltstone, does not reflect an igneous parentage: high Fe_2O_3 (14.6 wt. %) and LOI (16.9 wt. %) and extreme depletion in CaO (0.66 wt. %) and K_2O (0.07 wt %) are indicative of weathering, whereas the low rare earth element abundance (Fig. 9C) may reflect dilution of the tuff component by terrigenous sediment.

Sedimentary Geochemistry

Geochemical analysis of sedimentary rock units from the Centralia and Violet Prairie quadrangles (Polenz and others, 2018) suggests that systematic differences may exist between the mostly terrestrial Skookumchuck Formation and the marine McIntosh and Lincoln Creek Formations. Specifically, plots of (1) Rb/Al_2O_3 vs Zr/Al_2O_3 and (2) Ti/Al_2O_3 vs Zr/Al_2O_3 appear to systematically separate Skookumchuck Formation from the two marine units. Tentatively, the Skookumchuck Formation has higher Rb/Al_2O_3 and lower Ti/Al_2O_3 values compared to the marine units when controlling for Zr/Al_2O_3. The marine units have a similar range of values for Rb/Al_2O_3 and Ti/Al_2O_3, but the McIntosh Formation is generally lower in Zr/Al_2O_3 than the Lincoln Creek Formation. However, more work will be needed to confirm this relationship and assess if it resulted from something other than depositional environment, such as differing sediment sources.

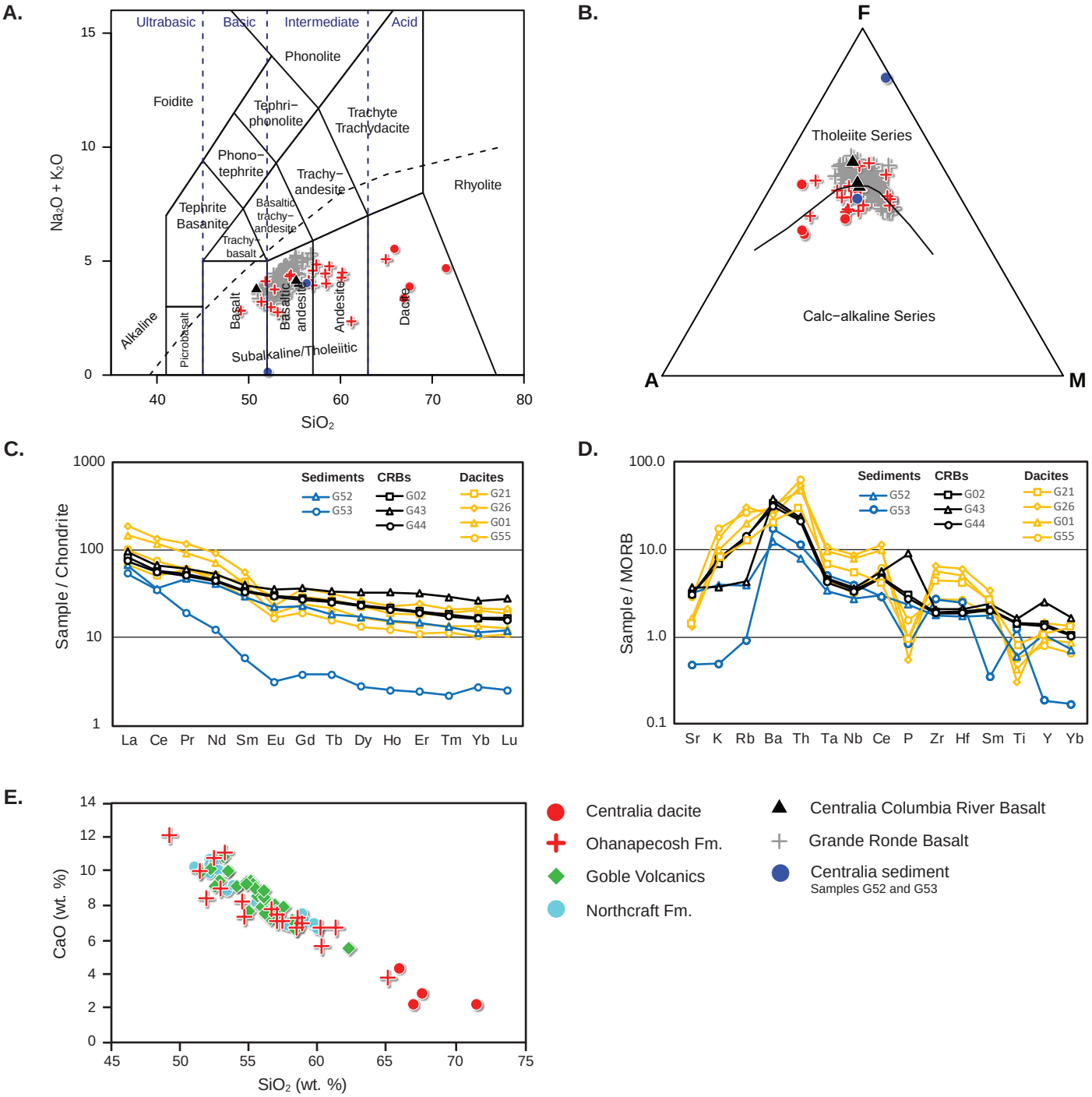

Figure 9. Geochemistry data. **A.** Total alkalis vs. silica plot (LeBas and others, 1986) for selected samples from Centralia quadrangle and other volcanic units for comparison. Notably, Ohanapecosh Formation data and sample G52 both overlap. This overlap suggests that sample G52 is heavily derived from basaltic andesite of the Ohanapecosh Formation. Grande Ronde data are from the GeoRoc database (GeoRoc database at http://georoc.mpch-mainz.gwdg.de/georoc/). Ohanapecosh data are from Polivka (1984), Shultz (1988) and Phillips and others (1989). **B.** AFM diagram (Irvine and Baragar, 1971) for selected samples from the Centralia quadrangle, with other volcanic units for comparison. Note that most dacite samples from the map area plot in the calc-alkaline field, which is similar to the Ohanapecosh Formation data. Also notable is that sample G52 overlaps with Ohanapecosh Formation data (Polivka, 1984; Shultz, 1988; Phillips and others, 1989). **C.** Rare earth element data for Centralia quadrangle rocks are shown normalized to the chondrite values of Boynton (1984). The similarities in patterns suggest common origins for: (1) the four dacite samples, and (2) the three Columbia River Basalt samples. Sample G52 plots similarly to the volcanic samples, whereas sedimentary sample G53 shows a lower REE enrichment pattern. **D.** MORB-normalized spider diagram (Sun and McDonough, 1989) for samples from the Centralia quadrangle. Note that all samples display relative depletions in Ta and Nb and enrichments in Rb and Ba, diagnostic features of subduction-related magmas and the Columbia River Basalts. The dacite samples also show depletions in P and Ti resulting from removal of apatite and Fe-Ti oxide minerals. **E.** Variation diagram comparing dacites from the Centralia quadrangle with data for early Cascade arc formations in the region. Other volcanic suites in the region (Grays River Volcanics, Crescent Formation, and Goble Volcanics) have generally higher total Fe_2O_3. Goble Volcanics data is from Phillips and others (1989). Northcraft Formation data is from Hagan (1987). The Centralia quadrangle dacite samples are more silica-rich than any of the other rocks shown on the diagram and appear to plot as a likely extension of the Ohanapecosh Formation data array. This is consistent with the suggestion that the dacites represent facies of the Ohanapecosh Formation.

X-Ray Diffraction

XRD results proved inconclusive in the map area and in the adjacent Violet Prairie quadrangle. The combined sample set from both quadrangles is presented here. Five clays were analyzed across 47 samples, including nontronite, kaolinite/halloysite, vermiculite, mica, and chlorite/montmorillonite. Most of the units in the quadrangle were poorly characterized by their clay mineral composition, although clays indicative of marine and terrestrial weathering environments can provide insight into the depositional environments of these formations. Nontronite is produced in alkaline conditions, which suggests a marine depositional environment and an iron-rich environment. Halloysite/kaolinite typically suggests a terrestrial depositional environment. Vermiculite suggests a magnesium-rich environment related to the weathering of biotite and (or) phlogopite. Overall, the clays that are detected are assumed to be authigenic, and not detrital (Table DS9).

The primary findings from XRD analysis differ for bedrock and glacial units. For bedrock units, neither nontronite nor halloysite/kaolinite were consistently detected in marine and terrestrial rocks, respectively. Therefore, inconsistent clay compositions suggest complicated or multiple depositional environments or shifted analytical data caused by interlayered clays. These inconsistencies may also call into question the assumptions that the clays are all authigenic and not detrital. Essentially, XRD clay mineral analysis reveals no clear differences between the sedimentary rock units in either quadrangle. For the Logan Hill Formation, nontronite was not detected in either sample and may suggest a nonmarine characterization with a larger sample size.

AGES OF DEPOSITS AND PALEOENVIRONMENTAL INTERPRETATIONS

Bedrock Units

Bedrock units, in order of decreasing age, include the Skookumchuck Formation, the Lincoln Creek Formation, the Grande Ronde Basalt, and the Wilkes Formation. With the exception of the Grande Ronde Basalt, the other bedrock units are well exposed along a north-northeast to south-southwest railroad segment in the north-central portion of the Centralia quadrangle (hereafter, “railroad section”). The Grande Ronde Basalt is unambiguously exposed on the western flank of Newaukum Hill in the southwestern map area. Biostratigraphic samples collected from the Centralia quadrangle aided paleoenvironmental interpretations but were not age diagnostic (Table DS1).

U-Pb analysis of detrital zircons is used to assess ages of bedrock units. This analysis provides information about maximum depositional ages and sediment provenance (Fedo and others, 2003) with caveats (Vermeesch, 2012). A compilation probability distribution plot for all zircon ages (Fig. 10) is arbitrarily cropped at 100 Ma to focus on the local geochronology using the most recent ages of the first peaks. A more detailed study of regional provenance offered by consideration of the older U-Pb peaks is outside the scope of this study (Appendix B and Tables DS2–DS6).

SKOOKUMCHUCK FORMATION

The age of the upper Skookumchuck Formation is loosely constrained in the Centralia quadrangle by the stratigraphic positions of coal beds that are well exposed to the east and their inferred locations as projected westward into the map area along with six unpublished K-Ar ages from tonsteins (ash partings) within those coal beds (40–41.5 Ma, D.M. Triplehorn, USGS, written commun., 1991, as cited in Flores and Johnson, 1995; Bohor and Triplehorn, 1993). The K-Ar sampling locations and which specific coal beds were sampled are unknown. Despite these spatial uncertainties, these ages are consistent with published ages of the Skookumchuck Formation from Armentrout and others (1983) and Wells and others (2014). A detrital zircon sample of Skookumchuck Formation collected in the Violet Prairie quadrangle (Polenz and others, 2018) also corroborated these late Eocene ages (Fig. 10). Paleomagnetic samples of the Skookumchuck Formation returned inconclusive results with considerable uncertainty due to structural complications, pervasive remagnetization, poor induration, and (or) sufficient weathering that included hematite and goethite.

At two locations (photo sites P01 and P02), trace fossil evidence of *Thalassinoides* (*Glossifungites* ichnofacies) (filled burrows) directly underlying a 6-in.-wide coal seam suggests a low-energy marine intertidal or shallow subtidal paleoenvironment, where sediments are firm but not lithified. Paleoenvironments that fit these characteristics include salt marshes, mud bars, intertidal flats, or shallow marine environments where erosion has stripped off unconsolidated sediments (Fig. 11)(Bromley, 1996; Benton and Harper, 1997; Seilacher, 2007). The relationship between the filled burrows overlying coal deposits shows that the terrestrial environment was inundated and became a shallow marine environment, suggesting a transgression; either deposition could not keep up with subsidence or eustatic sea level rise occurred at least once during deposition of the upper coal group of the Skookumchuck Formation. Other biostratigraphic paleoenvironmental indicators include a gastropod fossil mold of *Turritella uvasana washingtoniana* (Weaver and Palmer, 1922) found near the Mendota coal seam (age site GD38). This *Turritella* subspecies had only previously been observed in the lower Cowlitz Formation (Table DS1).

The feldspathic, micaceous and coal-bearing, trough-crossbedded, medium sandstone of the Skookumchuck Formation is inferred to have been deposited in paleoenvironments ranging from nearshore marine (foreshore to upper shoreface) to a terrestrial, tidally influenced coastal plain during the late Eocene (Flores and Johnson, 1995). Biostratigraphic markers (sites GD38, P02) further corroborate these interpretations. The regional depositional environment is likely a combination of broader distributary channels and interdistributary interfluves of an abandoned(?) lower delta plain (older) to delta front (younger) of a tidally-influenced delta (Buckovic, 1979). This regional setting assumes that the time-stratigraphic framework is correct and post-Eocene deformation has not significantly altered the Eocene paleogeographic fluvial drainage patterns east of and likely within the Centralia quadrangle. The deposits within this setting also suggest a slow, westward progradation of deposits with minor(?) lateral shifts of the distributary channels (Buckovic 1979). These distributary channels were located between major fluvial systems,

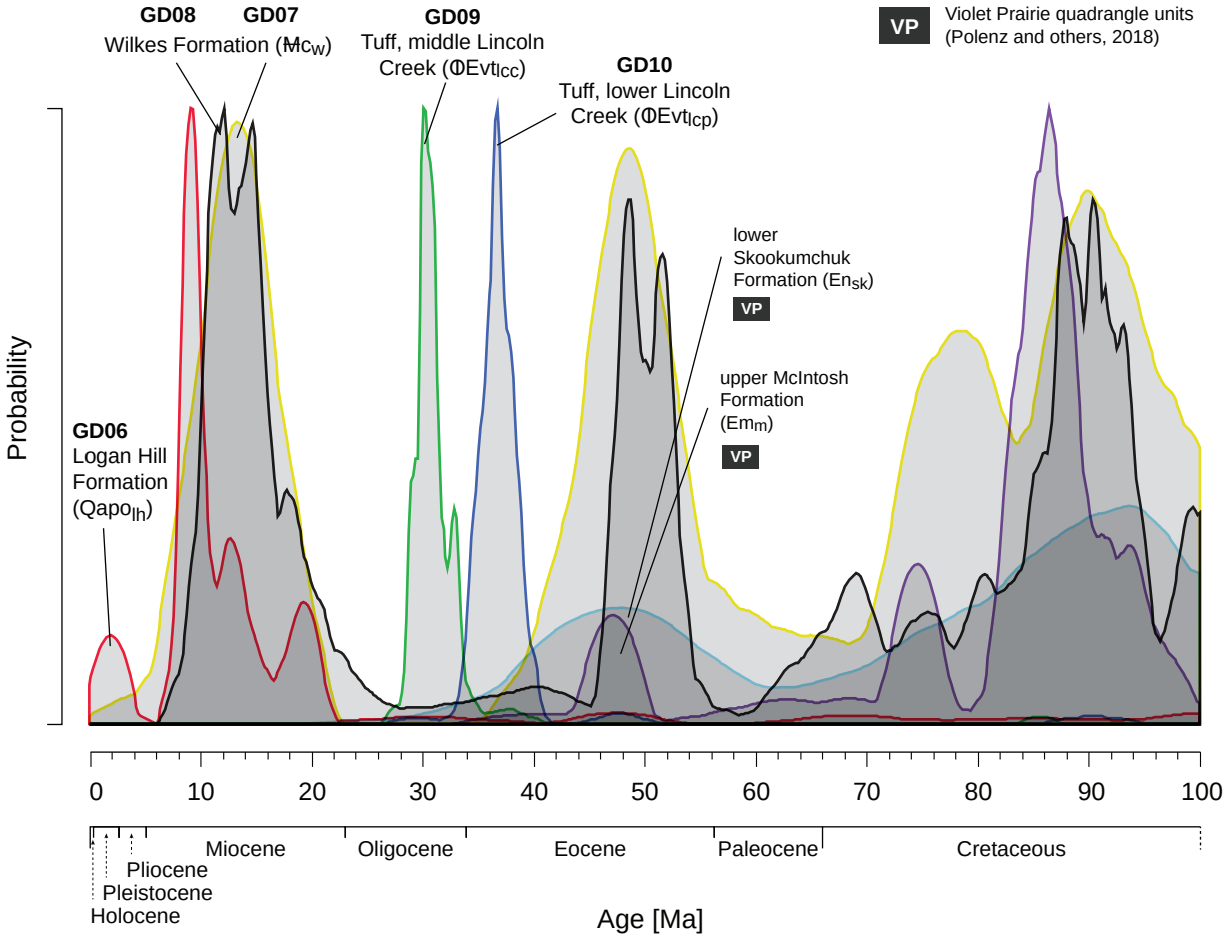

Figure 10. Compilation probability distribution plot of U-Pb analyses of zircon grains for the Centralia (this study) and Violet Prairie quadrangles (Polenz and others, 2018). The youngest peak for each age spectrum represents the maximum depositional age for that sample. Tall, narrow peaks represent well-constrained probabilities for a tight age range (single-event age: tuffs of sites GD09 and GD10). Smoother, wider peaks are less well constrained, have fewer analyzed detrital zircons, and represent a detrital signature with provenance implications (youngest single age: GD06, GD07, and GD08). While a histogram shows the distribution of age peaks for a sample (Appendix B and Data Supplement), the probability density function shown here provides the relative likelihood of different ages within a detrital zircon sample; higher peaks indicate a higher likelihood and sharper peaks have a greater number of samples constraining the age of the peak.

which were deflected by the Northcraft volcanic center farther east (Flores and Johnson, 1995)(Fig. 12). Additional evidence that corroborates such a river system comes from geochemical analysis of mica from northwestern Oregon (Kadri, 1982; Heller and Ryberg, 1983). The composition of the mica shows that the source area for the feldspathic sand of southwestern Washington is likely the Idaho Batholith (Armentrout, 1987). This suggests that a significant river system or multiple generations of smaller pre-Cascades rivers would have been needed to collect and transport material from such a distal source area. Notably, the coal rank decreases westward from the coal mines in the Bucoda quadrangle, suggesting either that there was less burial (perhaps due to uplift) or a lower geothermal gradient in the map area (Walsh and Phillips, 1983).

LINCOLN CREEK FORMATION

The age of the Lincoln Creek Formation in the map area is constrained by two new U-Pb zircon ages. Zircon grains collected from a basal, unwelded lapilli ash flow tuff and a middle, poorly welded lithic tuff return sharp U-Pb youngest age peaks of 36.70 ±0.32 Ma (unit ΦEvtlcp) and 30.58 ±0.35 Ma (unit ΦEvtlcc), respectively (sites GD10, G09)(Fig. 10, Appendix B, and Tables DS6 and DS7). These dacitic tuff samples each yielded a sharp, single age peak, which means the sampled layer represents a single volcanic event. These peaks therefore provide a maximum depositional age but do not provide insight into the mix of detrital constituents in the Lincoln Creek Formation. Ages are consistent within the uncertainties of Armentrout and others (1983), and suggest correlation with the Ohanapecosh Formation. Also magnetostratigraphic correlation on the Lincoln Creek Formation was used to better refine the age of the Eocene/Oligocene boundary, and report an age of about 36 to 37 Ma (Prothero and Armentrout, 1985).

At the base of the Lincoln Creek Formation, an unwelded lapilli ash flow tuff (36.70 ±0.32 Ma [unit ΦEvtlcp][site GD10, Fig. B1]) directly overlying the Skookumchuck Formation is a significant marker horizon in the map area and likely represents a regionally significant correlative horizon as well. This tuff likely represents the voluminous volcanic ash derived from explosive volcanism marking the onset of ancestral Cascade arc magmatism and thus the incipient Cascade Range and (or) local volcanic centers that are correlative with the unconformity at the base of the Cascade Range volcanic sequence (Armentrout, 1973a; Wells and others, 1984; Armentrout, 1987). Water-lain ash textures

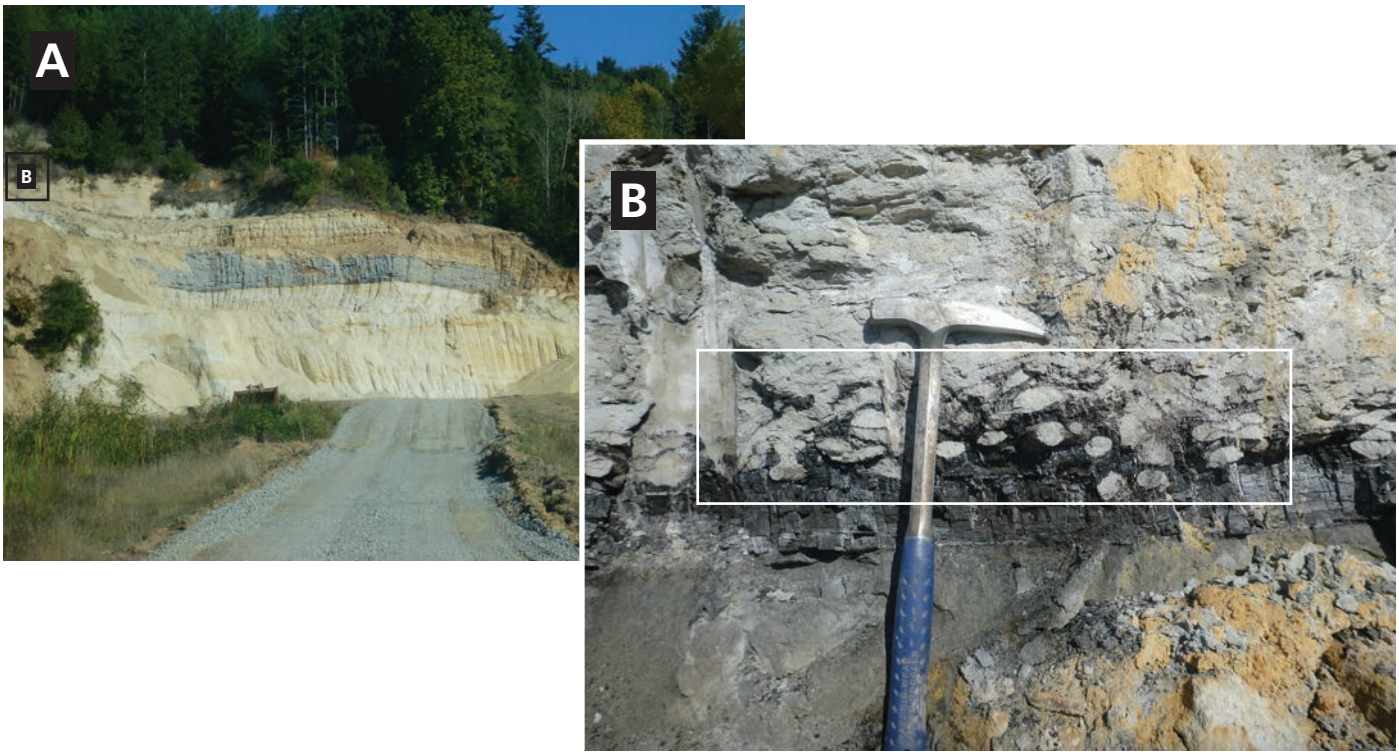

Figure 11. *Thalassinoides* (*Glossifungites* ichnofacies) trace fossils overlying a small coal seam at photo site P02 and close-up of photo site P01. **A.** Prominent bluish gray bed is highly carbonaceous, but not coal, and gently dipping into the slope to the northeast. **B.** Cylindrical trace fossil burrows (white box) above coal bed suggest a marine intertidal or shallow subtidal paleoenvironment, where sediments were firm, but not lithified.

and interfingering contact relationships with marine siltstone support a subaqueous depositional environment. Therefore, a submarine paleoenvironment is very likely for the lapilli tuff in the map area, which is further correlated with the subaqueous unwelded pyroclastic flows of the latest Eocene to earliest Oligocene Ohanapecosh Formation near Mt. Rainier (Fiske, 1963; Polivka, 1984; Shultz, 1988). The rocks may also be correlative with the latest Eocene or earliest Oligocene Goble Volcanic suite (Livingstone, 1966; Armentrout, 1975; Beck and Burr, 1979; Wells and Coe, 1985), and the Hatchet Mountain Formation of Roberts (1958).

Geochemical analysis of these tuffs tentatively correlates with the Wildcat Creek facies of the Ohanapecosh Formation. The lack of welding of the Centralia and Ohanapecosh lapilli tuffs suggests that sufficient heat was not present in the pyroclastic flows from the longitude of the map area to Mount Rainier in order to produce fiamme and compaction foliation. This notion is compatible with the Wildcat Creek facies of Shultz (1988), and it is possible that the heat of the pyroclastic flow was quickly leached by rapid cooling by the surrounding water.

Above the basal lapilli tuff, the Lincoln Creek Formation commonly consists of massive siltstone (to fine sandstone) along with macro- and microfossils (Table DS1). Both lithology and biostratigraphy strongly suggest a lower shoreface to offshore depositional environment. Constituents of the siltstone include erosional material shed from the proximal, coal-bearing Skookumchuck Formation, which left remnant carbonaceous material with rare pyrite within the Lincoln Creek Formation. This also mixed with Cascade arc-derived volcanic material, including, but not limited to glass shards, ash (pumiceous/"tuffaceous"), and basaltic-to-andesitic rock fragments. This material further mixed with feldspathic sediments from farther east, transported by west-flowing rivers, before likely deposition as forearc tuffaceous sediments (Beikman and others, 1967; Snavely and Wagner, 1963, 1982; Snavely and others, 1980a; Armentrout and Franz, 1983; Heller and Ryberg, 1983; Wells and others, 1984; Armentrout, 1987).

The middle, poorly welded (to unwelded) lithic tuff—30.58 ±0.35 Ma (unit ΦEvt_{lcc})(GD09, Fig. B2)—marks a subtle change in lithology between the underlying volcaniclastic siltstone and overlying tuffaceous siltstone. The change in lithology may suggest a transition in depositional environment from shallow to deeper marine.

Lastly, a complete transgressive-regressive cycle was defined from stratigraphic sections west and west-northwest of the Black Hills (~25–35 mi northwest of the map area), based on an unconformity-bound sequence containing the latest Eocene-Oligocene Lincoln Creek Formation and the Miocene Astoria(?) Formation (not observed in map area). These units represent a transition from nearshore and non-marine basin-margin facies in the east to deep shelf-margin basin facies in the west of the map area (Armentrout, 1987). The question mark after Astoria follows Snavely and others (1958) and Wells (1979, 1981, 1989), denoting probable correlation with the now-inaccessible type section of the Astoria Formation mapped south of the Columbia River (Howe, 1926; Beaulieu, 1971).

During the Oligocene through the Miocene, the inferred roughly north-south-oriented paleo-shoreline was likely irregularly migrating east and west through the map area under the influence of the competing forces of tectonics and eustasy. This transgressive-regressive cycle was governed dominantly by local tectonism, where subsidence exceeds sediment supply,

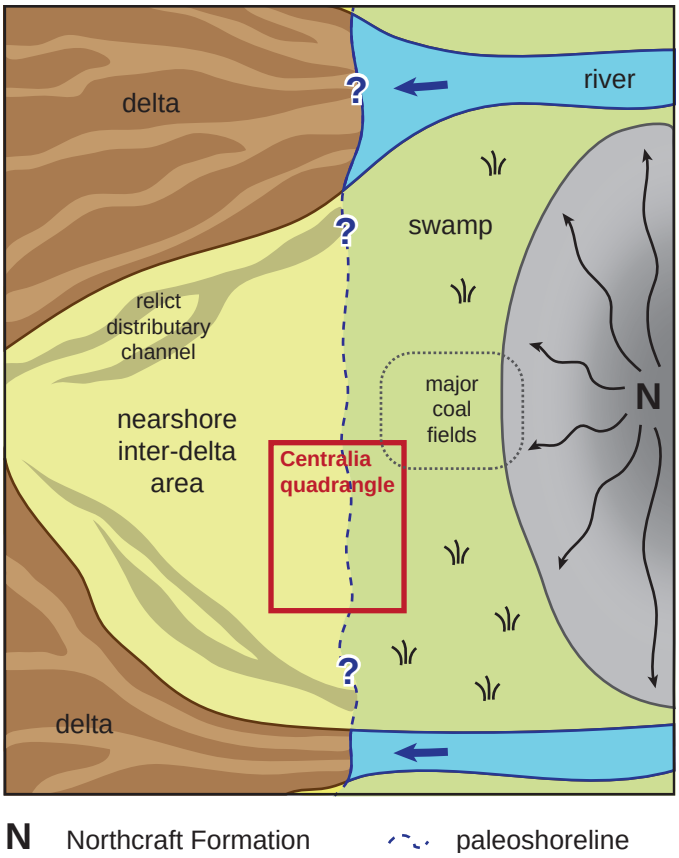

Figure 12. Schematic map showing inferred paleogeography of the Centralia area during the latest medial and late Eocene, modified from Flores and Johnson (1995). Nearshore, inter-delta areas with minor distributary channels as well as terrestrial, coal-bearing areas (swamps) both reside between major fluvial systems that are diverted around the Northcraft volcanic edifice (N). Arrows (black) in the Northcraft Formation illustrate movement direction of eruptive material. Rock types ranging from medium sandstone to siltstone in the Skookumchuck Formation suggest an inferred paleoshoreline (blue dashed line) that migrated east and west into and out of the Centralia quadrangle during this epoch.

and less so by global eustatic sea-level fluctuations, which are out of phase with basin bathymetry curves for southwest Washington (Armentrout, 1987). It is conceivable that similar tectonic processes operated in the map area at this time. These rapid changes in paleoenvironment generated a zone of stratigraphic complexity in the map area.

WILKES FORMATION

Prominent populations of U-Pb ages from detrital zircon grains at two localities (Fig. 10) suggest maximum depositional ages of 8.57 ±0.92 Ma (age site GD08, Fig. B3) and 7.54 ±1.04 Ma (age site GD07, Fig. B4), both based on the youngest single grains. These ages suggest a late Miocene or younger age, which is compatible with the Wilkes Formation (Roberts, 1958), also known as the Tertiary unnamed nonmarine unit (Pease and Hoover, 1957; Snavely and others, 1958; Armentrout, 1987). These ages are consistent with Armentrout and others (1983). A sand dike was observed at age site GD07. The dike was generated either by 1) seismic activity, 2) landslides in poorly consolidated material, or 3) loading without either triggers, and may reflect the terrestrial depositional environment of the Wilkes Formation (Fig. 13).

In the Centralia quadrangle, the cross-bedded, sandy conglomerate to pebbly sandstone of the Wilkes Formation was deposited on erosional surfaces of the Lincoln Creek Formation (scour-and-fill channels) and directly underlies the Logan Hill Formation. In the map area, bedding from the Wilkes Formation generally dips more gently and in different directions (as much as 90° difference) compared to the underlying Lincoln Creek Formation. Contact patterns of the Wilkes Formation show channelized deposition along these erosional surfaces and within larger synclinal structural troughs of the Lincoln Creek Formation, thus suggesting an unconformity (angular and (or) disconformity) with Oligocene units. No biostratigraphic age markers (foraminiferal assemblages, macrofossils, or trace fossils) were found in samples collected from Wilkes Formation biostratigraphic sites (GD20, GD27). Fossilized wood, leaf impressions, and partially macerated carbonaceous material, which are common in previous descriptions of the nonmarine unit (Pease and Hoover, 1957; Snavely and others, 1958), were not observed in the map area. Broadly, Miocene marine rocks are uncommon in the Centralia quadrangle, supporting a terrestrial to nearshore paleoenvironment for the Miocene Wilkes Formation.

Quaternary Surficial Units

LOGAN HILL FORMATION

Severe weathering of cobbles and pebbles in the Logan Hill Formation strongly suggests a pre-Vashon age, older than ~15.7 ka (Porter, 1975; Lea, 1984; Polenz and others, 2015, 2016, 2017). Weathering characteristics similar to the Miocene Wilkes Formation further suggest that the Logan Hill Formation is relatively old for glacial drift. Detrital zircon ages from the Logan Hill Formation show a youngest single age of 1.68 ±0.97 Ma (age site GD06, Fig. B5)(Fig. 10). This early(?) Pleistocene age is consistent within the geochronologic uncertainties with Armentrout and others (1983). The poor sorting of Cascade-sourced cobbles, mantling of topography, and common overlying of bedrock units are interpreted to represent distal outwash from glaciofluvial(?) processes for the Logan Hill Formation.

Contacts between the Logan Hill Formation and the Lincoln Creek Formation across the map area are consistently concealed by landslides. This may suggest that the basal contact of the Logan Hill Formation is favorable for landslide initiation by forming a slide plane for mass transport. Alternatively, this contact relationship is meaningless and landslides simply initiate at higher elevations in general. Geotechnical work for landslide and seismic hazard assessment should be considered on a site-by-site basis along this contact.

QUATERNARY ALLUVIUM, TERRACES, ALLUVIAL FANS, AND LANDSLIDES

Radiocarbon dating of a stick lodged in an outcrop of floodplain deposits weakly constrains the age of alluvium in the Chehalis River valley from recent to older than 1,650 ±30 years before present (radiocarbon site GD01, unit Qa). This age confirms the alluvium is a recent floodplain deposit. Quaternary alluvium in the Chehalis River valley is fed by its tributaries, which include the Skookumchuck River and China, Salzer, Coal, and Dillenbaugh Creeks. The sediments lie in a valley underfit for

its stream, where the Chehalis River meanders within the wider Chehalis River valley.

Basement elevation contours modeled from water wells near the Chehalis–Skookumchuck River confluence show the thickness of alluvium is 70 to 80 ft in the Chehalis River valley (D. Eungard, WGS, written commun., 2018). Local well logs across the river valley also support alluvial thicknesses >40 to 50 ft. Thickness of alluvium from the seismic reflection profile near the Chehalis–Centralia airport (W. Stephenson, USGS, written commun., 2018) is roughly 60 to 70 ft in the central portion of the quadrangle. Considering that alluvium can be as thick as 250 ft for the much larger Mississippi River, it is reasonable to infer that the Chehalis River valley alluvium is far less than 250 ft thick.

It is unclear what formed the 5- to 20-ft tall alluvial terraces (unit Qoa) in the map area, and the age of these terraces is unknown. Fluvial processes, tectonism, or a combination of the two processes may be contributing to the presence of these terraces. In the elbow of the Chehalis River, west of the Mellen St. Bridge, where the river takes a 90° bend to the west, a conspicuous and elevated alluvial terrace records a relict erosion and fill level (age site GD54). This location would be a good place to test for possible neotectonic signals using dating methods with younger age ranges, including but not limited to radiocarbon, luminescence, and cosmogenic nuclide dating.

Numerous, small alluvial fans are at the foot of every hill in the mapping area, especially at the mouths of minor drainages and small tributaries, which represent fluvial processes (flash floods) and erosion.

Numerous landslides and landslide complexes form on many of the hillslopes of the Centralia quadrangle. Locations of these features are compatible with some of the features delineated by Fiksdal (1979). The age, timing, and re-activation of these features is unknown, and the level of activity should be evaluated on a site-by-site basis with field visits. The more than 270 landslides identified in the quadrangle are large (~11.5 acres average, standard deviation ~25 acres, and a maximum area ~290 acres) and exhibit a range of morphologies from unambiguously mature to juvenile. Mass wasting features are also numerous (~150 mass-wasting zones), large (~14 acres average), and exhibit ambiguous morphologies that may or may not be landslides and thus warrant closer investigation.

STRUCTURES IN THE MAP AREA

At regional scale, the Centralia quadrangle is in a broad zone of interacting faults. The interplay between northwest-striking and west-striking faults suggests a zone of structural complexity. Faulting and folding is recognized in Paleogene and Neogene strata within the Centralia quadrangle. Poor exposures combined with similar looking Paleogene formations present a significant challenge when identifying, delineating, and interpreting structures throughout the map area. As a result, many contacts are inferred. To address this challenge, the inferred locations of coal bed outcrops by Snavely and others (1958) are relied upon to identify some folds (Fig. 14). Given the poor exposure, fault displacements should not be calculated from offset contacts and fold axes in the Centralia quadrangle. Future research

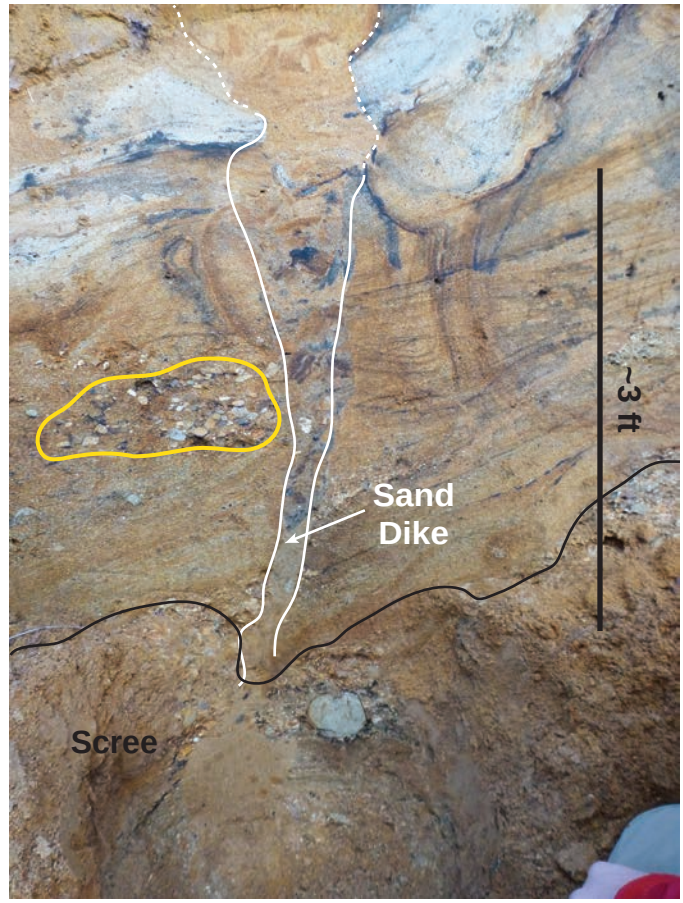

Figure 13. Photo of sand dike at GD07 (between white lines) above a small scree slope (black line). Scale of the sand dike is ~1 m (3 ft). The dike is to the right of a lens of pebbles in a pebbly sandstone (yellow outline) and disturbs the upper light gray layering (dashed white outline). Subtle, brown liesegang banding and black manganese nodules (<1 mm) coat parts of the outcrop. This picture was taken below the erosional unconformity at the base of the Logan Hill Formation.

utilizing deep paleoseismic trenches should be used to determine displacements and slip rates in the Centralia quadrangle. No unambiguous fault-related escarpments were observed in the Quaternary alluvium (unit Qa) or in the modified land (unit ml) of the Chehalis River valley associated with the Salzer Creek, Doty, or Chehalis faults. Therefore, these structures may be (a) inactive and older than the Quaternary alluvium, (b) active(?) and muted by the regional climate and active fluvial processes, or (c) active and blind.

Our mapping refines the locations, extents, and characteristics of faults and folds originally characterized and named by Snavely and others (1958) before the widespread acceptance of plate tectonics. Therefore, significant refinements have been made to the characterizations of the Salzer Creek fault, Kopiah fault and related folds, and associated minor faults. However, in the central portion of the map area, characterization of the Doty and Scammon Creek faults is on-going because the lateral extents of their traces are concealed beneath the alluvium of the Chehalis River valley. Likewise, their interaction with the concealed Salzer Creek fault is unclear.

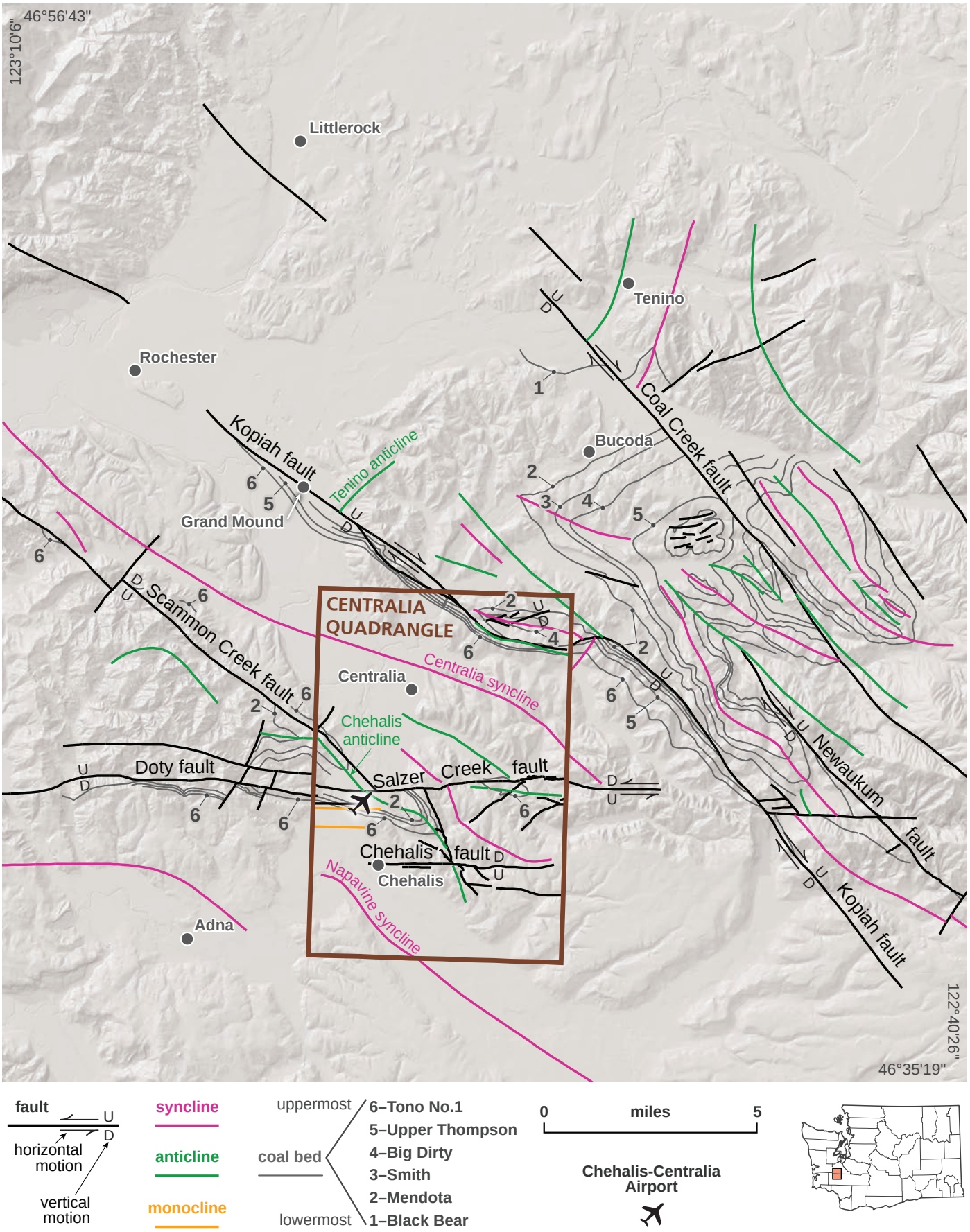

Figure 14. Structural map of the Centralia quadrangle and adjacent areas showing faults, folds, and coal beds. Structures outside of the Centralia quadrangle are adapted from Snavely and others (1958) and Polenz and others (2018). Coal beds adapted from Snavely and others (1958). West- and northwest-striking oblique faults and similarly trending folds show the prevailing structural fabric.

Faults

Five major fault strands are mapped in the Centralia quadrangle including: the Salzer Creek, Doty, Scammon Creek, Kopiah, and Chehalis faults. These faults fall into two interacting fault pattern categories. The Kopiah and Scammon Creek faults are northwest-striking, whereas the other major faults are west-striking. Poor exposure of fault traces prevents the calculation of precise slip estimates and slip rate along fault planes in bedrock lithologies, therefore the amounts of displacement along faults are adopted or modified from Snavely and others (1958), Pease and Hoover (1957), or otherwise inferred. Likewise, the lack of kinematic data on fault surfaces precludes precise calculations for principal strain axis orientations and inversion for local principal stress directions and magnitudes.

DOTY–SALZER CREEK FAULT SYSTEM

The Doty–Salzer Creek fault system consists of the Doty fault and Salzer Creek fault, both of which strike east-west through the Centralia quadrangle, effectively dividing the quadrangle in half (Fig. 14). The Doty fault is approximately 2,000 ft south of the Salzer Creek fault and their proximity suggests that they may share a genetic association and are possibly related to a deeper crustal structure.

The Doty fault is a west-striking, steeply(?) north(?)-dipping, high-angle reverse fault, where strata are upthrown along its north side. No surface exposures of the Doty fault were observed in the Centralia quadrangle, and the structure is inferred to be concealed through the alluvium of a small, east-draining creek valley (south of age site GD34). The orientation of this creek valley may also provide surface evidence for the location of the Doty fault. The Doty fault is inferred to terminate eastward in the central portion of the Chehalis River valley. Like the Scammon Creek fault, no surficial evidence collected from within the Centralia quadrangle suggests disagreement with the fault type, sense of slip, and dip direction proposed by Snavely and others (1958) for the Doty fault. Surface evidence of the Doty fault is more likely in exposures to the west and outside of the Chehalis River valley. Thus geologic mapping of the Adna quadrangle adjacent to and west of the map area may elucidate the character of this regionally significant structure.

The Salzer Creek fault is a continuous, east-striking, steeply south(?)-dipping, oblique-slip fault with sinistral sense of movement greater than or equal to reverse components of slip, where strata are upthrown along its south side. This ratio of slip senses is inferred from field relationships of contacts. Dip-slip displacement along the fault is inferred to be less than 1,000 ft. A conspicuous scarp at significant site S03 and nearby separation of depositional contacts to the west provide surface evidence for the Salzer Creek fault (Fig. 15A). At significant site S03, an escarpment that represents either a landslide headscarp or fault scarp is between a landslide deposit and the Logan Hill Formation. Also near this locality, a left-laterally separated magnetic anomaly in the shallow (reduced to pole) aeromagnetic survey (R. Blakely, USGS emeritus, written commun., 2018) may provide additional evidence for a sinistral sense of slip (Fig. M2).

The Salzer Creek fault is also exposed at the surface in the eastern portion of the quadrangle area, particularly in a small, north-draining creek located to the south of Salzer Valley Road and west of Reinke Road (significant site S01). Here, the exposure contains a sub-vertical fault surface with sub-horizontal slickenlines and a Riedel shear(?) exhibiting a left-lateral sense of slip as well as a collection of closely spaced (6–18 in.), very steeply north-dipping to sub-vertical joints with moderately-dipping conjugate joints (shears?). Near this fault surface a conspicuous, east-trending topographic break in slope provides additional geomorphic evidence for a fault. Following this topographic break for 2,000 to 4,000 ft to the east from the fault surface, the geomorphic feature aligns with an escarpment through a landslide deposit at the eastern edge of the map area (significant site S02; Fig. 15B). Arguably, this longitudinal escarpment through the middle of the landslide deposit may be landslide-related. Therefore, surface evidence at sites S02 and S03 suggest that the Salzer Creek fault may have neotectonic significance in the map area and that the Salzer Creek fault may exhibit recent slip.

Also in the eastern portion of the quadrangle, proximal to the Salzer Creek fault, are several shorter, discontinuous, west- to southwest-striking, left-lateral(?) fault segments. South of an east-trending, gently doubly-plunging anticline, the longest minor fault associated with the Salzer Creek fault is defined from offset of the Golden Glow and Tono coal beds (coal records 20, 21, and 50 of Snavely and others, 1958)(Fig. 14). Southwest-trending topographic lineaments are also parallel to the strike of this minor fault.

In the central portion of the quadrangle, a north-northeast-striking, west-dipping, high-angle normal(?) fault between the Salzer Creek and Chehalis faults is identified from Reliance and Leonard coal mine maps of 1932. This short fault segment is inferred to have little to no offset (< 250 ft) and its north and south extent is unclear beyond either of the major, west-striking, bounding faults.

Snavely and others (1958) showed the Doty and Scammon Creek faults as concealed and terminating at the Salzer Creek fault in the Chehalis River valley. Another interpretation would be that these three faults do not all intersect in the shallow subsurface but may be related to a deeper structure. This second interpretation is reflected as terminating faults. Future work in the Adna quadrangle will further characterize the Doty and Salzer Creek faults and their relationship to each other.

SCAMMON CREEK FAULT

The Scammon Creek fault is a northwest-striking, southwest-dipping, reverse(?) fault that terminates to the southeast in the Chehalis River valley of the Centralia quadrangle (Fig. 14). The location of the fault trace was adopted from Snavely and others (1958) and modified using magnetic and gravity geophysical surveys (this report). This characterization differs from that originally proposed by Snavely and others (1958), where they characterized the Scammon Creek fault as a northeast-dipping normal fault. This difference is prompted by observations of regional compressional tectonics and a local transpressional stress regime in order to accommodate uplift on the northeastern flank of the Lincoln Creek uplift in the Willapa Hills. Therefore, an inference of reverse rather than normal displacement is primarily model-driven given that most of the fault trace is concealed in the Chehalis River valley. The fault is inferred to be steep

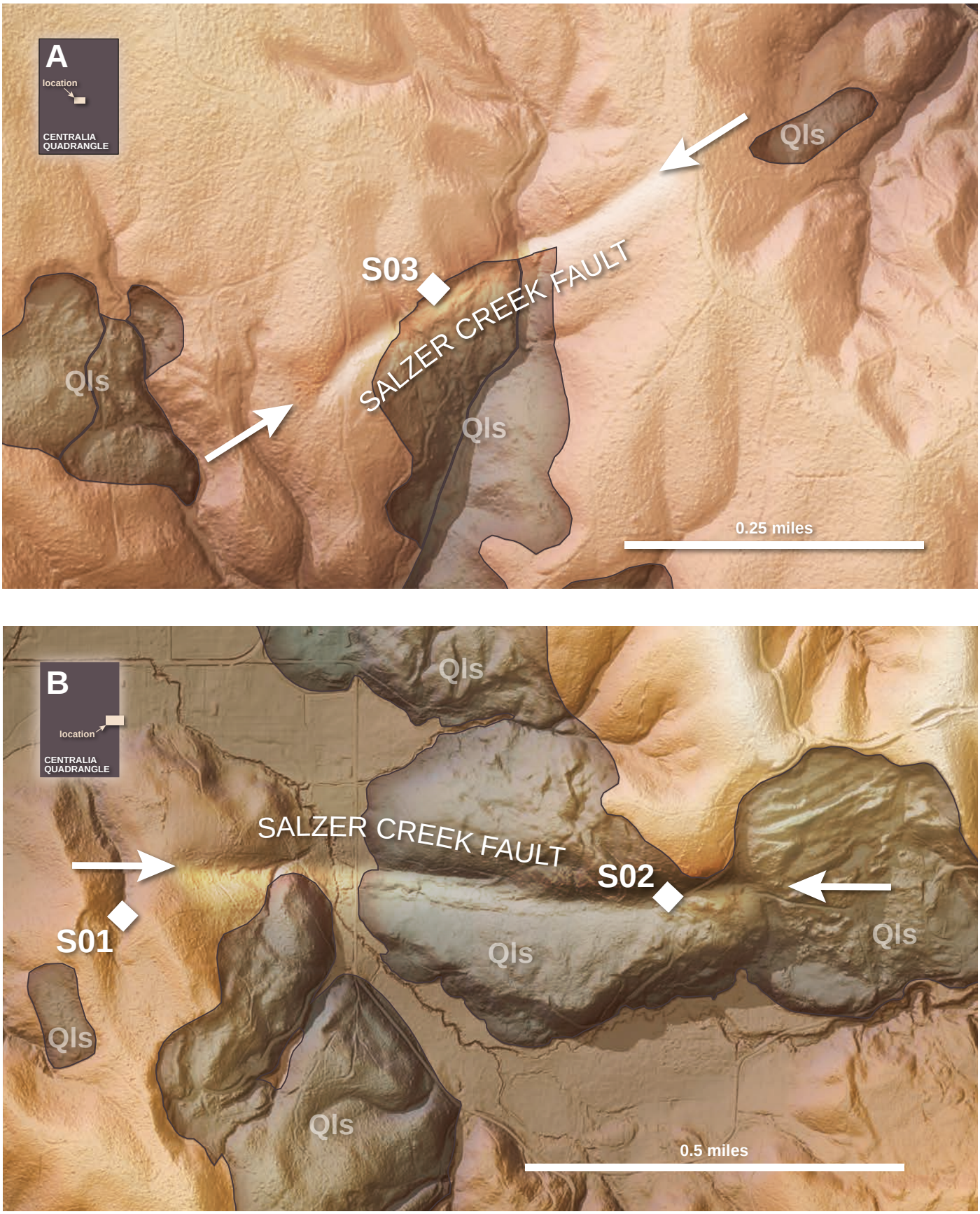

Figure 15. Lidar images showing the Salzer Creek fault (white arrows) in the center and the eastern portion of the map area. **A.** Linear escarpment along the trace of the Salzer Creek fault near significant site S03. **B.** Landslide deposits possibly deformed by the Salzer Creek fault near significant site S02 that suggest neotectonic significance and recent seismic activity. Fault surface with slickenlines and Riedel shears observed at significant site S01 (Fig. 16).

to near vertical in the Centralia quadrangle. The concealed southeastern trace of the Scammon Creek fault interacts with the concealed trace of the Salzer Creek fault. The interaction is likely a fault termination of the Scammon Creek fault at the through-going Salzer Creek fault. This association may suggest that these structures are related and possibly antithetic(?) to each other. Fault slip along the Scammon Creek fault is inferred to diminish to the southeast toward the zone of intersection. Bedrock exposures in the adjacent quadrangles to the northwest and west (Rochester and Adna 7.5-minute quadrangles) may aid further characterization of the Scammon Creek fault.

KOPIAH FAULT

The Kopiah fault was originally identified by a change in dip domain over a short distance (<1,000 ft) within the Skookumchuck Formation in the north-central portion of the Centralia quadrangle (Fig. 14). There, a fault delineated the boundary between a steep southerly (~40–90°S) to overturned dip domain and a gentle northerly dip domain (~10–40°N)(Snavely and others, 1958). Contrary to Snavely and others (1958), observations from this study identify an asymmetric, south-verging anticline at the surface rather than a fault. However, a laterally extensive, steep gradient in the regional aeromagnetic survey (R. Blakely, USGS, written commun., 2018) suggests a deep (blind?), northwest-oriented structure with a short, west-striking bend. Co-located at this west-striking bend is this newly identified fold (see Folds Associated with the Kopiah Fault), which is also along the previously mapped trace of the Kopiah fault (Fig. M1).

Elsewhere, in the Violet Prairie and Logan Hill quadrangles, the Kopiah fault strikes predominantly northwest and takes a small, westward bend or left step (<9,000 ft wide) within the Centralia quadrangle. In nearby quadrangles to the east, recent coal mining excavations near Hanaford Creek and South Hanaford Creek show lateral offsets with lesser amounts of localized "overthrusting" (tens of feet) along many of the major northwest-striking faults, including the Kopiah, Newaukum, and Coal Creek faults (W. Greenough, TransAlta Coal, oral commun., 2017; Stanley and others, 1994). The highly localized, episodic "overthrusting" is restricted to shallow coal excavations in multiple areas (see Nelson, 1981). The causative stresses for overthrusting may be unrelated to northwest-striking fault segments and instead related to non-tectonic gravitational collapse.

Therefore, the northwest-striking segments of the Kopiah fault are understood to be oblique with greater dextral movement than reverse movement (W. Greenough, oral commun., 2017). Furthermore, mapping by Snavely and others (1958) shows a bifurcation of the Kopiah fault near the northern boundary of the Centralia quadrangle. Our new mapping does not find evidence to confirm or dispute this bifurcation, and therefore this geometry is accepted. Northwest-trending folding in the Violet Prairie quadrangle (Polenz and others, 2018), dextral offset, and fault bifurcation may possibly be the expression of a larger flower structure that may encompass multiple northwest-striking oblique faults (Figs. M1 and 14). The displacement is inferred from offset coal beds to be approximately 200 to 250 ft on each fault strand where the Kopiah fault splits and strikes northwest (Snavely and others, 1958).

Evidence suggests that the west-striking segment of the Kopiah fault in the Centralia quadrangle is a restraining bend. Therefore, in the Centralia quadrangle, the short, west-striking segment of the Kopiah fault is a north-dipping, blind, reverse-to-thrust fault with attendant fault-related folds (See *Folds Associated with the Kopiah Fault*). There are multiple hypotheses for the causative stresses for the sense of slip on this fault, and may either be: (1) related to localized transpression from a left-step in a dextral-reverse fault; (2) related to regional shortening associated with Cascadia subduction processes; or (3) both. Also, a short, synthetic(?) reverse fault within the northern fault block of the Kopiah fault is identified from the separation of the Mendota coal bed. The fault type and sense of slip of this minor fault are consistent with deformation within a restraining bend. Characterizing the northwest-striking faults farther to the east—the Newaukum and Coal Creek faults—would aid understanding of the local stress perturbation near the westward bend in the Kopiah fault.

CHEHALIS FAULT

The Chehalis fault is a west-striking, steeply(?) north-dipping, normal fault that terminates to the west in the Chehalis River valley and continues eastward off the Centralia quadrangle. Repetition of southwest-dipping bedrock strata that identify the Chehalis fault crop out west of the Chehalis River and south of Coal Creek Road. A prominent east-west oriented segment of the headwaters of Coal Creek provides geomorphic evidence to extend the Chehalis fault eastward to the quadrangle boundary and likely beyond into the Logan Hill quadrangle. The Chehalis fault is inferred to terminate westward in the Chehalis River valley. Slip along the Chehalis fault is inferred to be relatively small and less than 1,000 ft (Snavely and others, 1958).

Timing of movement along the Chehalis fault and the fault's western extent are not well constrained from observations in the Centralia quadrangle, but Snavely and others (1958) posit that movement occurred (and ceased) prior to the Miocene because Miocene strata along fault strike to the west in the Adna quadrangle are undisturbed. Future geologic mapping of this adjacent quadrangle would help constrain the timing and extent of the Chehalis fault.

Folds

Numerous, west-, northwest-, and southeast-trending folds are present in the Centralia quadrangle. These folds include: Kopiah fault-related folds, the Centralia syncline, the Chehalis anticline, the Napavine syncline, and other unnamed folds.

The relative timing of faulting and folding in the Centralia quadrangle is difficult to discern because of poor exposure along faults and the broad geometry of folds. Slip rate calculations should not be attempted from offset axial surface traces that are approximately located or inferred.

FOLDS ASSOCIATED WITH THE KOPIAH FAULT

An anticline and syncline are along and north of the west-striking bend of the Kopiah fault, respectively. The anticline is an asymmetric, closed, south-verging fold and may have smaller-scale associated geomorphic features including pressure ridges. Structural data (n=11) yield an approximate axial plane that

strikes west and dips ~70°N. A near-vertical to overturned coal bed at significant site S04 may suggest other dip magnitudes for the axial plane of this anticline, but additional attitudes are necessary to determine a more precise orientation.

North of the concealed westward bend of the Kopiah fault, the syncline is less asymmetric, more open, and upright compared to the anticline. The syncline is geomorphically expressed as an area of relatively lower elevation with irregular "hummocky" surface morphology. Structural data (n=14) yield an approximate axial plane orientation that strikes west-northwest and dips sub-vertically. Within the west-striking segment of the Kopiah fault, these folds have a restricted lateral extent and have only been mapped in the Centralia quadrangle.

These folds may be: (1) transpressive features along a restraining bend in the Kopiah fault; (2) a fault propagation fold (anticline) with a subparallel syncline to the north; or (3) a combination of both 1 and 2. The second hypothesis implies that the west-striking segment of the Kopiah fault is part of an inferred, more extensive, and continuous blind thrust, whereas the first hypothesis has fewer inherent assumptions. Given the restricted lateral extent of the folds, the first hypothesis seems more likely and further supports a dextral motion on the Kopiah fault.

CENTRALIA SYNCLINE

The Centralia syncline was originally identified by Weaver (1937) and named by Snavely and others (1958). Sparse structural data and clear contact relationships define the Centralia syncline. Lack of bedding attitudes in the generally massive and hackly weathered Lincoln Creek Formation preclude any stereonet-based structural analysis of the Centralia syncline and the dip of the axial plane is assumed to dip vertically to sub-vertically north. The Centralia syncline is a gentle fold, and it trends west-northwest across the entire map area, which suggests that it may be a regionally extensive structure.

South of the Centralia syncline and north of the Salzer Creek fault, a previously unrecognized anticline is concealed in Salzer Valley. This west-northwest-trending anticline is inferred from field relationships, where its northern and southern limbs contain Skookumchuck Formation underlying Lincoln Creek. Given that it is concealed, the extent of this anticline is unknown. It is inferred to be paired with the Centralia syncline, based on its proximity to it.

SYNCLINE NEAR SALZER CREEK FAULT

A syncline in the central portion of the map area was originally identified by Snavely and others (1958). This fold is located south of the Salzer Creek fault and may extend north of the fault, where the syncline is queried. The location of the fold is approximated from field relationships between the Lincoln Creek and Skookumchuck Formations. West of Centralia Alpha Road, the syncline extends farther southeast, where it bends subparallel to the Chehalis fault between the Chehalis anticline and a doubly-plunging anticline south of Salzer Creek fault. The Pleistocene surface of the Logan Hill Formation along this syncline near age site GD07 shows no warping that can be unambiguously attributed to tectonism when examined with lidar topographic profiles. The fold is thus likely concealed. Additional topographic profile analysis should be performed to assess if the Logan Hill Formation is undeformed everywhere this fold is concealed, further supporting that the deformation is not recent.

CHEHALIS ANTICLINE

Like the Centralia syncline, the Chehalis anticline was originally identified by Weaver (1937) and named by Snavely and others (1958). The fold is well constrained by bedding attitudes in the Skookumchuck Formation at the surface and by subsurface coal mine data. It is an open (interlimb angle ~90°), southeast-plunging anticline with an approximate axial plane orientation striking northwest to west and dipping ~83°SSW (n=18 measurements). The southern extent of the Chehalis anticline is unclear farther south of the Chehalis fault because bedding attitudes in the massive Lincoln Creek Formation are rare. The anticline likely continues farther northwest, concealed under the Chehalis River valley and likely exposed at the surface in the core of the Lincoln Creek uplift in the adjacent quadrangle. Its relationship to the Doty–Salzer Creek fault system is unclear due to the concealment of these structures in the Chehalis River valley.

NAPAVINE SYNCLINE

Originally named by Snavely and others (1958), the Napavine syncline is identified from field relationships, where Columbia River Basalt is flanked by Lincoln Creek Formation to the northeast within the map area and to the southwest outside of the map area. In the southwestern portion of the Centralia quadrangle, the fold is concealed and inferred to be northwest-trending and upright, and previous mapping shows this structure extending farther southeast and west. It is conceivable that the Napavine syncline is the same structure as the west-trending Chehalis River syncline that is located farther west (Snavely and others, 1958).

Lincoln Creek Uplift

The faults and folds of the Centralia quadrangle help define a broad zone of uplift along the western edge of the map area. The Lincoln Creek uplift of Snavely and others (1958) is concealed beneath alluvium of the Chehalis River valley and continues farther west beyond the quadrangle boundary. The zone of uplift is a broad structural high of shallow basement that is bounded by the Doty–Salzer Creek fault system on the south and the Scammon Creek fault and possibly other structures(?) on the northeast (Fig. M2). The displacement along these boundary faults reflects accommodation of regional stresses and is likely the cause of uplift for this basement high. This notion is at odds with Snavely and others (1958), who suggested that the Lincoln Creek uplift is caused by geosynclinal(?) flexure, but this hypothesis is not informed by plate tectonics. The Chehalis anticline likely extends farther west along the axis of this structural high, which is cored by Eocene units. This major anticline is not the cause of uplift, but rather a product of the tectonic process driving the uplift.

GEOPHYSICAL DATA AND INTERPRETATION

Gravity and Magnetic Geophysical Data

Gravity and ground magnetic geophysical data was collected by the Washington Geological Survey (WGS) in the Centralia quadrangle in 2017 (this report). These data are merged with regional gravity (Bowman, 2013) and reduced-to-pole, residual aeromagnetic surveys (R. Blakely, written commun., 2016), respectively, where the latter highlights shallow magnetic anomalies. Bedrock with similar densities and magnetic properties, such as the Skookumchuck and Lincoln Creek Formations, may be difficult to distinguish geophysically from one another. Therefore, significant differences in geophysical measurements (strong anomalies) are attributed to significant differences in rock type, such as contrasts between sedimentary rocks and denser, more magnetically susceptible volcanic rocks including the Grande Ronde Basalt, Northcraft Formation volcanic rocks, or Crescent Formation basalt. Likewise, strong magnetic anomalies may be associated with shallow highly magnetic rocks, and conversely, weak magnetic anomalies may be associated with deeper magnetic rocks with appreciable thicknesses of sedimentary rocks overlying them. However, weaker gravity and magnetic anomalies may also be the result of subtle differences between similar rock types or structures and are interpreted with caution.

The Complete Bouguer anomaly grid (CBA) of a Centralia-centered, coarsely-spaced gravity survey (<6,000-ft spacing, or <2 km) shows a basin geometry with lower accelerations south of the airport in Chehalis, WA. These lower accelerations are attributed to lower densities, which represent basin fill, and are interpreted to be an area with a greater depth to basement (Fig. M3). The boundary between these inferred density changes is delineated by the Doty–Salzer Creek fault system. Conversely, the higher values north of the fault system suggest shallower, dense basement, which is interpreted to be basalt of the Crescent Formation. Similarly, the aeromagnetic data show moderate to high anomalies north of the fault system, suggesting that rock types with higher magnetic values are closer to the surface in this part of the map area. These magnetic anomalies are also consistent with an interpretation of shallow Crescent Formation basalt. Therefore, the gravity and magnetic surveys strongly suggest tectonic uplift near the Doty–Salzer Creek fault system. Note that neither survey addresses the timing of tectonic activity.

Along the western edge of the map area, gravity and magnetic measurements along the South Scheuber Road geophysical survey line exhibit anomalies near the mapped traces of the Doty–Salzer Creek fault system and Scammon Creek fault (Fig. M3 and M2). Gravity measurements and inferred rock densities are higher between these fault traces than north and south of these faults (Fig. 16). Also along this geophysical line, the ground magnetics show relative minimums on either side of the Lincoln Creek uplift. One of these minimums is part of a northwest-oriented magnetic geophysical lineament located to the north of the Scammon Creek fault. The other minimum coincides with the Doty–Salzer Creek fault system located to the south. The co-location of two types of geophysical anomalies with mapped structures suggests a fault-bounded, structural high of elevated basement in the subsurface of the east flank of the Lincoln Creek uplift. Minor magnetic highs and lows within the uplift represent deformation associated with the Scammon Creek fault and Chehalis anticline or other concealed structures.

The magnetic and gravity anomalies along the Doty–Salzer Creek fault system are muted east of the Chehalis River valley (Fig. M2). The clear, east-west gravity contrast of the Doty fault in the valley is subtle to the east, and the magnetic contrast along the Salzer Creek fault is muted to the east. This change in geophysical character may suggest less uplift, a change in fault type, or a change in the amount of fault displacement. We speculate that the displacement along the Doty reverse(?) fault decreases to the east and strain is transferred to the Salzer Creek sinistral-reverse fault.

The alignment of geophysical lineaments and topographic lineaments expressed as northwest-, west-northwest-, and west-oriented valleys, tributaries, and drainage basins may suggest a structural grain in the subsurface. Most notably, aeromagnetics show multiple northwest-oriented features that overlap with the Kopiah and Scammon Creek faults, and a west-oriented feature that aligns with the Doty fault. Ground magnetics collected orthogonally across these structures confirm the aeromagnetic data (Figs. M2 and 17).

Taken together, gravity and magnetic geophysical data strongly suggest uplift near the western flank of the Chehalis River valley bounded by the Doty fault and other structures. The relationships between these faults and timing of the structures flanking the Lincoln Creek uplift is still poorly understood.

Active and Passive Seismic Interpretation

Clear dispersion curves were obtained (Fig. 17) after recorded ambient noise data was processed using the common midpoint spatial autocorrelation method (CMP-SPAC) (Hayashi and others, 2018). The relative maximum in phase velocity near the central portion of these curves at ~400 to 500 m (~1,300–1,640 ft) depth shows that there are layers that have different velocities in the horizontal direction ("horizontally differentiated layers") surrounding the latitude of the Doty–Salzer Creek fault system. This is interpreted to be a fracture zone with a width of ~4,265 ft (~1,300 m), where the width is approximated from the 100-m leap-frog-like station spacing (Fig. A2).

A 2D shear-wave velocity image inverted from these dispersion curves shows two geophysical anomalies (Fig. 18): (1) a subtle, deep structure of higher velocities (1,300–1,500 m\sec) that shallowly ramps upward from the south at 600 to 700 m (~1,970–2,300 ft) depth and to the north at ~500 m (1,640 ft) depth, and (2) a shallow moderate velocity layer (800–1,000 m/sec). The ramping structure of higher velocities (anomaly 1) broadly coincides with the concealed eastern flank of the Lincoln Creek uplift in the Chehalis River valley, and the shallow moderate velocity layer (anomaly 2) coincides with the Doty–Salzer Creek fault system. The combined understanding of the gravity and magnetics with these seismic surveys aids the characterization of the Doty–Salzer Creek fault system, where uplift has occurred north of the fault system, but timing is poorly understood.

Unpublished seismic reflection profiles (W. Stephenson, USGS, written commun., 2018) have contributed to our interpretation of a concealed monocline south of the Centralia–Chehalis

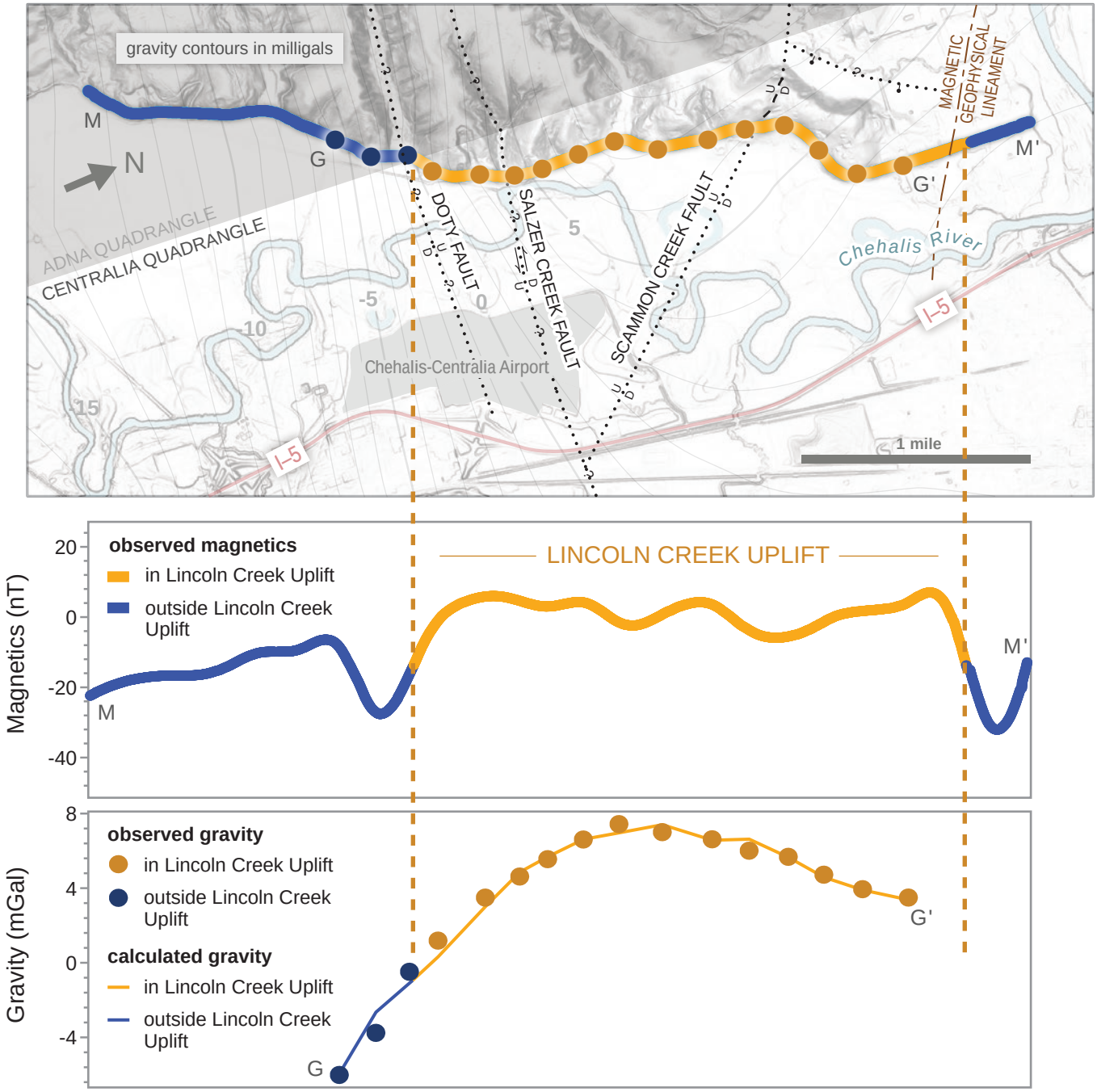

Figure 16. South Scheuber Road geophysical survey results highlighting the location of the Lincoln Creek uplift (yellow) on the western flank of the Chehalis River valley. The uplift is bound by the Doty–Salzer Creek fault system to the south (left) and the Scammon Creek fault and a magnetic geophysical lineament (brown dashed line) to the north (right). Areas outside of the Lincoln Creek uplift are shown in blue. **Top.** Simplified structural map with gravity contours (milligal), gravity stations (yellow and blue dots), and ground magnetic line (yellow and blue). **Middle.** Ground magnetic profile from M to M'. Data has been filtered using a low-pass filter with a cut-off wavelength of 1000 ft. Minor magnetic highs and lows (5 nanotesla amplitude undulations) within the Lincoln Creek uplift suggest deformation related to the Scammon Creek fault and Chehalis anticline, or other structures. **Bottom.** Gravity profile G to G'. The map and profiles are aligned with each other (yellow dashed line). Both magnetic and density (gravity) highs provide evidence of uplift that suggests shallow basement, likely Crescent Formation, representing the Lincoln Creek uplift.

municipal airport. This monocline coincides with geophysical anomalies from WGS geophysical investigations and the Doty–Salzer Creek fault system. These data also suggest that deformation related to the Doty fault is the cause for the monocline, and vertical displacement on the southern flank of the Lincoln Creek uplift is solely accommodated by the Doty fault and not the Salzer Creek fault.

STRUCTURAL SYNTHESIS

The Cascadia forearc exhibits a history of north-south compression accompanied by block rotation and dextral shear (Wells, 1981; Wells and Coe, 1985; McCaffrey and others, 2007; Wells and Sawlan, 2014; Brocher and others, 2017) that continues today (Wells and Coe, 1985; Wells and McCaffrey, 2013). Within the Centralia quadrangle, major structures include northwest-striking

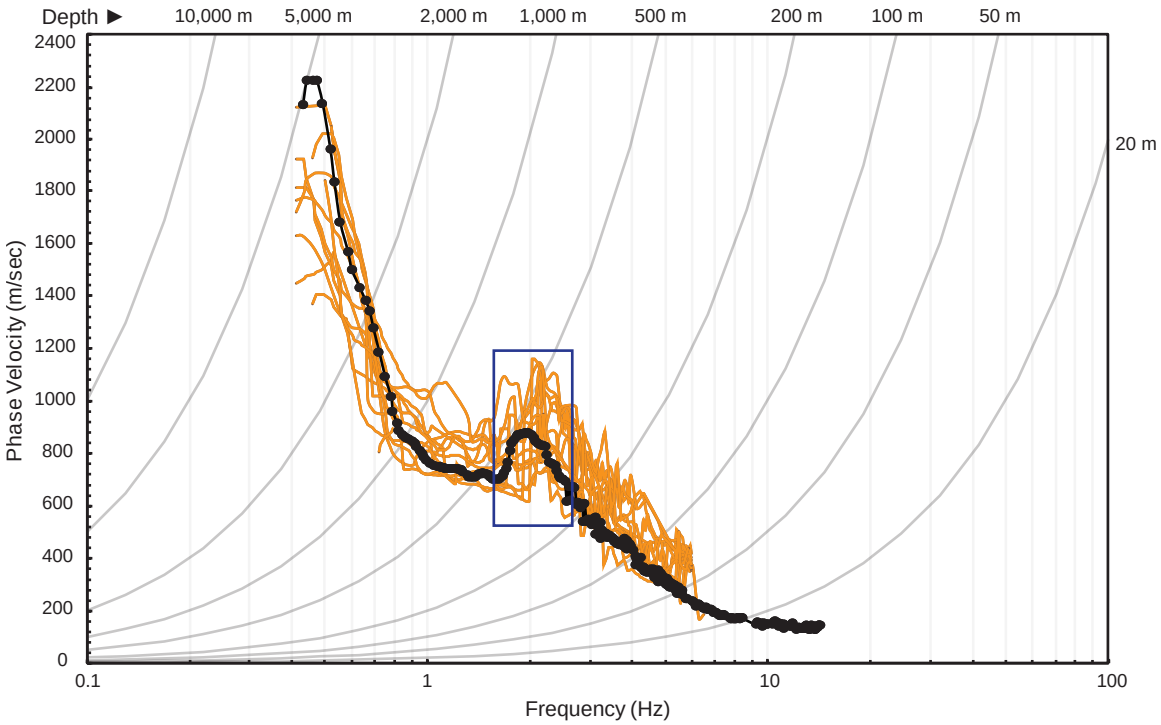

Figure 17. Results of new wireless passive seismic experiment. Figure shows all dispersion curves from ambient noise data processing using the common midpoint spatial autocorrelation method (CMP-SPAC) (Hayashi and others, 2018). Black line is a selected curve, shown as an example of what a single profile might look like. Horizontally differentiated layers (blue box) are at ~400–500 m (~1,300–1,640 ft) depth and are interpreted to be a fracture zone representing the Doty fault. Note: for depth calculations, velocity = wavelength × frequency.

dextral reverse faults, west-striking sinistral-reverse to purely(?) reverse faults, and west- to northwest-trending folds. Structures with similar orientations are also found regionally and include the St. Helens seismic zone (Weaver and Smith, 1981; 1983) and fault systems both east and west of the Centralia quadrangle (Snavely and others, 1951; 1958). Farther north, active faults of the Puget Lowland also have broadly similar geometries to those found in the Centralia quadrangle. These active fault systems include (1) northwest-striking dextral faults such as the Southern Whidbey Island fault zone and (2) west-striking faults such as the Seattle and Tacoma faults. The similarity of structural elements across such a broad region suggests a shared deformation history in the Cascadia forearc of southwest Washington.

A simple transpressional strain ellipse (McClay, 2013) with maximum-horizontal stress oriented parallel to the modern plate vector (McCaffrey and others, 2013), provides a simple, yet compelling model to explain the orientation and kinematics of major structures in the area (Fig. 19). This model implies that many of the structures would be active at the same time and interacting with each other. Because the current plate motion is similar to plate motions throughout much of the Neogene, it is not possible to use the geometric relationship of mapped faults to the modern stress field to determine if they are presently active or if they merely formed under similar stress conditions in the past. Sparse seismicity in the Centralia quadrangle—only 4 events with magnitudes between 1.0M and 2.4M at depths ranging from ~35 to ~53 km (22 to 33 mi) recorded since 1993 (Bowman and Czajkowski, 2016)—suggests one of the following: (1) significant strain is accumulating and the faults are locked, (2) the area is accumulating strain very slowly, or (3) the area is not seismically active. Since many of the structures have an orientation that is near optimal for continued deformation in the modern stress field and there appears to be evidence for Quaternary faulting of a landslide deposit (Fig. 15, significant sites S02 and S03), it is likely that the faults are active but moving at a slow rate.

CONCLUSIONS

Geologic mapping of the Centralia 7.5 minute quadrangle found possible evidence for active faults. Evidence included possible fault escarpments through landslides along the trace of the Salzer Creek fault. Newly acquired gravity, ground magnetic, and passive seismic geophysical data constrained the locations of several concealed fault strands and associated uplift. Together, mapping and geophysical data aided the characterization of structures throughout the map area that may pose a seismic hazard and could impact construction of a proposed flood retention dam on the upper Chehalis River, south of Pe Ell, WA.

Our 1:24,000-scale mapping raises new questions about the activity of the Doty, Salzer Creek, and Scammon Creek faults, while confirming much of the bedrock stratigraphy in the map area. Though the stratigraphic framework was not significantly modified from older 1:48,000-scale maps published in 1958, new geochronologic methods provided more detailed insight into the ages of several local Cenozoic formations including the Lincoln Creek, Wilkes, and Logan Hill Formations. Our work also shows that dextral-reverse and sinistral-reverse faults interact in the map area, and we hypothesize that these structures may be part of an active transpressional stress regime. Additionally, lidar and mapping revealed numerous previously unrecognized landslide deposits.

Lastly, the fault interaction zone within the Centralia quadrangle is not the optimal place to characterize active structures because the stress regime may be locally perturbed. Quadrangles farther west and farther east may best characterize the west-striking and northwest-striking faults, respectively. Therefore, the Centralia quadrangle is not the ideal place to characterize the Doty fault or the main strand of the Kopiah

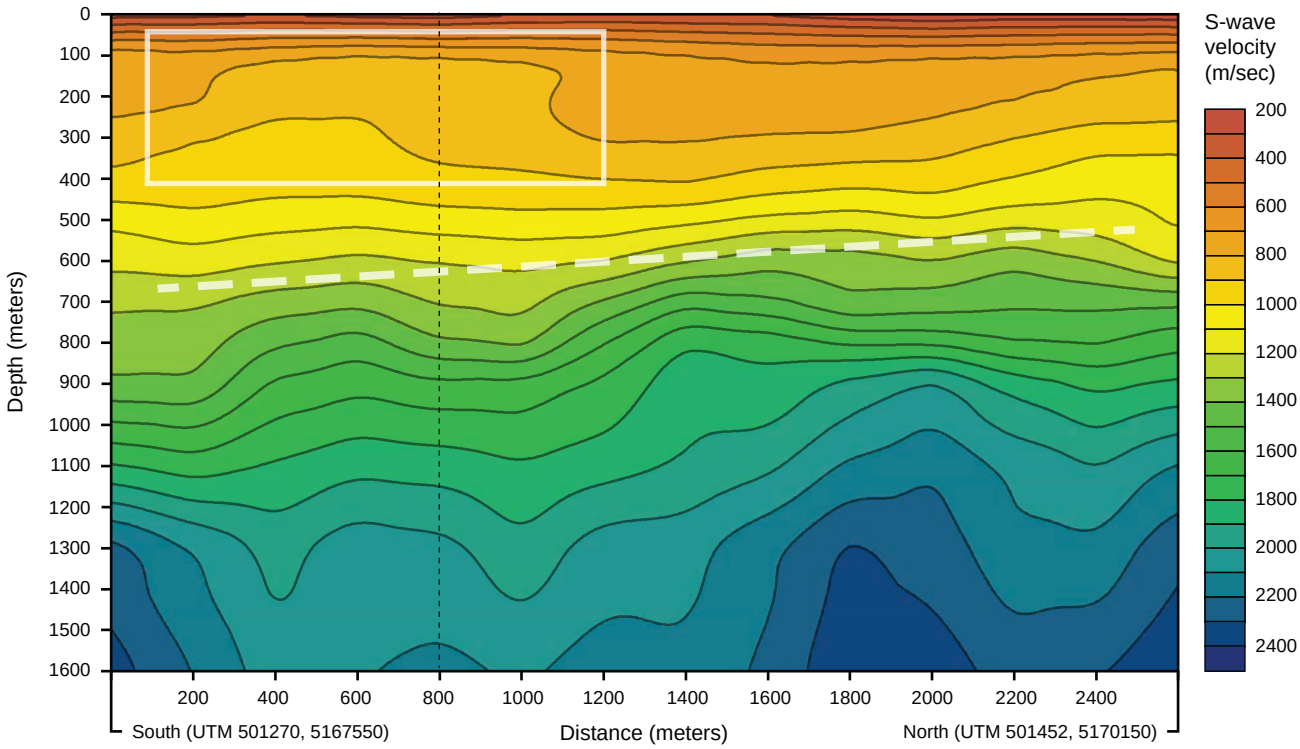

Figure 18. Two-dimensional shear-wave velocity image estimated using the dispersion curves obtained from the large passive seismic array method described in Hayashi and others (2015, 2018)(Hayashi, Geometrics Inc., written commun., 2018)(Fig. 18). A shallow moderate velocity anomaly coincides with the Doty–Salzer Creek fault system (box), and a subtle, deep velocity anomaly is gently south dipping (white dotted line). Black dotted line indicates approximate location of velocity profile highlighted in black in Fig. 18. Location of profile is shown in Figure A1.

fault, especially since potentially active structures may be better exposed in the adjacent Adna quadrangle to the west.

Recommendations for Future Work

- Future neotectonics research on both the Doty–Salzer Creek fault system and Kopiah fault (S04) in the Centralia quadrangle may greatly benefit from paleoseismic trenches at these localities to determine the activity and slip rates of mapped faults.
- Future investigations of the Kopiah fault would greatly benefit from seismic reflection surveys in the Centralia and Violet Prairie quadrangles. North–south oriented seismic reflection profiles in Zenkner Valley, the Skookumchuck River valley, and South Hanaford Creek valley could be useful in assessing the depth, sense of slip, dip direction, and dip value of the Kopiah fault.
- Additional gravity observations are needed to decrease the spacing of the station array and achieve finer resolution. These changes would allow for a more robust first-horizontal gradient calculation that could better delineate fault locations and possibly aid interpretations of slip sense.
- Additional work focused on understanding the Lincoln Creek Formation in southwest Washington may help elucidate the geochronology and paleoenvironment during the latest Eocene to the Oligocene in this area, especially because local biostratigraphic age constraints are tied to distal southern(?) California faunal systems. This additional work would require a biostratigraphic sampling campaign to re-evaluate the micro- and macrofaunal assemblages in the Lincoln Creek Formation. This would allow us to assess the bathymetry of the Chehalis basin and evaluate the tectonic controls on transgression-regression from the Eocene to Miocene (similar to Armentrout, 1987).
- Detailed soil profiles of the alluvial terraces near Mellen St bridge and near Chehalis, WA (unit Qoa) are needed to better characterize the feature and constrain its age for use in future neotectonic studies.
- A detailed hydrologic study in the Chehalis River valley to assess how groundwater may or may not be affected by folding and concealed faults.
- Additional geochronological methods need to be applied to the Logan Hill Formation to better constrain its absolute age, but given the estimated age and severe weathering of this unit, several questions remain:

  1. Using newer dating methods, precisely how old is the Logan Hill Formation? Finding a suitable dating method may be challenging.
  2. What was the ice extent for the glaciation associated with the Logan Hill Formation? Where is the transition from glacial outwash to the distal fluvial system?
  3. Are there multiple episodes of glaciation that produced Logan Hill-type deposits? If so, how many members does it have?

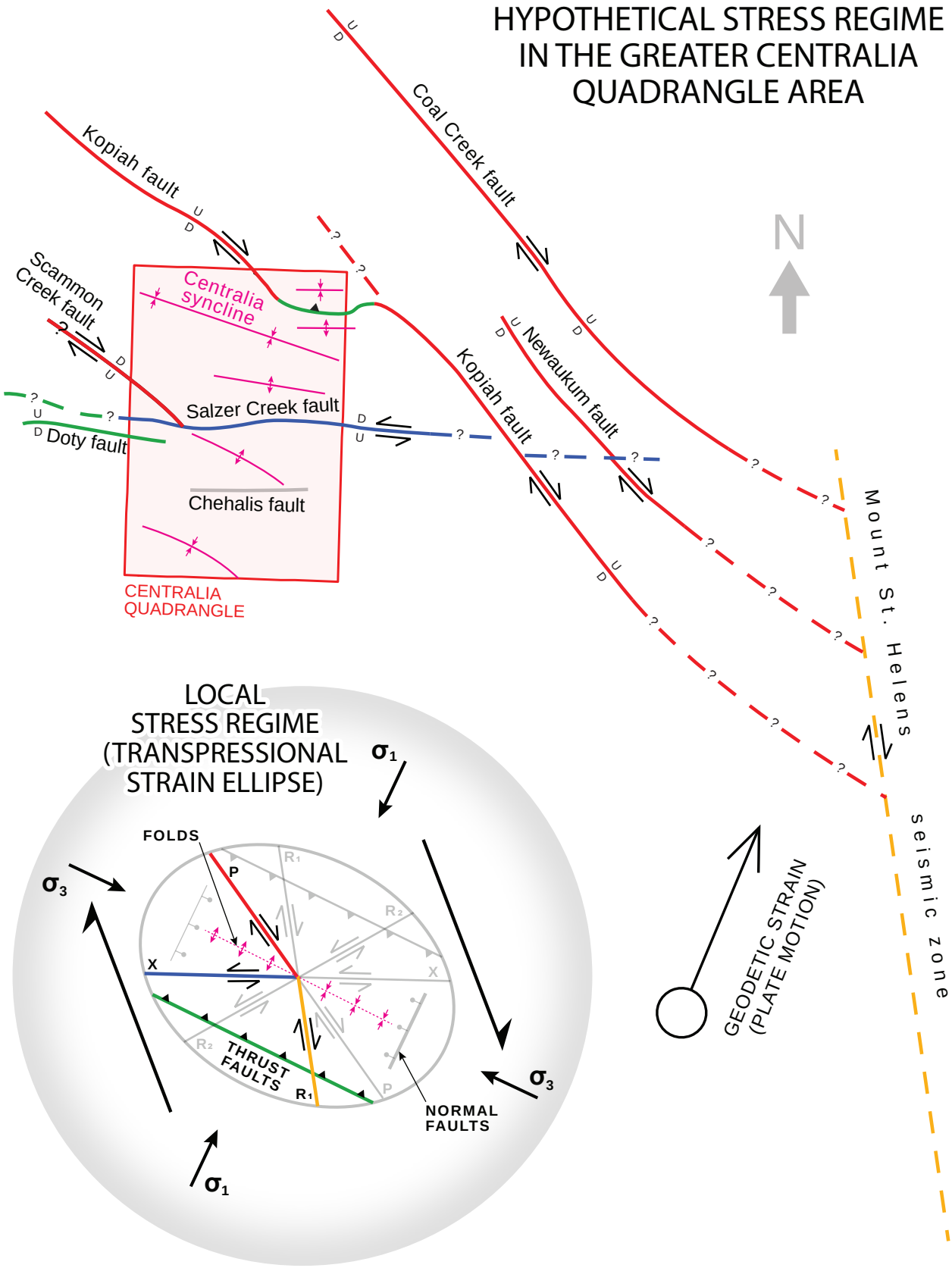

Figure 19. Hypothetical stress regime in the greater Centralia quadrangle area. This model synthesizes structures into a transpressional stress regime within the broader compressional stress regime of the Cascadia forearc. Assuming that geodetic strain from plate motions is subparallel to the orientation of σ1, then according to the strike-slip strain ellipse modified from McClay (2013), named faults are synthetic, dextral Riedel shears (orange, R1), synthetic dextral shears (red, P), antithetical, sinistral shears (blue, X), or thrust faults (green), or folds (pink). This synthesis cannot address the timing or recency of activity, but based on potentially faulted landslides at significant sites S02 and S03, these faults could be active.

4. The unit is less widespread than previously mapped by Snavely and others (1958). How spatially and temporally widespread is the Logan Hill Formation?

ACKNOWLEDGMENTS

This geologic map was funded in part by the U.S. Geological Survey (USGS) National Cooperative Geologic Mapping program under award no. G17AC00262.

We thank: Ruth Martin of the Burke Museum for analysis of biostratigraphic samples for fossils and their ages; John Wolff, director of the Peter Hooper GeoAnalytical Lab at the Washington State University, Pullman, WA for his group's analysis of samples from the Columbia River Basalt; Will Greenough (TransAlta) and Grant Newport (Weyerhaeuser) for helpful discussions and insights from proprietary exploration records; Richard Blakely (USGS) for aeromagnetic anomaly maps; Washington DNR Natural Heritage staff Joe Arnett, Tynan Gramm-Ramm-Granberg, and Joe Rocchio for assistance with identification and paleoenvironmental interpretation of plant samples; Kat Szatkowski, Lauren Burch, and WGS staff Spenser Scott, Rachel Noonan, Ian Hubert, Kara Jacobacci, Abigail Gleason, and Guy McWethy for help with field work; the WGS landslide hazard group (Kara Jacobacci, Kate Mickelson, Trevor Contreras and Stephen Slaughter) for lidar-based reconnaissance assessment of potentially unstable slopes; Mitchell Allen (DNR Forest Practices Division) for assistance with GIS project set-up and field work; Bernard Housen (Western Washington University) for paleomagnetic analyses; Timothy Walsh,Alex Steely, and Stephanie Earls of WGS for helpful discussions and research literature needs. WGS volunteer Angela Blanks-Bennett on geochemical sample analysis and geophysical data collection. We thank the private and public landowners for sharing local knowledge and permitting us to map on their land. This project was greatly aided by the kindness, generosity, and curiosity of countless Lewis County landowners, especially Sam Madsen, who allowed us onto their properties.

REFERENCES

Allmendinger, R. W.; Cardozo, Nestor; Fisher, D. M., 2013, Structural geology algorithms: Vectors and tensors: Cambridge University Press, 289 p.

Anderson, H. E.; Davis, D. W., 1995, U-Pb geochronology of the Moyie sills, Purcell Supergroup, southeastern British Columbia—Implications for the Mesoproterozoic geological history of the Purcell (Belt) basin: Canadian Journal of Earth Sciences, v. 32, no. 8, p. 1180-1193.

Armentrout, J. M., I973, Stratigraphic relationships of the Narizian-Refugian boundary in Washington (abstract): Geological Society of America Abstracts with Program, v. 5, no. 1, p. 4.

Armentrout, J. M., 1975, Molluscan biostratigraphy of the Lincoln Creek Formation, southwest Washington. *In* Weaver, D. W.; Hornaday, G. R.; Tipton, Ann, editors, Paleogene symposium and selected technical papers—Conference on future energy horizons of the Pacific coast: American Association of Petroleum Geologists Pacific Section, 50th Annual Meeting, p. 14-18.

Armentrout, J. M., 1987, Cenozoic stratigraphy, unconformity-bounded sequences, and tectonic history of southwestern Washington: Washington Division of Geology and Earth Resources Bulletin 77, p. 291-320. [http://www.dnr.wa.gov/Publications/ger_b77_papers_on_wa_geology_pt3of3.pdf; http://www.dnr.wa.gov/Publications/ger_b77_papers_on_wa_geology_pt2of3.pdf; http://www.dnr.wa.gov/Publications/ger_b77_papers_on_wa_geology_pt3of3.pdf]

Armentrout, J. M.; Franz, U. A., 1983, Tectonic control of Eocene arkosic sediment deposition, Oregon and Washington [abstract]: American Association of Petroleum Geologists, v. 67, no. 3, p. 413-414.

Armentrout, J. M.; Hull, D. A.; Beaulieu, J. D.; Rau, W. W., 1983, Correlation of Cenozoic stratigraphic units of western Oregon and Washington: Oregon Department of Geology and Mineral Industries Oil and Gas Investigation 7, 90 p., 1 plate. [http://www.oregongeology.org/pubs/ogi/OGI-07.pdf]

Beaulieu, J. D., 1971, Geologic formations of western Oregon (west of longitude 121° 30′): Oregon Department of Geology and Mineral Industries Bulletin 70, 72 p. [http://www.oregongeology.org/pubs/B/B-070.pdf]

Beck, M. E., Jr.; Burr, C. D., 1979, Paleomagnetism and tectonic significance of the Goble volcanic series, southwestern Washington: Geology, v. 7, no. 4, p. 175-179.

Beikman, H. M.; Rau, W. W.; Wagner, H. C., 1967, The Lincoln Creek Formation, Grays Harbor basin, southwestern Washington: U.S. Geological Survey Bulletin 1244-I, 14 p. [https://pubs.usgs.gov/bul/1244i/report.pdf]

Benton, M. J.; Harper, D. A., 1997, Basic palaeontology: Prentice Hall, 360 p.

Bohor, B. F.; Triplehorn, D. M., 1993, Tonsteins: altered volcanic-ash layers in coal-bearing sequences: Geological Society of America, Special Paper 285, 44 p.

Bowman, J. D.; Czajkowski, J. L., 2016, Washington State seismogenic features database—GIS data: Washington Division of Geology and Earth Resources Digital Data Series 1, version 4.1, originally issued December 2013. [http://www.dnr.wa.gov/publications/ger_portal_seismogenic_features.zip]

Boynton, W. V., 1984, Cosmochemistry of the rare earth elements: Meteorite studies. *In* Henderson, P., editor, Rare Earth Element Geochemistry: Elsevier, p. 63–114.

Bretz, J. H., 1913, Glaciation of the Puget Sound region: Washington Geological Survey Bulletin 8, 244 p., 3 plates. [http://www.dnr.wa.gov/publications/ger_b8_glaciation_pugetsound.pdf]

Brocher, T. M.; Wells, R. E.; Lamb, A. P.; Weaver, C. S., 2017, Evidence for distributed clockwise rotation of the crust in the northwestern United States from fault geometries and focal mechanisms: Tectonics, v. 36, no. 5, p. 787-818.

Bromley, R. G., 1996, Trace fossils—Biology, taphonomy and applications: Chapman & Hall, 361 p.

Buckovic, W. A., 1979, The Eocene deltaic system of west-central Washington. *In* Armentrout, J. M.; Cole, M. R.; Ter Best, Harry, Jr., editors, Cenozoic paleogeography of the western United States: Society of Economic Paleontologists and Mineralogists Pacific Section, Pacific Coast Paleogeography Symposium 3, p. 147-163.

Cardozo, Nestor; Allmendinger, R. W., 2013, Spherical projections with OSXStereonet: Computers & Geosciences, v. 51, p. 193-205.

Clowes, R. M.; Brandon, M. T.; Green, A. G.; Yorath, C. J.; Sutherland Brown, A.; Kanasewich, E. R.; Spencer, C. J., 1987, LITHOPROBE—Southern Vancouver Island—Cenozoic subduction complex imaged by deep seismic reflections: Canadian Journal of Earth Sciences, v. 24, no. 1, p. 31-51.

Dethier, D. P.; Bethel, J. P., 1981, Surficial deposits along the Cowlitz River near Toledo, Lewis County, Washington: U.S. Geological Survey Open File Report 81-1043, 10 p., 1 plate. [http://pubs.er.usgs.gov/usgspubs/ofr/ofr811043]

Dickinson, W. R.; Gehrels, G. E., 2009, Use of U-Pb ages of detrital zircons to infer maximum depositional ages of strata: a test against a Colorado Plateau Mesozoic database: Earth and Planetary Science Letters, v. 288, no. 1-2, p. 115-125.

Dragovich, J. D.; Gilbertson, L. A.; Lingley, W. S., Jr.; Polenz, Michael; Glenn, Jennifer, 2002, Geologic map of the Fortson 7.5-minute quadrangle, Skagit and Snohomish Counties, Washington: Washington Division of Geology and Earth Resources Open File Report 2002-6, 1 sheet, scale 1:24,000. [http://www.dnr.wa.gov/Publications/ger_ofr2002-6_geol_map_fortson_24k.pdf]

Evans, K. V.; Aleinikoff, J. N.; Obradovich, J. D.; Fanning, C. M., 2000, SHRIMP U–Pb geochronology of volcanic rocks, Belt Supergroup, western Montana: evidence for rapid deposition of sedimentary strata: Canadian Journal of Earth Sciences, v. 37, no. 9, p. 1287-1300.

Fossen, Haakon; Schultz, R. A.; Shipton, Z. K.; Mair, Karen, 2007, Deformation bands in sandstone: a review: Journal of the Geological Society, v. 164, no. 4, p. 755-769. [https://folk.uib.no/nglhe/Papers/JGS%202007%20DB%20review%20paper.pdf]

Fedo, C. M.; Sircombe, K. N.; Rainbird, R. H., 2003, Detrital zircon analysis of the sedimentary record: Reviews in Mineralogy and Geochemistry, v. 53, no. 1, p. 277-303.

Fiksdal, A. J., 1978, Slope stability of the Centralia-Chehalis area, Lewis County, Washington: Washington Division of Geology and Earth Resources Open File Report 78-2, 4 p., 1 plate, scale 1:62,500. [http://www.dnr.wa.gov/publications/ger_ofr78-2_slope_stability_centralia_chehalis_62k.pdf]

Finn, C. A., 1990, Geophysical constraints on Washington convergent margin structure: Journal of Geophysical Research, v. 95, no. B12, p. 19,533-19,546.

Fiske, R. S., 1963, Subaqueous pyroclastic flows in the Ohanapecosh Formation, Washington: Geological Society of America Bulletin, v. 74, no. 4, p. 391-406.

Flores, R. M.; Johnson, S. Y., 1995, Sedimentology and lithofacies of the Eocene Skookumchuck Formation in the Centralia coal mine, southwest Washington [abstract]: American Association of Petroleum Geologists Bulletin, v. 79, no. 4, p. 584-585.

Gaschnig, R. M.; Vervoort, J. D.; Lewis, R. S.; McClelland, W. C., 2010, Migrating magmatism in the northern US Cordillera: in situ U–Pb geochronology of the Idaho batholith: Contributions to Mineralogy and Petrology, v. 159, no. 6, p. 863-883.

Geometrics, 2009, SeisImager/SWTM Manual, Version 3.0: Geometrics, 314 p.

Geometrics, 2016, SeisImager/SW-ProTM Manual, Version 1.2: Geometrics, 74 p.

Hagen, R. A., 1987, The geology and petrology of the Northcraft Formation, Lewis County, Washington: University of Oregon Master of Science thesis, 252 p., 1 plate.

Hayashi, Koichi; Craig, Mitchell; Kita, Takaho; Inazaki, Tomio, 2015, CMP spatial autocorrelation analysis of multichannel passive surface-wave data [abstract]: SEG Technical Program Expanded Abstracts, p. 2200-2204. [https://library.seg.org/doi/abs/10.1190/segam2015-5913708.1]

Hayashi, Koichi; Lorenzo, J. M.; Gostic, Adam, 2018, Application of 2D ambient noise tomography to levee safety assessment in New Orleans [abstract]: Proceedings, 31st Symposium on the Application of Geophysics to Engineering and Environmental Problems (SAGEEP), 5 p. [https://www.xcdsystem.com/sageep/abstract/File1988/43_UploadExtendedAbstract_1221073301.pdf]

Heller, P. L.; Ryberg, P. T., 1983, Sedimentary record of subduction to forearc transition in the rotated Eocene basin of western Oregon: Geology, v. 11, no. 7, p. 380-383.

Howe, H. V., 1926, Astoria—Mid-Tertic type of Pacific coast: Pan-American Geologist, v. 45, no. 4, p. 295-306.

Irvine T. N.; Baragar, W. R. A., 1971, A guide to the chemical classification of common volcanic rocks: Canadian Journal of Earth Sciences, v. 8, no. 5, p. 523-548.

Johnson, S. Y.; Blakely, R. J.; Stephenson, W. J.; Dadisman, S. V.; Fisher, M. A., 2004, Active shortening of the Cascadia forearc and implications for seismic hazards of the Puget Lowland: Tectonics, v. 23, no. 1, 27 p. [https://agupubs.onlinelibrary.wiley.com/doi/epdf/10.1029/2003TC001507]

Johnson, S. Y.; Potter, C. J.; Armentrout, J. M.; Miller, J. J.; Finn, C. A.; Weaver, C. S., 1996, The southern Whidbey Island fault—An active structure in the Puget Lowland, Washington: Geological Society of America Bulletin, v. 108, no. 3, p. 334-354, 1 plate.

Kadri, M. M., 1982, Structure and influence of the Tillamook uplift on the stratigraphy of the Mist Area, Oregon Portland State University Master of Science thesis, 105 p., 1 plate.

Kant, L. B.; Tepper, J. H.; Eddy, M. P., 2015, Basalt of Summit Creek—Eocene Magmatism Associated with Farallon Slab Break Off [abstract]: Eos (American Geophysical Union Transactions), 2015 Fall Meeting, Abstract V23C-03. [https://agu.confex.com/agu/fm15/meetingapp.cgi/Paper/69408]

LaMaskin, T. A., 2012, Detrital zircon facies of Cordilleran terranes in western North America: GSA Today, v. 22, no. 3, p. 4-11. [http://www.geosociety.org/gsatoday/archive/22/3/article/i1052-5173-22-3-4.htm]

Lea, P. D., 1984, Pleistocene glaciation at the southern margin of the Puget lobe, western Washington: University of Washington Master of Science thesis, 96 p., 3 plates.

LeBas M. J.; LeMaitre, R. W.; Streckeisen, Albert; Zanettin, Bruno, 1986, A chemical classification of volcanic rocks based on the total alkali silica diagram: Journal of Petrology, v. 27, no. 3, p. 745-750.

Lewis, J. C.; Unruh, J. R.; Twiss, R. J., 2003, Seismogenic strain and motion of the Oregon coast block: Geology, v. 31, no. 2, p. 183-186.

Lewis, R. S.; Vervoort, J. D.; Burmester, R. F.; Oswald, P. J., 2010, Detrital zircon analysis of Mesoproterozoic and Neoproterozoic metasedimentary rocks of north central Idaho: implications for development of the Belt-Purcell basin: Canadian Journal of Earth Sciences, v. 47, no. 11, p. 1383-1404.

Livingston, V. E., Jr., 1966, Geology and mineral resources of the Kelso-Cathlamet area, Cowlitz and Wahkiakum Counties, Washington: Washington Division of Mines and Geology Bulletin 54, 110 p., 2 plates, scale 1:24,000. [http://www.dnr.wa.gov/publications/ger_b54_geol_min_res_kelso_cathlemet.pdf]

Logan, R. L.; Walsh, T. J.; Stanton, B. W.; Sarikhan, I. Y., 2009, Geologic map of the Maytown 7.5-minute quadrangle, Thurston County, Washington: Washington Division of Geology and Earth Resources Geologic Map GM-72, 1 sheet, scale 1:24,000. [http://www.dnr.wa.gov/publications/ger_ gm72_geol_map_maytown_24k.pdf]

McCaffrey, Robert; King, R. W.; Payne, S. J.; Lancaster, Matthew, 2013, Active tectonics of northwestern U. S. inferred from GPS-derived surface velocities: Journal of Geophysical Research Solid Earth, v. 118, p. 709-723. [https://agupubs.onlinelibrary.wiley.com/doi/epdf/10.1029/2012JB009473]

McCaffrey, Robert; Qamar, A. I.; King, R. W.; Wells, Ray; Khazaradze, Giorgi; Williams, C. A.; Stevens, C. W.; Vollick, J. J.; Zwick, P. C., 2007, Fault locking, block rotation and crustal deformation in the Pacific Northwest: Geophysical Journal International, v. 169, no. 3, p. 1315-1340.

McClay, K. R., 2013, The mapping of geological structures: John Wiley & Sons, 168 p.

Nelson, W. J., 1981, Faults and their effect on coal mining in Illinois: Illinois Institute of Natural Resources, State Geological Survey Division Circular 523, 38 p. [https://www.ideals.illinois.edu/bitstream/handle/2142/44642/faultstheireffec523nels.pdf?sequence=2]

Nilsen, T. H., 1976, Washington gravity base station network: Washington Division of Geology and Earth Resources Information Circular 59, 83 p. [http://www.dnr.wa.gov/Publications/ger_ic59_wa_gravity_base_network.pdf]

Pratt, T. L.; Johnson, S. Y.; Potter, C. J.; Stephenson, W. J.; Finn, C. A., 1997, Seismic reflection images beneath Puget Sound, western Washington State—The Puget Lowland thrust sheet hypothesis: Journal of Geophysical Research, v. 102, no. B12, p. 27,469-27,489. [https://agupubs.onlinelibrary.wiley.com/doi/pdf/10.1029/97JB01830]

Phillips, W. M.; Walsh, T. J.; Hagen, R. A., 1989, Eocene transition from oceanic to arc volcanism, southwest Washington. *In* Muffler, L. J. P.; Weaver, C. S.; Blackwell, D.D., editors, Proceedings of workshop XLIV—Geological, geophysical, and tectonic setting of the Cascade Range: U.S. Geological Survey Open-File Report 89-178, p. 199-256. [https://pubs.er.usgs.gov/publication/ofr89178]

Polenz, Michael; Allen, M. D.; Legorreta Paulín, Gabriel; Eungard, D. W.; Cakir, Recep; Scott, S. P.; Mahan, S. A., 2016, Geologic map of the Shelton Valley 7.5-minute quadrangle, Mason County, Washington: Washington Division of Geology and Earth Resources Map Series 2016-02, 1 sheet, scale 1:24,000, 45 p. text. [http://www.dnr.wa.gov/publications/ger_ms2016-02_geol_map_shelton_valley_24k.zip]

Polenz, Michael; Favia, J. G.; Hubert, I. J.; Legorreta Paulín, Gabriel; Cakir, Recep, 2015, Geologic map of the Port Ludlow and southern half of the Hansville 7.5-minute quadrangles, Kitsap and Jefferson Counties, Washington: Washington Division of Geology and Earth Resources Map Series 2015-02, 1 sheet, scale 1:24,000, 40 p. text. [http://www.dnr.wa.gov/publications/ger_ms2015-02_geol_map_port_ludlow_hansville_24k.zip]

Polenz, Michael; Ostrom, B. A.; Lau, T. R.; Sadowski, A. J.; Blanks-Bennett, A. L.; Cakir, Recep; Tepper, J. H.; DuFrane, S. A.; Legorreta Paulín, Gabriel, 2017, Geologic map of the Violet Prairie 7.5-minute quadrangle, Thurston and Lewis counties, Washington: Washington Geological Survey Map Series 2018-04, 1 sheet, scale 1:24,000, XY p. text. [http://www.dnr. wa.gov/publications/ger_ms2018-0X_geol_map_violet_prairie_24k.zip]

Polenz, Michael; Vermeer, J. L.; Legoretta Paulín, G.; Tepper, J. H.; Mahan, S. A.; Cakir, Recep, 2017, Geologic map of the Littlerock 7.5-minute quadrangle, Thurston County, Washington; Washington Geological Survey Map Series 2017-01, 1 sheet, scale 1:24,000, 36 p. text. [http://www.dnr.wa.gov/publications/ger_ms2017-01_geol_map_littlerock_24k.zip]

Porter, S. C., 1975, Weathering rinds as a relative-age criterion—Application to subdivision of glacial deposits in the Cascade Range: Geology, v. 3, no. 3, p. 101-104.

Polivka, D. R., 1984, Quaternary volcanology of the West Crater-Soda Peaks area, southern Washington Cascade Range: Portland State University Master of Science thesis, 78 p., 1 plate. [http://pdxscholar.library.pdx.edu/cgi/viewcontent.cgi?article=4404&context=open_access_etds]

Prothero, D. R.; Armentrout, J. M., 1985, Magnetostratigraphic correlation of the Lincoln Creek Formation, Washington Implications for the age of the Eocene/Oligocene boundary: Geology, v. 13, no. 3, p. 208-211.

Reidel, S. P.; Camp, V. E.; Tolan, T. L.; Martin, B. S.; Ross, M. E.; Wolff, J. A.; Wells, R. E., 2013, The Columbia River flood basalt province: Stratigraphy, areal extent, volume, and physical volcanology. *In* Reidel, S. P.; Camp, V. E.; Ross, M. E.; Wolff, J. A.; Martin, B. S.; Tolan, T. L.; Wells, R. E., editors, The Columbia River flood basalt province: Geological Society of America Special Paper 497, p. 1-43.

Reidel, S. P.; Tolan, T. L., 2013, The Grande Ronde Basalt, Columbia River Basalt Group. *In* Reidel, S. P.; Camp, V. E.; Ross, M. E.; Wolff, J. A.; Martin, B. S.; Tolan, T. L.; Wells, R. E., editors, The Columbia River flood basalt province: Geological Society of America Special Paper 497, p. 117–153.

Roberts, A. E., 1958, Geology and coal resources of the Toledo-Castle Rock district, Cowlitz and Lewis Counties, Washington: U.S. Geological Survey Bulletin 1062, 71 p., 6 plates. [https://pubs.er.usgs.gov/publication/b1062]

Ross, G. M.; Parrish, R. R.; Winston, Don, 1992, Provenance and U-Pb geochronology of the Mesoproterozoic Belt Supergroup (northwestern United States): implications for age of deposition and pre-Panthalassa plate reconstructions: Earth & Planetary Science Letters, v. 113, no. 1-2, p. 57-76.

Seilacher, A., 2007, Trace fossil analysis: Springer, 226 p.

Shultz, J. M., 1988, Mid-Tertiary volcanic rocks of the Timberwolf Mountain area, south-central Cascades, Washington: Western Washington University Master of Science thesis, 145 p., 1 plate, 1:24,000.

Snavely, P. D., Jr.; Brown, R. D., Jr.; Roberts, A. E.; Rau, W. W., 1958, Geology and coal resources of the Centralia–Chehalis district, Washington, with a section on Microscopical character of Centralia–Chehalis coal, by J. M. Schopf: U.S. Geological Survey Bulletin 1053, 159 p., 6 plates. [https://pubs.er.usgs.gov/publication/b1053]

Snavely, P. D., Jr.; Roberts, A. E.; Hoover, Linn, Jr.; Pease, M. H., Jr., 1951, Geology of the eastern part of the Centralia–Chehalis coal district, Lewis and Thurston Counties, Washington: U.S. Geological Survey Coal Investigations Map, C-8, 2 sheets, scale 1:31,680. [https://pubs.er.usgs.gov/publication/coal8]

Snavely, P. D., Jr.; Wagner, H. C., 1963, Tertiary geologic history of western Oregon and Washington: Washington Division of Mines and Geology Reports of Investigations 22, 25 p. [http://www.dnr.wa.gov/publications/ger_ri22_tert_geol_west_or_wa.pdf]

Snavely, P. D., Jr.; Wagner, H. C., 1982, Geologic cross section across the continental margin of southwestern Washington: U.S. Geological Survey Open-File Report 82-459, 10 p., 1 plate. [http://pubs.er.usgs.gov/publication/ofr82459]

Snavely, P. D., Jr.; Wagner, H. C.; Lander, D. L., 1980, Interpretation of the Cenozoic geologic history, central Oregon continental margin: Geological Society of America Bulletin, v. 91, no. 3, p. 143-146.

Stanley, W. D.; Johnson, S. Y.; Nuccio, V. F., 1994, Analysis of deep seismic reflection and other data from the southern Washington Cascades: U.S. Geological Survey Open-File Report 94-159, 180 p. [https://pubs.er.usgs.gov/publication/ofr94159]

Starkey, H. C.; Blackmon, P. D.; Hauff, P. L., 1984, The routine mineralogical analysis of clay-bearing samples: U.S. Geological Survey Bulletin 1563, 32 p., 1 plate. [https://pubs.er.usgs.gov/publication/b1563]

Sun, S.-s.; McDonough; W. F., 1989, Chemical and isotopic systematics of oceanic basalts: Implications for mantle composition and processes. *In* Saunders, A. D; Norry, M. J., editors, Magmatism in the Ocean Basins: Geological Society of London Special Publication 42, p. 313-345.

Telford, W. M.; Geldart, L. P.; Sheriff, R. E., 1990, Applied geophysics; 2nd ed.: Cambridge University Press, 770 p.

Trehu, A. M.; Asudeh, Isa; Brocher, T. M.; Luetgert, J. H.; Mooney, W. D.; Nabelek, J. L.; Nakamura, Y., 1994, Crustal architecture of the Cascadia forearc: Science, v. 266, no. 5183, p. 237-243.

USGS, 2016, SWWA Foothills 2017 project, Western Washington 3DEP LiDAR, Collected March 17, 2016 to September 30, 2016 by Quantum Spatial Inc., 3-ft resolution, accessed May 16, 2018 [http://lidarportal.dnr.wa.gov/], metadata available on portal [ger_swwa_foothills_2017_lidar_report.pdf].

Vermeesch, Pieter, 2012, On the visualisation of detrital age distributions: Chemical Geology, v. 312-313, p. 190-194.

Walsh, T. J.; Logan, R. L., 2005, Geologic map of the East Olympia 7.5-minute quadrangle, Thurston County, Washington: Washington Division of Geology and Earth Resources Geologic Map GM-56, 1 sheet, scale 1:24,000. [http://www.dnr.wa.gov/Publications/ger_gm56_geol_map_eastolympia_24k.pdf]

Walsh, T. J.; Phillips, W. M., 1983, Rank of Eocene coals in western and central Washington State—A reflection of Cascade plutonism?: Washington Division of Geology and Earth Resources Open File Report 83-16, 21 p. [http://www.dnr.wa.gov/publications/ger_ofr83-16_eocene_coal_rank.pdf]

Washington Division of Geology and Earth Resources, 2016, Surface geology, 1:100,000—GIS data, November 2016: Washington Division of Geology and Earth Resources Digital Data Series 18, version 3.1, previously released June 2010. [https://www.dnr.wa.gov/publications/ger_portal_surface_geology_100k.zip]

Wang, Kelin, 1996, Simplified analysis of horizontal stresses in a buttressed fore arc sliver at an oblique subduction zone: Geophysical Research Letters, v.23, no. 16, p. 2021-2024.

Weaver, C. E., 1912, A preliminary report on the Tertiary paleontology of western Washington: Washington Geological Survey Bulletin 15, 80 p. [http://www.dnr.wa.gov/publications/ger_b15_prelim_rep_teriary_paleo_western_wa.pdf]

Weaver, C. E., 1937, Tertiary stratigraphy of western Washington and northwestern Oregon: University of Washington Publications in Geology, v. 4, 266 p. [http://babel.hathitrust.org/cgi/pt?id=uc1.b3666455;view=1up;seq=5]

Weaver, C. E.; Beck, Stanley; Bramlette, M. N.; Carlson, Stanley; Clark, B. L.; Dibblee, T. W., Jr.; Durham, Wyatt; Ferguson, G. C.; Forest, L. C.; Grant, U. S., IV; Hill, Mason; Kelley, F. R.; Kleinpell, R. M.; Kleinpell, W. D.; Marks, J.; Putnam, W. C.; Schenck, H. G.; Taliaferro, N. L.; Thorup, R. R.; Watson, Elizabeth; White, R. T., 1944, Correlation of the marine Cenozoic formations of western North America: Geological Society of America Bulletin, v. 55, no. 5, p. 569-598.

Weaver, C. E.; Palmer, K. V. W., 1922, Fauna from the Eocene of Washington: University of Washington Publications in Geology, v. 1, no. 3, 55 p. [http://www.archive.org/details/faunaeocene00weavrich]

Weaver, C. S.; Smith, S. W., 1981, The St. Helens seismic zone—A major crustal fault zone in western Washington [abstract]: Eos (American Geophysical Union Transactions), v. 62, no. 45, p. 966.

Weaver, C. S.; Smith, S. W., 1983, Regional tectonic and earthquake hazard implications of a crustal fault zone in southwestern Washington: Journal of Geophysical Research, v. 88, p. 10371-10383.

Wells, R. E., 1979, Geologic map of the Cape Disappointment-Naselle River area, Pacific County, Washington: U.S. Geological Survey Open-File Report 79-389, 1 sheet, scale 1:48,000. [https://pubs.er.usgs.gov/publication/ofr79389]

Wells, R. E., 1981, Geologic map of the eastern Willapa Hills, Cowlitz, Lewis, Pacific, and Wahkiakum Counties, Washington: U.S. Geological Survey Open-File Report 81-674, 1 sheet, scale 1:62,500. [https://pubs.er.usgs.gov/publication/ofr81674]

Wells, Ray E., 1989, Geologic map of the Cape Disappointment-Naselle River area, Pacific and Wahkiakum Counties, Washington: U.S. Geological Survey Miscellaneous Investigations Series Map I-1832, 1 sheet, scale 1:62,500. [http://pubs.er.usgs.gov/publication/i1832]

Wells, R. E.; Coe, R. S., 1985, Paleomagnetism and geology of Eocene volcanic rocks of southwest Washington, implications for mechanisms of tectonic rotation: Journal of Geophysical Research Solid Earth, v. 90, no. B2, p. 1925-1947.

Wells, R. E.; Engebretson, D. C.; Snavely, P. D., Jr.; Coe, R. S., 1984, Cenozoic plate motions and the volcano-tectonic evolution of western Oregon and Washington: Tectonics, v. 3, no. 2, p. 275-294.

Wells, R. E.; McCaffrey, Robert, 2013, Steady rotation of the Cascade arc: Geology, v. 41, no. 9, p. 1027-1030.

Wells, R. E.; Blakely, R. J.; Wech, A. G.; McCrory, P. A.; Michael, Andrew, 2017, Cascadia subduction tremor muted by crustal faults: Geology, v. 45, no. 6, p. 515-518. [https://pubs.geoscienceworld.org/gsa/geology/article/45/6/515/207933/cascadia-subduction-tremor-muted-by-crustal-faults]

Wells, Ray; Bukry, David; Friedman, Richard; Pyle, Doug; Duncan, Robert; Haeussler, Peter; Wooden, Joe, 2014, Geologic history of Siletzia, a large igneous province in the Oregon and Washington Coast Range: Correlation to the geomagnetic polarity time scale and implications for a long-lived Yellowstone hotspot: Geosphere, July 14th, 2014, 28 p.

Wells, Ray E.; Sawlan, Michael G., 2014, Preliminary geologic map of the eastern Willapa Hills, Cowlitz, Lewis, and Wahkiakum Counties, Washington: U.S. Geological Survey Open-File Report 2014-1063, 2 sheets, scale 1:50,000.

Wells, R. E.; Weaver, C. S.; Blakely, R. J., 1998, Fore-arc migration in Cascadia and its neotectonic significance: Geology, v. 26, no. 8, p. 759-762.

Appendix A. Geophysical Methods: Data Collection and Analysis

MAGNETICS

Ground magnetic surveys were conducted using two portable magnetometers: a G-859 Cesium Vapor Magnetometer and G-857 Proton Procession (both manufactured by Geometrics, Inc.). The former was used for survey lines at a 0.5 Hz sample rate, whereas the latter was used for lines at a 0.2 Hz sample rate for the base station measurements. Daily checks were made for calibration purposes between the two magnetometers. The Centralia base station was located at 46.67537°N, 122.93258°W and the Violet Prairie base station at 46.77675°N, 123.06137°W (Fig. M2). Internal clocks on both instruments were synchronized using a handheld GPS (Garmin GPSmap 60CSx). Ground magnetic measurements were then completed with efforts to minimize the interference of magnetic objects on and near the observer. These efforts included removing magnetic materials such as jewelry and cell phones, waiting for cars to pass before sampling, and avoiding areas with large electromagnetic sources such as power lines and junkyards.

Before modeling, ground magnetic data were pre-processed through Geometrics Magmap2000 software for de-spiking and correcting diurnal variations measured at the base station. Pre-processed data was transferred to the OasisMontaj modeling software. In OasisMontaj, a band-pass filter was applied to further eliminate local spikes in the data. The result is a map that isolates the anomalies produced by near-surface magnetic rocks. Geophysical cross section models were produced with 2D GM-SYS Modeling software (Geosoft, Inc.). Model geometry (depth) and material properties (magnetic susceptibilities) are constrained from the literature (Finn, 1990; Telford and others, 1990) and local borehole information, where available.

GRAVITY

Microgravity surveys were conducted using a LaCoste Romberg Model G-908 gravimeter at a total of 183 stations with 820-ft spacing (0.25 km) along profiles. Gravity readings were collected in structurally significant areas that were identified using current observations, previous studies, and reduced-to-pole, residual “shallow” aeromagnetic anomalies (R. Blakely, U.S. Geological Survey, written commun., 2017). We also conducted gravity surveys in the Centralia quadrangle with approximately 3,281- to 4,922-ft grid spacing (1.0–1.5 km)(Fig. M3). These measurements significantly enhanced the 2D and 3D gravity anomalies in the quadrangle areas. A regional gravity base station called Chehalis B (46.394169°N, 122.580970°W)(Nielsen, 1976) was selected for calibration of the readings, specifically to observe and correct for tidal effects. A minimum of three gravity readings with a 0.00 to 0.02 milligal sensitivity range were collected at each station. Time was recorded during the measurements, and readings at each station were averaged for the data reduction process. Average readings were imported into Geosoft’s OasisMontaj software and tidal, drift, latitude, and terrain corrections were performed with an assigned crustal density of 2.67 g/cm^3. A grid of regional terrain was created in OasisMontaj that combines a regional 10 m DEM clipped at a distance of 50 kilometers from the map area and centered on the survey area and a local 2 m lidar DEM clipped at a distance of 7 kilometers from the map area. Terrain corrections were calculated from this grid using an outer distance of 50 km and an inner correction distance of 100 m. A Complete Bouguer Anomaly grid (CBA) was created using minimum surface curvature in OasisMontaj. Geophysical cross section models were calculated with the 2D GM-SYS Modeling software. The CBA grid was used to model areas of interest. Block model densities were constrained using previous regional studies (Finn, 1990) or averaged values (Telford and others, 1990).

ACTIVE AND PASSIVE SEISMIC SURVEY METHODS

One active and four passive seismic surveys were performed in the Centralia quadrangle, near the Centralia–Chehalis Airport. Multi-channel Analysis Surface Waves (MASW) and Microtremor Array Measurement (MAM) survey methods were used to estimate 1D and 2D shear-wave velocity profiles. Two passive seismic surveys were conducted using 48- and 72-channel Geode seismographs with natural frequency 4.5 Hz geophones with 5 meter spacing. These experiments provided constraints on surface wave dispersion at shallow depths (0–200 m).

Additionally, new wireless seismographs called “Atoms” (manufactured by Geometrics Inc.) with 2-Hz geophones were used to investigate deeper structures in the area (1–2 km). A long-range passive array method (Hayashi and others, 2018; Hayashi and others, 2015) was employed, with 13 wireless stations having varying sensor separations (10 and 100 m). To run a two-dimensional long-range passive array survey for a maximum desirable separation (target depth >1.5 km), 4 wireless seismographs were expanded leap-frog-like from the southern end to the north end of the seismic line, until the maximum separation (~2.6 km) was reached (see Fig. A2). Total data acquisition took about 6 hours for all overlapping leap-frogged lines, where each line was surveyed in ~30 minutes. The placement of sensors provided a variety of triangular geometries (Fig. A1). The recorded ambient noise data were processed using the common midpoint spatial autocorrelation method (CMP-SPAC)(Hayashi and others, 2018) and clear dispersion curves were obtained.

Dispersion curves for the long-range passive seismic survey are shown in Figure 18. The curves show layers that have different velocities in the horizontal direction (“horizontally differentiated layers”). The relative maximum in phase velocity near

the central portion of these curves at ~400–500 m depth shows that there are horizontally differentiated layers surrounding the latitude of the Doty fault. These layers suggest the presence of a fracture zone with a width of ~4,265 ft (~1,300 m), where the width is approximated from the 100 m leap-frog-like station spacing. Figure A3 shows selected dispersion curves for all of the active and passive seismic surveys that were conducted. The overlap between the original shallow-focused methods and the new deep-focused surveys at lower frequencies indicates that the two survey methods are in agreement with each other.

PALEOMAGNETISM

Four samples of the Skookumchuck Formation (3–5 plastic sample vials of sediment per sample site) and one sample of Columbia River Basalt (whole rock) were obtained to measure paleomagnetic properties. The orientations of the sampling surfaces were measured and recorded as well as the bedding orientations at the sampling localities. The Columbia River Basalt was further characterized with a portable, custom-built fluxgate magnetometer (built in 1982 by Dr. J. Hinthorne, Univ. of Texas Rio Grande Valley, written commun., 2018) to determine normal or reverse polarity of 12 hand specimens. The four samples from the Skookumchuck Formation were collected near the Chehalis anticline. Of those samples, two were collected on the south limb, one near the fold axis, and another on the north limb but in a different fault block.

All five paleomagnetism samples returned inconclusive results possibly due to their being poorly indurated (Skookumchuck Formation), exhibiting too much variability in the oriented surface thus preventing reorientation for drilling (Grande Ronde Basalt), or being sufficiently weathered with hematite or goethite (both units)(B. Housen, Western Washington Univ., written commun., 2018). Generally, demagnetization behavior of most specimens is poor, likely owing to their low intensities, and the samples carry a complex remanence. Furthermore, lower hemisphere projections of the stratigraphic and geographic paleomagnetic results show considerable uncertainty likely due to either structural complications (multiple generations of folding) and (or) pervasive remagnetization.

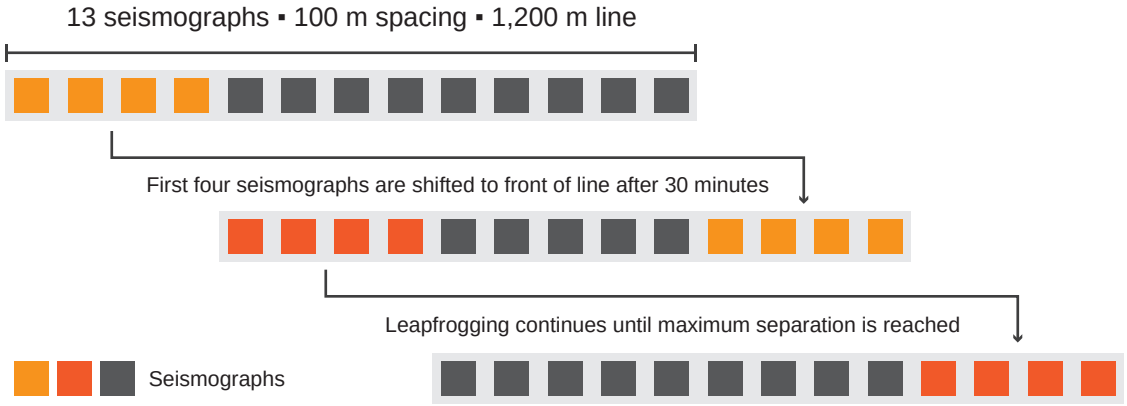

Figure A1. Geometry of the long-range passive seismic array using Atoms (wireless seismographs). Thirteen seismographs were expanded five times in a leapfrog pattern in order to reach a maximum separation of about 2.6 km. GPS clocks included in the seismographs were used for time synchronization (Hayashi, 2018).

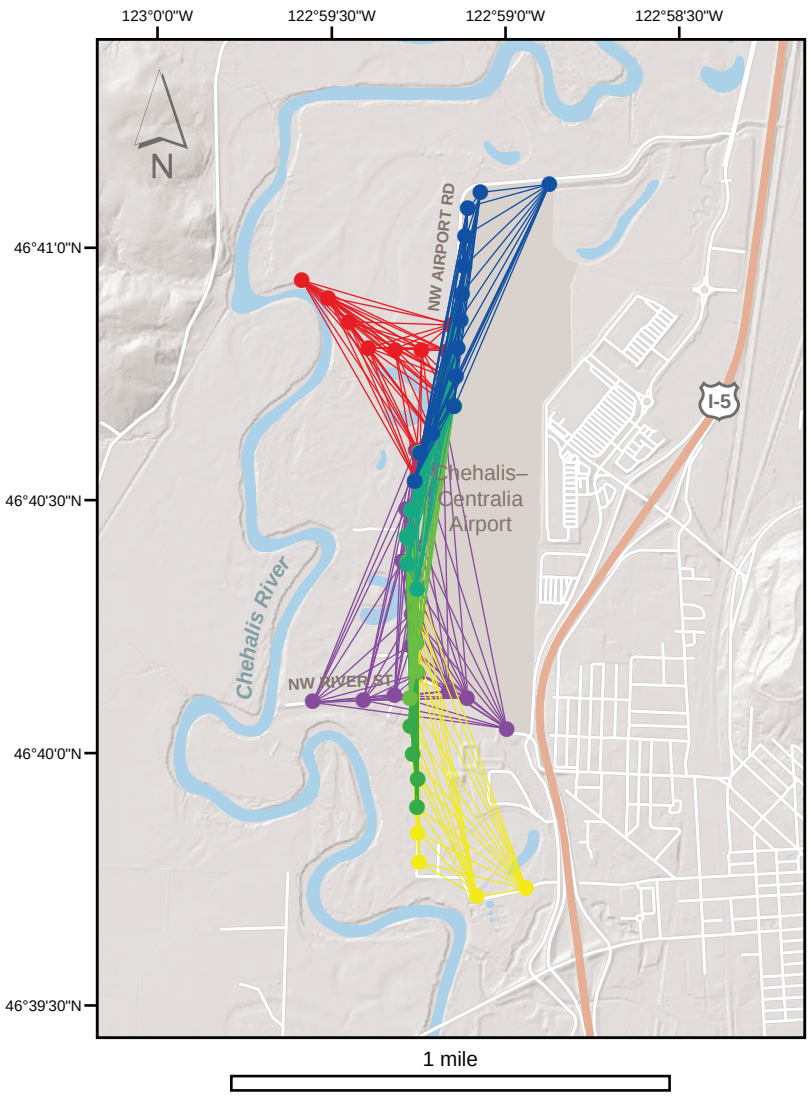

Figure A2. Long-range passive array measurement locations and corresponding triangular geometries used for data processing (Hayashi, 2018, written communication). Point colors correspond to groups of 13 sensors used in each 30-minute data collection session. East-west spread of sensors was used to improve triangulation.

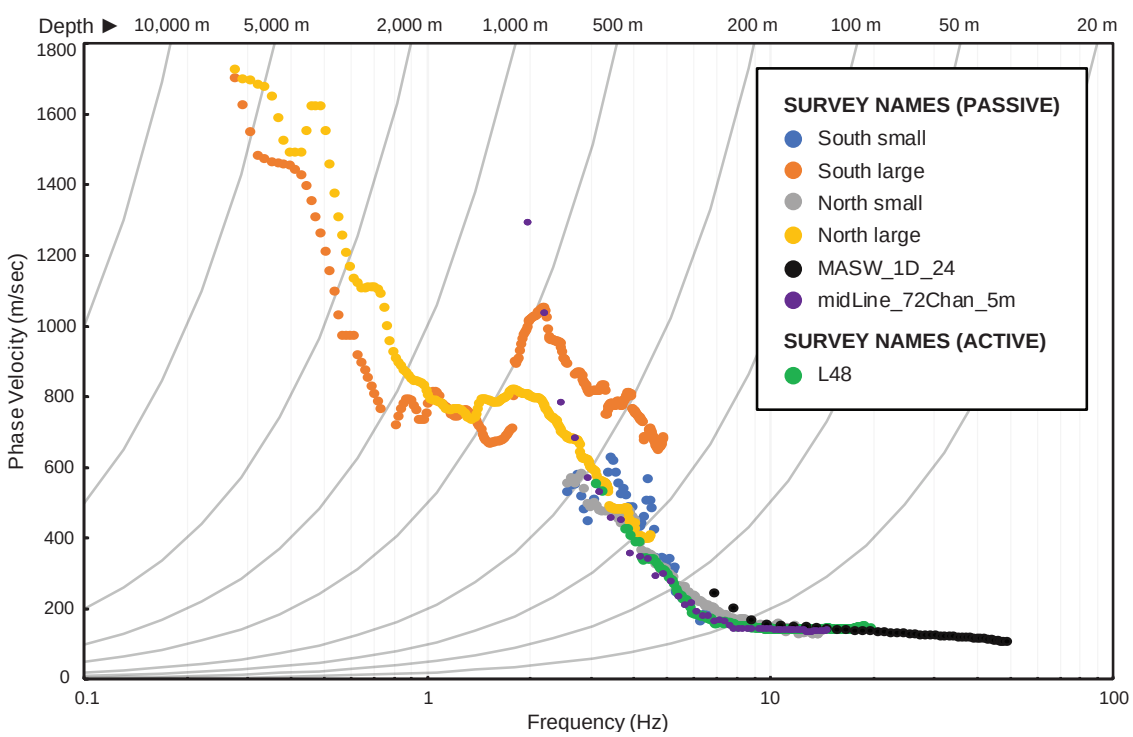

Figure A3. Comparison of simplified dispersion curves obtained from all active and passive array survey methods. Surveys L48, MASW_1D_24, and midline_72Chan_5m provide constraints on shallow seismic velocities. These experiments were used to confirm the validity of the new wireless passive seismic survey (small and large), which was designed to provide information on seismic velocities at greater depths. The overlap between the deep and shallow experiments at frequencies between 1 and 10Hz confirms that the methods are in agreement. Note: for depth calculations, velocity = wavelength × frequency.

Appendix B. New U-Pb Age Estimates

U-PB ANALYSIS METHODS

Each sample (~5 kg) was crushed to fine sand-sized particles. Heavy minerals were then concentrated using a Wilfley table. Between each sample, great care was taken to clean crushing plates and the Wilfley table to reduce the risk of contamination. The zircon concentrate was then passed through a 220 µm sieve and the <220 µm fraction was further refined using a Frantz LB1 magnetic separator to remove undesirable magnetic minerals. Zircons were then separated by density from the non-magnetic fraction using di-methylene iodide heavy liquid. From the zircon separate, ~50–300 individual zircon grains were hand selected from each sample and mounted in epoxy. The grain mount was polished to expose the grain centers and regions suitable for analysis were identified from Cathodoluminescense imaging.

U-Pb zircon data were collected at the Canadian Center for Isotopic Micro-analysis (CCIM) at the University of Alberta using procedures modified from Simonetti and others (2005). The analytical setup consists of a New Wave UP-213 laser ablation system interfaced with a Nu plasma MC-ICPMS equipped with three ion counters for static collection of Pb isotopes. The laser operated at a 4 Hz pulse rate with a beam diameter of 30 µm at a fluence of ~3 J/cm^2. Ablations were conducted in a He atmosphere at a flow rate of 1 L/min through the cell. Output from the cell was joined to the output from a standard Nu plasma desolvating nebulizer (DSN-100). On peak gas + acid blanks (30s) were measured prior to a set of 10–20 analyses. Data were collected statically, consisting of 30 1-second integrations. Before and after each set of analyses, we analyzed zircon reference materials, GJ-1 (Jackson and others, 2004; Heaman, unpublished data), and 94–35 (Klepeis and others, 1998) to monitor U-Pb fractionation, reproducibility, and instrument drift. Mass bias for Pb isotopes was corrected by simultaneously measuring $^{205}Tl/^{203}Tl$ from an aspirated 0.5 ppb Tl solution (NIST SRM 997) using an exponential mass fractionation law and assuming a natural $^{205}Tl/^{203}Tl$ of 2.3871.

All data were reduced offline using an Excel©-based spreadsheet. Unknowns were normalized to the zircon reference material GJ-1 and the uncertainties reported are a quadratic combination of: (1) the standard error of the measured isotope ratio (internal precision) and (2) the standard deviation of the standard means (external precision). The external precision of the GJ1 zircon reference material is estimated to be ~1% at 2σ for $^{207}Pb/^{206}Pb$ and 2%, 2σ for $^{206}Pb/^{238}U$ during these analytical sessions. The secondary standard 94–35 treated as an unknown yielded a lower Tera-Wasserberg concordia intercept age of 55.61 ±0.39 Ma (2σ, MSWD= 0.65, n = 18), in excellent agreement with the 55.5 Ma ID-TIMS age of Klepeis and others (1998). Data points were discarded if it was obvious that an inclusion contributed to the analysis, if there was an extreme common Pb component, or if the grain was in fact not zircon. All plots were generated using the Isoplot software of Ludwig (2003).

For detrital samples where zircon ages are thought to reflect the ages of contributing geologic units (provenance), the distribution of ages is plotted in two ways: as a histogram and as a probability density function; each has advantages and drawbacks (for example, Vermeesch, 2012). A histogram shows the distribution of age peaks for a sample, whereas a probability density function shows the relative likelihood of different ages within a detrital zircon sample; higher peaks indicate a higher likelihood and sharper peaks have a greater number of samples constraining its location on the horizontal axis (age), whereas rounder peaks have fewer samples.

Table B1. U-Pb data . Analysis by Andrew DuFrane and staff at ICPMS Lab, Canadian Center for Isotopic Micro-analysis, Department of Earth & Atmospheric Sciences, University of Alberta, Edmonton, Alberta, Canada T6G 2E3. Uncertainty values are at the 2σ level. Systematic errors from unrecognized sample characteristics are not well understood, but likely amount to 2% (Marillo-Sialer and others, 2016, and references therein). Thus a realistic estimate of the total uncertainty for the youngest peak age is 2 percent and conservatively 5 percent. * indicates common Pb correction by the method of Andersen (2002). See Data Supplement for analytical results and age estimates from individual crystals.

U-Pb site ID (sample no.) (geologic unit)		Age estimate	Maximum depositional age
GD10 (A174) (ⓅEvt$_{lcp}$)		No older than 36.70 ±0.32 Ma	single event, first peak average
TRS	sec. 33, T15N R02W	Analysis marks ages of 100 zircon grains from an unwelded lapilli ash flow tuff that is crystal- and lithic-poor, with a water-lain ash texture. The youngest age peak is tall and narrow, ranges from ~35 to 37 Ma, is formed from ~58 individual zircon ages and centered at 36.70 ±0.32 Ma. This is interpreted to be the maximum depositional age for a single volcanic event (eruption of tuff). The youngest single zircon yielded an age of 29.59 ±9.64 Ma.	
Lat/Long. (degrees)	46.74147 -122.94087		
Elev. (ft)	257	This locality was sampled from a steep, west-facing exposure that is east of a segment of active, north-south railroad tracks and east of the Skookumchuck River in the northernmost and central portion of the Centralia 7.5-minute quadrangle. The outcrop is to the east of and along a major railroad track in the northern map area and north of the site GD08 exposure. The exposure is a broad, steep slope laden with soil. This segment of railroad showcases the best stratigraphic succession of bedrock units for the Centralia 7.5-minute quadrangle. The attendant bedrock formations are moderately to steeply south-southwesterly dipping (southward is upsection). Outcrop color is a bluish medium gray, unweathered to mildly weathered with poorly welded to unwelded, lapilli tuff with abundant pumice. Field relationships place it within the lowermost portion of the Oligocene–Eocene Lincoln Creek Fm or uppermost portion of the Eocene Skookumchuck Fm. Notably, this lithology is consistently observed overlying the micaceous sandstone member of the Skookumchuck Fm, and commonly interfingers with the volcaniclastic siltstone member of the Lincoln Creek Fm. Snavely and others (1958) have this locality mapped within the Lincoln Creek Fm and to the south of a contact with the Skookumchuck Fm. The 1958 field relationship is further supported with coal mine data through a south-trending adit that runs through the hillside parallel to the railroad tracks. A U-Pb age from this locality may precisely place this lithology in either the Eocene or Oligocene, and thus within its respective formation.	
GD09 (A131) (ⓅEvt$_{lcc}$)		No older than 30.58 ±0.35 Ma	single event, first peak average
TRS	sec. 33, T14N R2W	Analysis marks ages of 100 zircon grains from a poorly welded lithic ash flow tuff.	
Lat/Long. (degrees)	46.65560 -122.94586	The youngest age peak is tall and narrow, ranges from ~29 to 30 Ma, is formed from ~44 individual zircon ages, and is centered at 30.58 ±0.35 Ma. This is interpreted to be the maximum depositional age for a single volcanic event (eruption of tuff). The youngest single zircon yielded an age of 27.72 ±2.50 Ma.	
Elev. (ft)	423	The outcrop is along SE Prospect St and to the east of downtown Chehalis, WA. The outcrop is exposed under tree roots at the top of a poorly maintained and partially overgrown roadcut.	
GD08 (A175) (Ⓜc$_{w}$)		No older than 8.57 ±0.92 Ma	youngest single grain
TRS	sec. 33, T15N R2W	Analysis marks ages of 283 zircon grains from a sandy conglomerate in the northern portion of the Centralia quadrangle. (300 grains total, 17 grains were >10% discordant).	
Lat/Long. (degrees)	46.73811 -122.94337	The youngest single zircon grain yielded an age of 8.57 ±0.92 Ma and is interpreted to represent the oldest possible age of the deposit. The youngest age peak is tall and bimodal, ranging from ~8 to 12 Ma and is formed from 12 individual zircon ages. An average maximum depositional age of the first peak is 10.58 ±0.50 Ma (Concordia, MSWD=1.01). Minor differences between curves GD08 and GD07 can be attributed to the greater number of zircons analyzed in GD08 (n=300), which is more likely to pick up less prominent populations compared to GD07 (n=100).	
Elev. (ft)	228	The outcrop is to the east of and along a major railroad track in the northern map area and south of the site GD10 exposure. The exposure is a large near-vertical wall of hackly, weathered Lincoln Creek Formation and very treacherous when wet. The horizon that was sampled is near the top of the exposure above an irregular, paleoerosional surface of the siltstone of the Lincoln Creek Formation, which is unconformably overlain by the sandy conglomerate of the Wilkes Formation (Fig. 4). Pebbles are rotten. Any imbrication is extremely subtle or non-existent.	

Table B1. continued.

U-Pb site ID (sample no.) (geologic unit)		Age estimate	Maximum depositional age
GD07 (A109r) (Ꝑc$_W$)		No older than 7.54 ±1.04 Ma	youngest single grain
TRS	sec. 28, T14N R2W	Analysis marks ages of 97 zircon grains from a pebbly sandstone in the central portion of the Centralia quadrangle. (100 grains total, 3 grains were >10% discordant) The youngest single zircon grain yielded an age of 7.54 ±1.04 Ma and is interpreted to represent the oldest possible age of the deposit. The youngest age peak is tall and smooth, ranging from ~10 to 16 Ma and is formed from 5 individual zircon ages. An average maximum depositional age of the first peak is 11.05 ±0.63 Ma (Concordia, MSWD=0.83). Minor differences between curves GD08 and GD07 can be attributed to the greater number of zircons analyzed in GD08 (n=300), which is more likely to pick up less prominent populations compared to GD07 (n=100). The outcrop is along a well-maintained, north-south forestry road on the property of Sam Madsen. Exposure is approximately 6 to 8 ft tall with greater depth gained by a ditch that flanks the exposure. A sand blow, formed by landslide or seismic activity, disturbs fine laminations and pebble lenses. The Logan Hill Formation directly and unconformably overlies this outcrop. To the south of the outcrop is a well-exposed contact with the lapilli ash flow tuff of the Lincoln Creek Formation.	
Lat/Long. (degrees)	46.67397 -122.93276		
Elev. (ft)	421		
GD06 (A095) (Qapo$_{lh}$)		No older than 1.68 ±0.97 Ma	Youngest Single Grain
TRS	sec. 36, T14N R2W	Analysis marks ages of 90 zircon grains from a pre-Vashon glaciofluvial outwash plain that mantles topography in the southeastern portion of the Centralia quadrangle. (100 grains total, 10 grains were >10% discordant) The youngest single zircon yielded an age of 1.68 ±0.97 Ma and is interpreted to represent the oldest possible age of the deposit. The youngest age peak is low and wide, ranging approximately from ~0 to 4 Ma and is formed from 7 individual zircon ages. An average maximum depositional age of the first peak is 1.86 ±0.19 Ma (Concordia, MSWD=0.29). The outcrop is multi-colored with severely weathered cobbles and pebbles in a sandy matrix along Centralia Alpha Rd on Logan Hill. Matrix was sampled for U-Pb, Cascade-sourced cobbles were sorted and not sampled. Weather was light drizzle with mildly muddy conditions, water was not streaming over the outcrop. Matrix was sorted by hand and with small digging tools at the outcrop and samplers were careful not to touch modern soils during sample bagging.	
Lat/Long. (degrees)	46.65947 -122.87760		
Elev. (ft)	545		

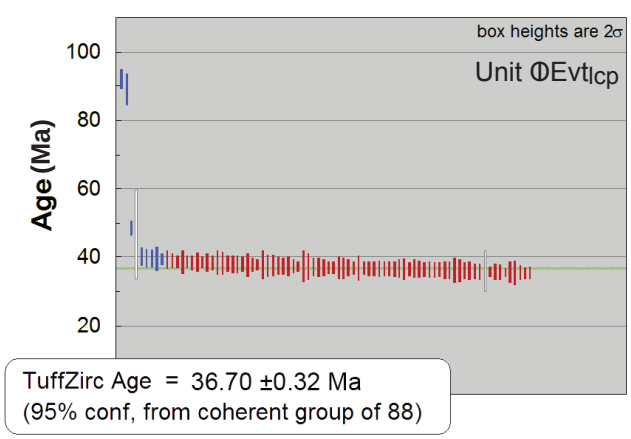

Figure B1. Younger zircon age peaks for sample from site GD10.

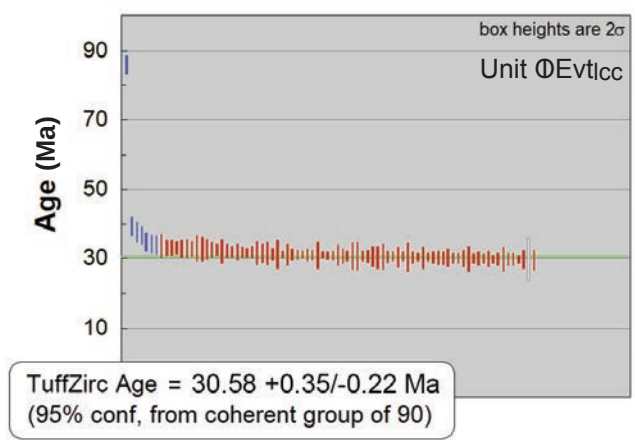

Figure B2. Younger zircon age peaks for sample from site GD09.

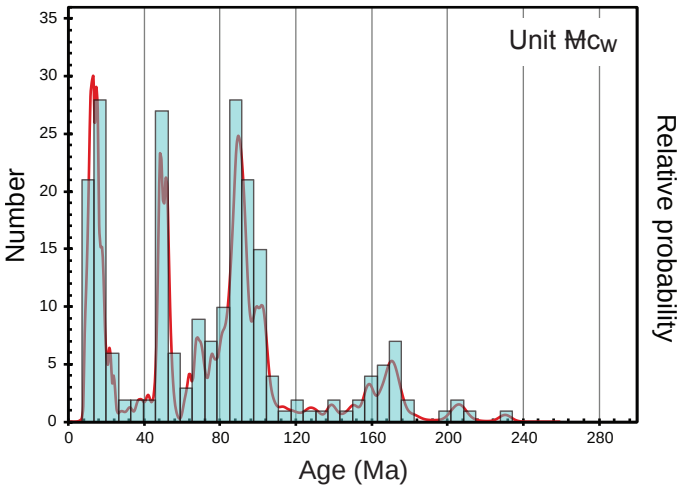

Figure B3A. Younger zircon age peaks for sample from site GD08.

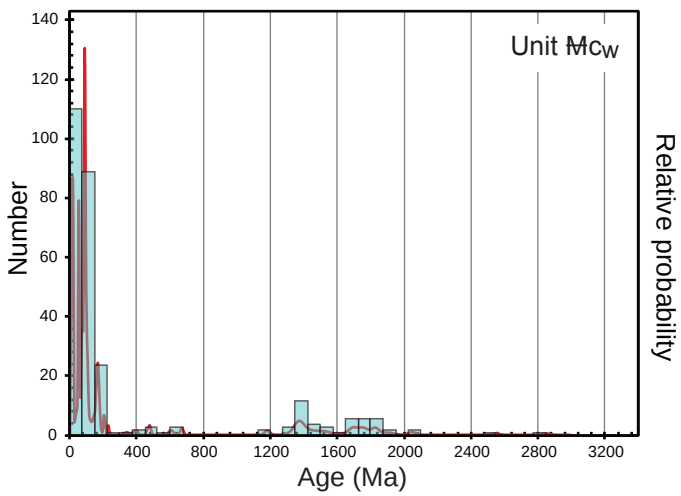

Figure B3B. Older zircon age peaks for sample from site GD08.

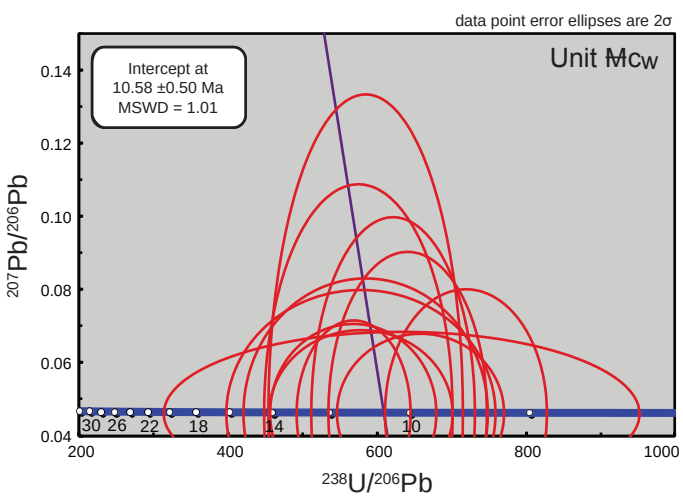

Figure B3C. Concordia diagram for sample from site GD08.

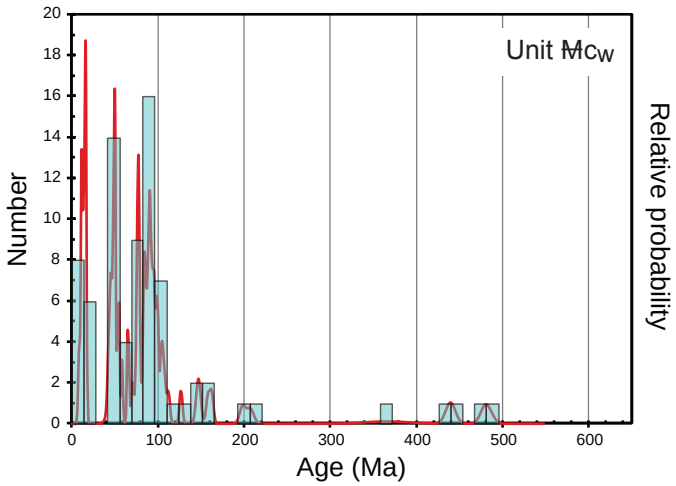

Figure B4A. Younger zircon age peaks for sample from site GD07.

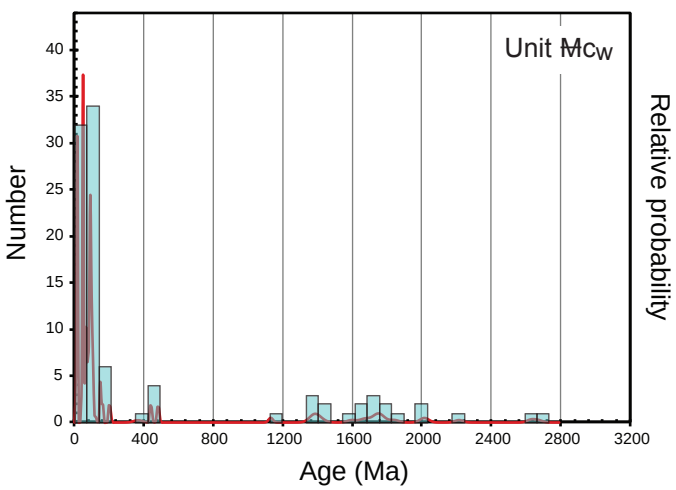

Figure B4B. Older zircon age peaks for sample from site GD07.

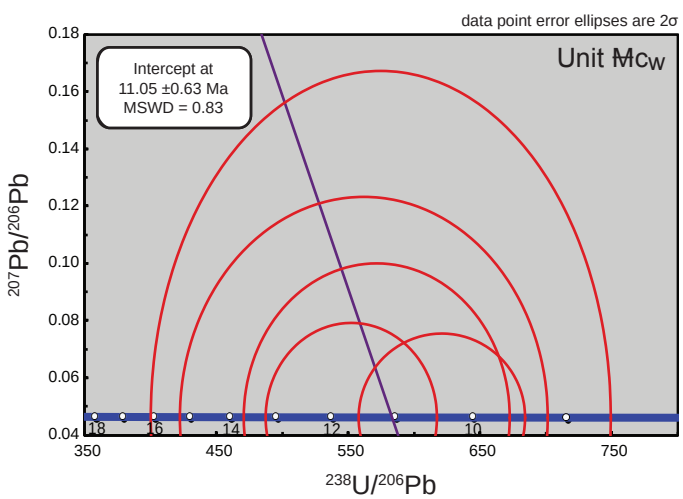

Figure B4C. Concordia diagram for sample from site GD07.

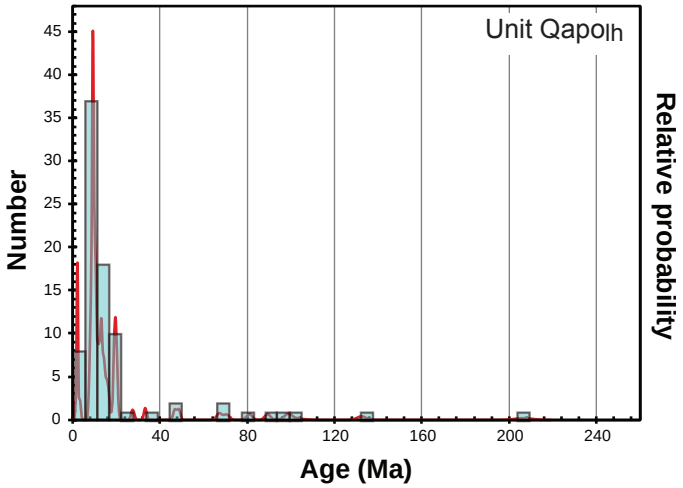

Figure B5A. Younger zircon age peaks for sample from site GD06.

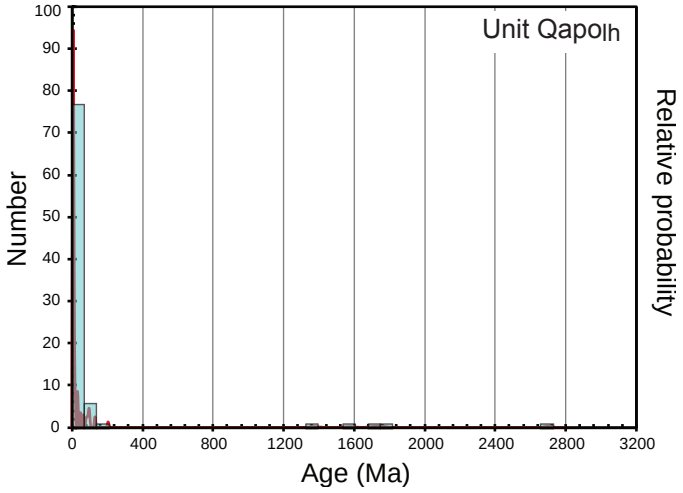

Figure B5B. Older zircon age peaks for sample from site GD06.

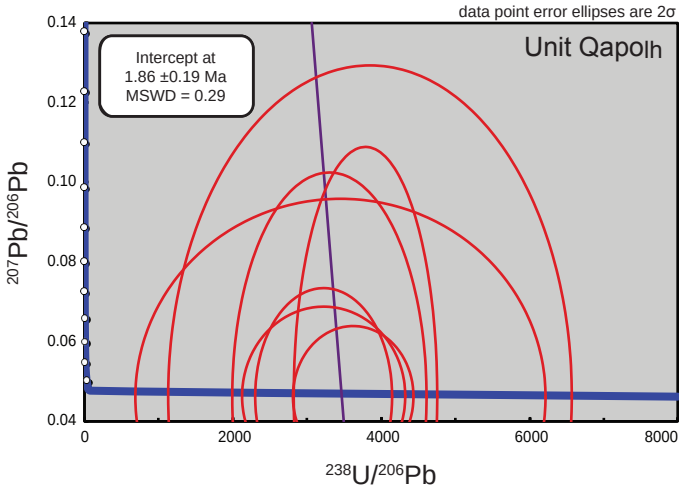

Figure B5C. Concordia diagram for sample from site GD06.

Appendix C. New Radiocarbon Age Estimate

Table C1. Radiocarbon data from site GD01 for unit Qa. ^{14}C yr BP age estimate is in radiocarbon years before 1950, and uncertainty estimates are reported at 1σ (68% confidence). Age in ka is in calendar years before 1950 divided by 1,000 and has 2σ uncertainty range. An age range is preferred because uncertainties are unequally distributed as a result of the calibrations curves used to convert between radiocarbon and calendar years. Uncertainty statements reflect random and lab errors; errors from unrecognized sample characteristics or flawed methodological assumptions (for example, 14C sample contamination from younger carbon flux) are not known. Age is adjusted for measured $^{13}C/^{12}C$ ratio (a 'conventional' age).

Elevations were estimated using Puget Sound Lidar Consortium Lidar data projected to State Plane South, NAD 83 HARN, U.S. Survey feet, supplemented by visual elevation estimates on-site. Lidar elevation statements were not adjusted to account for systematic projection differences relative to the base map. Lidar level '0' is theoretically 3.40 to 3.47 ft below base map level '0' [https://www.ngs.noaa.gov/cgi-bin/VERTCON/vert_con.prl]. Latitude and longitude coordinates are in WGS84 datum.

^{14}C site ID (sample no.) (geologic unit)		Reference	Material	Method	$^{13}C/^{12}C$ (o/oo)	Age estimate
GD01 (A304) (Qa)		this study	wood	^{14}C	-29.2	1,650 ±30 ^{14}C yr BP
Lab ID[a]	Beta-481940	~14 in.-long stick that was tightly lodged in floodplain deposit (unit Qa) on the downstream left side of Chehalis River. Sample was cleaned and carefully prepped before sending to Beta Analytical (Miami, FL).				
TRS	Sec. 24, T14N R03W					
Lat/Long. (degrees)	46.678997 -122.992962					
Elev. (ft)	162					

[a] Beta Analytic.

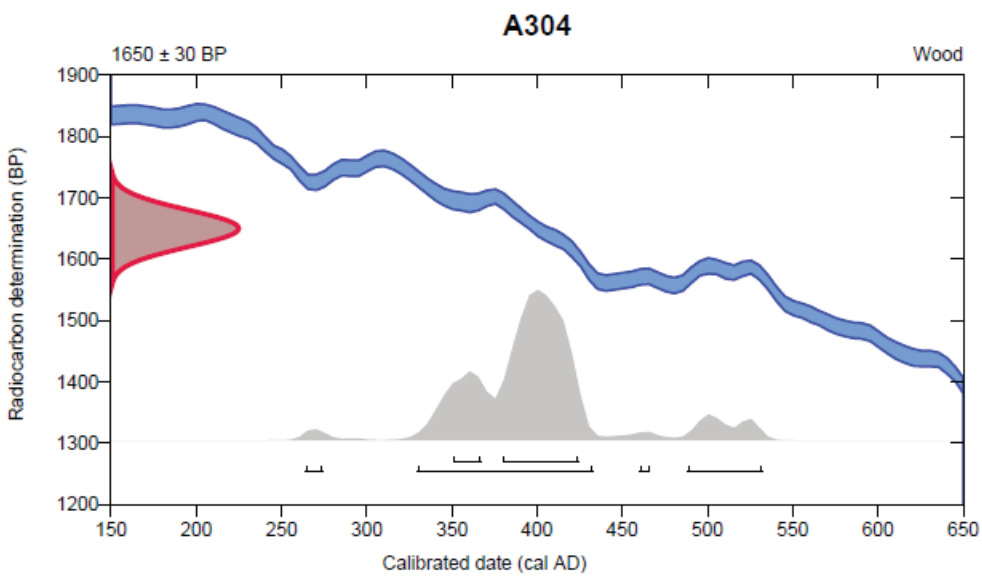

Figure C1. Radiocarbon age diagram for sample from site GD01.